ZAM Quadrotor VTOL UAV:
Prototype Development and Control Translator Dynamic Modelling

By

Cornelis Ambrosio Kok

Supervised by

Dr. Shane Pinder

A thesis submitted in fulfilment of the requirements

for the degree of Master of Engineering

School of Engineering

Auckland University of Technology

2010

ABSTRACT

ZAM Quadrotor VTOL Unmanned Aerial Vehicle: Prototype Development and Control Translator Dynamic Modelling

By

Cornelis A. Kok

Master of Engineering

AUT University, 2010

Dr. Shane D. Pinder

Motivated by the need to control a quadrotor tail-sitter unmanned aerial vehicle (QTUAV), the thesis presents the development of a method to convert user inputs and estimated measurements of QTUAV states into control set-points.

Pinder suggests control of the QTUAV using an optimal controller to achieve zero angular momentum (ZAM) and desired set-points [1]. The QTUAV dynamic model is dependent on previous states and has several phases of flight, which range from hover to forward flight. An Euler dynamic model relating desired set-points, system states, propeller velocities and angular momentum is developed in the work.

A pilot familiar with control of a Cessna-172 airplane is to command the craft. Cessna-172 airplane user inputs are transformed into desired set-points using a dynamic model of a Cessna-172 airplane. The user is provided a single intuitive concept of the system and is able to provide commands to the quadrotor without knowledge of the quadrotor dynamics. However command limitations exist due to differences between the user's concept of the flight envelope and the actual flight envelope. Alternative dynamic models that represent the user-system concept can be chosen to allow control translation and accommodate flight envelope differences.

Components for a prototype quadrotor helicopter were selected, and a quadrotor helicopter prototype constructed. Joystick inputs were converted into desired control states, transformed into a pulse-period-modulated (PPM) signal and output to a remote controller through a stereo sound port, using MATLAB. This basic control translator was used to control a tethered quadrotor however the inertia of the quadrotor was not sufficiently high to allow adequate control.

Thrust testing is completed to determine variation in thrust coefficients and equipment capabilities. The propeller assembly was attached to a base which was placed upon a digital balance to measure rotational speed and thrust at various controller settings. A coefficient of thrust of 2.94 x 10^{-6} N/rpm^2 was experimentally determined for the APC-E 7x5 propeller.

The selected electronic speed controller (ESC) did not provide speed control independent of power supply, showing that controller setting control is inadequate to control the motor rotational speeds[*]. Measurements of either propeller rotational speeds or thrusts are required in the control system to provide feedback of control set-points.

This work has accomplished further development of a method of control for a QTUAV. A dynamic model was developed which provides the relationships between current and future system states. It reviews current developments in unmanned aerial vehicles and presents several limitations to this method of control.

Future development of the dynamic model is required to enable complete attitude representation using the unit quaternion. Additionally, thrust and drag parameters must be determined for the wing. Furthermore, the dynamic models are to be modified to attain optimising functions. Implementation of the dynamic model will require the development of an observer to provide information about the craft states.

---

[*] A distinction is made between control (process of attempting to achieve a set-point) and controller setting (value displayed on radio controller indicating a set-point)

ACKNOWLEDGEMENTS

TABLE OF CONTENTS

LIST OF FIGURES

LIST OF TABLES

NOMENCLATURE

Symbol	Description	Units
$\mathcal{A}$	Coordinate of body axis origin, $\mathcal{A} = x_0, y_0, z_0$	m
A_{prop}	Characteristic area, $\pi R_{prop}{}^2$	m^2
A_{wing}	Characteristic wing area, top projection	m^2
AOA_{prop}	Propeller angle of attack	deg
B	Proportionality constant for static thrust	N.rpm^{-2}
C	Battery capacity	Ah
C$_{nominal}$	Nominal battery capacity	
$C_{D,2d}$	Two dimensional drag coefficient (wing)	-
$C_{L,2d}$	Two dimensional lift coefficient (wing)	-
$C_{M,2d}$	Two dimensional moment coefficient (wing)	-
C_M	Moment coefficient	-
C_T	Thrust coefficient	-
D	Proportionality constant for static moment	N.rpm^{-2}
D	Drag force	N
D_{2d}	Two dimensional drag force	N
$\hat{e}_i, \hat{e}_j, \hat{e}_k$	Unit vectors for body co-ordinate system	-
$\hat{e}_x, \hat{e}_y, \hat{e}_z$	Unit vectors for inertial co-ordinate system	-
F_{weight}	Force due to body mass	N
g	Gravitational constant, 9.81	m.s^{-2}
i, j, k	Coordinate in body coordinate system	M
I_{max}	Maximum current due to battery specifications	A
I_r	Mass moment of inertia for rotor about rotor axis	kg.m^2
$I_{G,x}, I_{G,y}, I_{G,z}$	Mass moment of inertia about x, y and z axis (**I**)	kg.m^2
K_V	Proportionality constant relating input voltage and rotational speed	rpm.V^{-1}
L	Lift force	N
L_{2d}	Two dimensional lift force	N
m	Mass	kg
$m_{battery}$	Battery mass	kg
m_{total}	All up weight of body	kg

Symbol	Description	Units
M_{drag}	Body moment due to air friction over the body (parasite)	Nm
$M_{drag-ind}$	Moment due to induced drag (wing force opposite to motion)	Nm
$M_{drag-para}$	Moment due to parasitic drag	Nm
M_{gyro}	Body moment due to gyroscopic effects of the propeller	Nm
M_{lift}	Moment due to lift force	Nm
M_n	Moment due to propeller-air interaction for propeller n, where $n \epsilon \{1,2,3,4\}$	Nm
M_{prop}	Moment due to propeller-air interaction	Nm
M_{static}	Moment due to propeller-air interaction in static conditions	Nm
M_R	Moments for rotor assembly	Nm
$Mach$	Mach number, ratio indicating speed relative to speed of sound	-
$pitch$	Pitch, forward movement of propeller per revolution	inch (")
$rpm_{\max\_prop}$	Maximum propeller rpm due to manufacturing requirements	rpm
R_{prop}	Propeller radius	m
r	Distance from oscillation point to center of gravity	m
T_n	Thrust due to propeller-air interaction for propeller n, $n \epsilon \{1,2,3,4\}$	N
T_{nR}	Propeller reaction force provided by frame	N
T_{prop}	Thrust due to propeller-air interaction	N
T_{rotor}	Thrust due to propeller-air interaction	N
t_{osc}	Time taken for single oscillation of quadrotor during inertia experiment	s
$t_{osc,tot}$	Time taken for 50 oscillations of quadrotor during inertia experiment	s
t_{rev}	Time taken for a single propeller revolution	s
$v_{prop,n}$	Translational velocity of propeller n	m.s⁻¹
$v_{proptip}$	Velocity of propeller tip	m.s⁻¹
$v_{n/air}$	Velocity of propeller n relative to air, $n \epsilon \{1,2,3,4\}$	m.s⁻¹
$v_{air/body}$	Velocity of air relative to body	m.s⁻¹
$v_{air/body,k}$	Velocity of air relative to air in the k body direction	m.s⁻¹
$v_{n/origin}$	Velocity of propeller n relative to body origin, $n \epsilon \{1,2,3,4\}$	m.s⁻¹
$v_{air/origin}$	Velocity of free stream air relative to body origin	m.s⁻¹
x, y, z	Coordinate relative to inertial coordinate system	m

Greek nomenclature

Symbol	Description	Units
α_n	Angular acceleration for propeller n, $n\epsilon\{1,2,3,4\}$	rad.s^{-2}
δ	Duration of negative pulse in trainer signal	s
Δ_a	Duration between negative pulses in trainer signal, $a\epsilon\{1,2\ldots8\}$	s
θ	Pitch angle	rad
ϕ	Roll angle	rad
ψ	Yaw angle	rad
ϑ	Generic angle used for formulation	rad
ρ	Air density	kg.m^{-3}
$\emptyset_{prop}$	Propeller diameter	inches
τ_n	Reaction torque for propeller assembly	N
ω	Propeller rotational velocity	rad.s^{-1}
ω_n	Propeller rotational velocity of propeller n, where $n\epsilon\{1,2,3,4\}$	rad.s^{-1}
ω_{prop}	Propeller rotational velocity	rad.s^{-1}
$\Omega_i, \Omega_j, \Omega_k$	Angular body rotation rate about i, j, and k body axis	rad.s^{-1}

Subscripts and Functions

Symbol	Description	Units
$c(\ )$	Cosine, i.e. $c\vartheta = cos\vartheta$	-
$s(\ )$	Sine, i.e. $s\vartheta = sin\vartheta$	-
$(\ )_{1stRot}$	First rotation	-
$(\ )_{2ndRot}$	Second rotation	-
$(\ )_{3rdRot}$	Third rotation	-
$(\ )_{max}$	Maximum possible/allowable	-
$(\ )_{prop}$	Of or relating to propeller	-
$(\ )_n$	Of or relating to propeller n, $n\epsilon\{1,2,3,4\}$	-

Matrices

Symbol	Description	Units
I	3 x 3 inertia matrix (mass moment of inertia of frame)	kg.m^2
M_{rotor}	Body moment due to rotor thrust and torque	Nm
R	3 x 3 rotation matrix (inertial coordinate system to body coordinate system)	
$R_{heading}$	3 x 3 rotation matrix (rotation due to heading angle)	
R_{pitch}	3 x 3 rotation matrix (rotation due to pitch angle)	
R_{roll}	3 x 3 rotation matrix (rotation due to roll)	
R_{yaw}	3 x 3 rotation matrix (rotation due to yaw)	
r	Inertial coordinate	
$sk(\Omega)$	3 x 3 skew symmetric matrix	
ξ	3 x 1 body coordinate matrix, where $\xi = [x \quad y \quad z]^T$	m
Ω	3 x 1 angular body rotation rates matrix, where $\Omega = [\Omega_i \quad \Omega_j \quad \Omega_k]^T$	rad.s^{-1}

ACRONYMS

AFV	Autonomous flying vehicle
AI	Artificial intelligence
AIAA	American Institute of Aeronautics and Astronautics
ANU	Australian national university
AOA	Angle of attack
APC	Manufacturer of propeller components
ARS	Attitude reference system
AFV	Autonomous flying vehicle
BQR	Buoyant quadrotor
C2	Command and control
DAQ	Data Acquisition
DC	Direct current
DCM	Direction cosines matrix
DOD	(American) Department of Defense
ESC	Electronic speed controller
FBD	Full body diagram
GPS	Global positioning system
HMI	Human machine interface
IMU	Inertial measurement unit
ISO	International organisation for standardisation
LED	Light emitting diode
LQ	Linear quadratic
MATLAB	Matrix laboratory™
MAUW	Maximum all-up weight
MAV	Micro air vehicles
MIMO	Multiple input multiple output
mUAV	Miniature unmanned aerial vehicle
NN	Neural network
PI	Proportional integral
PID	Proportional integral derivative
PD^2	Proportional derivative derivative
PWM	Pulse width modulation
QED	Quod erat demonstrandum

SISO	Single input single output
SNU	Seoul National University
STARMAC	Stanford testbed of autonomous rotorcraft for multi-agent control
TUAV	Tail-sitter unmanned aerial vehicle
TQUAV	Tail-sitter quadrotor unmanned aerial vehicle
VTOL	Vertical takeoff and landing
VTUAV	Vertical takeoff and landing unmanned aerial vehicle
QUAV	Quadrotor unmanned aerial vehicle
QTUAV	Quadrotor tail-sitter unmanned aircraft
UA	Unmanned aircraft
UAV	Unmanned aerial vehicle
USAR/WSAR	Urban search and rescue/wilderness search and rescue
ZAM	Zero net angular momentum

Other Abbreviations

xyz	Refers to the rotation of a body coordinate system to an inertial coordinate system
zyx	Refers to the rotation of a body coordinate system to an inertial coordinate system

ATTESTATION OF AUTHORSHIP

I hereby declare that this submission is my own work and that, to the best of my knowledge and belief, it contains no material previously published or written by another person (except where explicitly defined in the acknowledgements), nor material which to a substantial extent has been submitted for the award of any other degree or diploma of a university or other institution of higher learning.

_____

(Signature of Author)

_____

(Date)

Chapter 1 Introduction

1.1 Motivation and Objectives

An unmanned aircraft with four in-plane rotors, which is capable of flight as a helicopter and as a plane, is motivated by flight efficiencies and control challenges. The objective is to develop an unmanned aircraft that is intuitively controllable by a pilot. The research proceeds from undergraduate research undertaken at the University of Waterloo. Research motivations and objectives are further developed in the following section.

1.1.1 Unmanned Aircraft Preliminaries

Unmanned aircraft (UA) are defined as aircraft controlled without an onboard human pilot, and are used for a range of dull, dirty or dangerous missions where automation of the task or protection of the human user is necessary [2]. Applications that use UA include military reconnaissance, military combat, and filming and observation of structures. UA can carry a range of payloads to perform these functions including cameras, weaponry, and chemical and biological detection equipment. A selection of the diverse assortment of UA under development is presented in Figure 1.

The Stanford Meisocopter (Figure 1-a) is one of the smallest UA and is a quadrotor helicopter using tiny motors developed by Kroo et al [3]. Tethered flight tests for the Meisocopter have been achieved, and future advances in battery storage and control systems are expected to enable non-tethered flight. Kroo et al. hope to successfully deploy a system capable of controlling a large group of Meisocopters for reconnaissance missions on Mars (§1.2.1).
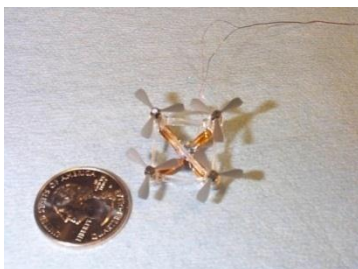
| a) Meisocopter [4] | b) Bidule-CSyRex [5] | c) Wasp [6] |

Figure 1: A sample of UAV under development

The Bidule-CSyRex (Figure 1-b), under development by KC Wong et al is a tail-sitter, an aircraft that can take-off like a helicopter and fly on its wing like an airplane. Tail-sitters provide the advantage of endurance during forward flight due to the potential of reducing the propeller thrust required to maintain the craft in the air. Manned tail-sitters, which include the Convair Pogo shown in Figure 2, have been historically unsuccessful due to the pilots' inability to view the ground during landing.

There is a distinction between tilt-rotor aircraft (such as the V22 Osprey) and tail-sitter aircraft (such as the Convair Pogo), where tilt-rotors have motors that rotate about the wing and tail-sitters have motors fixed with the wing.

Figure 2: Tilt-rotor (left) and tail-sitter aircraft (right); MV-22 Osprey in hover (left top) [7]; MV-22 Osprey forward flight (bottom left) [8]; Convair tail-sitter in hover (right) [9]

The Wasp™ (Figure 1 - right), by AeroVironment™ in conjunction with the Defence Advanced Research Projects Agency, represents the current endurance and functional capabilities of UA. Its flight endurance of 1.8 hours, ability to transfer real-time colour daylight images, and several autonomous flight modes make it useful for over-the-hill surveillance providing valuable intelligence [2].

The configuration of the aircraft, size, and control systems are different among UA as they are created under different design objectives including endurance, vertical take-off and landing (VTOL), manoeuvrability, stability, and tolerance to damage.

The rotation of an aircraft about its body is described by the terms pitch, roll, and yaw. The axes about which pitching, yawing, and rolling are respectively defined are shown

in Figure 3. Pitching is rotation around the lateral axis (left). Yawing is rotation around the normal axis (center). Rolling is rotation around the longitudinal axis (right).
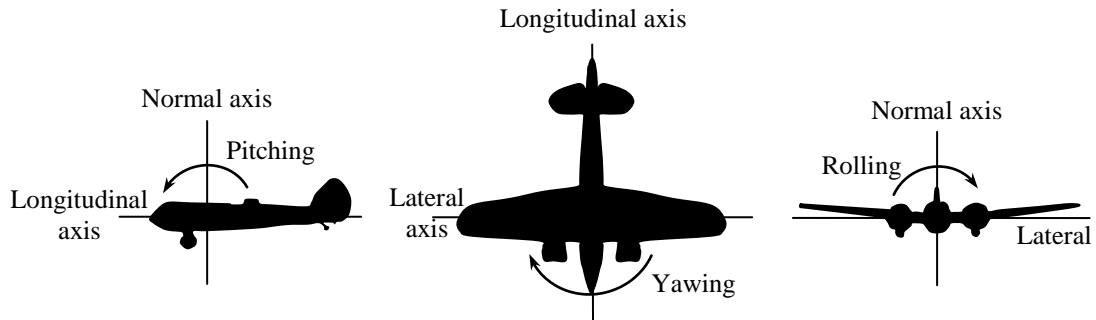
Figure 3: Axes and motions of aircraft; pitching (left), yawing (center), rolling (right); (reproduced from [10])

The conventional helicopter (Figure 4 - left) is a VTOL craft that uses a large spinning main rotor to generate the lift force required to support and manoeuvre the craft. The pilot can control the direction and magnitude of the thrust vector by controlling the angle of attack of the main rotor propeller blades. Pitch and roll movement of the helicopter is achieved by movement of a swashplate, which controls angle of attack as a function of angular displacement. Thrust magnitude is provided by collective control of the angle of attack for all angular displacements. However in addition to providing lift, the main rotor tends to rotate the body of the helicopter, so a rotor is placed at the rear of the helicopter to provide an opposite rotation force.

Torque generated by a single helicopter main rotor is alternatively balanced by using a second coaxial counter rotating propeller. The helicopter with two coaxial main rotors also has a swashplate to control the direction of motion.

Conventional   Co-axial   Quadrotor

Figure 4: Conventional helicopter [11] (left), co-axial helicopter [12] (center), and quadrotor helicopter [13] (right)

A four-rotor helicopter eliminates the need for the swashplate mechanism. The relationship between the thrust of each propeller and aircraft motion is simplified by placing the four rotors in the same plane. Rotating two propellers clockwise, and the

two remaining propellers counter-clockwise as shown in Figure 5, allows provision capability of zero net torque. This in-plane four-rotor craft with counter rotating propellers is described as a quadrotor in this text.

Changes in roll, pitch, yaw, and thrust are possible with the quadrotor configuration. The rotational speed of each rotor influences the torque and thrust provided by each rotor. Manipulation of the orientation and translation of the quadrotor is achieved through control of its linear and rotational accelerations. The relationship between motor speeds and quadrotor helicopter motion is described, with reference to Figure 5.
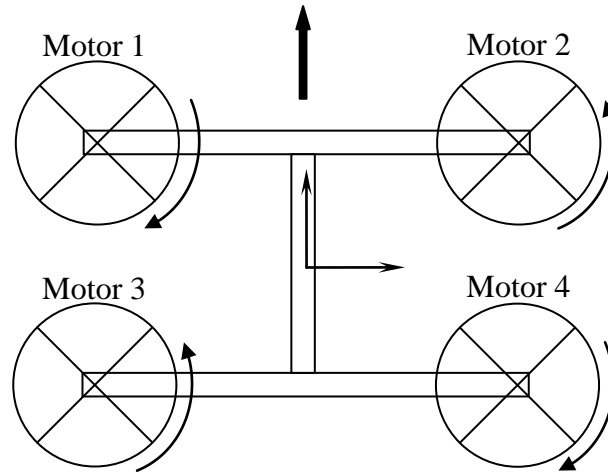
Figure 5: Top view of an H-configuration quadrotor aircraft indicating rotor rotation direction, motor number, and forward motion (wide black arrow)

Rotational acceleration about the lateral axis of the craft would be attained by decreasing the rotational speed of motors 1 and 2, and increasing the rotational speed of motors 3 and 4 (Figure 6-a). An increase in acceleration in the direction of the longitudinal axis would be attained by increasing the rotational speed of all four motors, thus increasing the net thrust. Rotational acceleration about the longitudinal axis would be attained by decreasing the rotational speed of motors 1 and 3, and increasing the rotational speed of motors 2 and 4 (Figure 6-b). Rotational acceleration about the normal axis would be attained by increasing the rotational speed of motors 1 and 4, and decreasing the rotational speed of motors 2 and 3 (Figure 6-c).

a) pitching   b) rolling   c) yawing
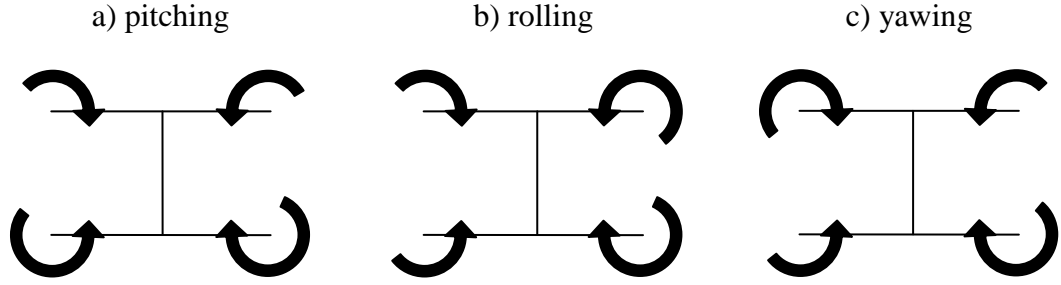
Figure 6: Achieving a) pitching, b) rolling, and c) yawing motions for a quadrotor

Changing the propeller speeds and therefore propeller thrusts alters the attitude/orientation of the quadrotor aircraft. Propulsion magnitude changes create a moment that tends to accelerate the aircraft linearly and rotationally. The quadrotor helicopter is unstable and requires a controller to achieve stable control of the system or must be designed to achieve increased angular inertia.

A range of control systems for quadrotor helicopters have been implemented and include a range of PID methods (PD, PI, PD^2), neural networks and optimal control. These methods are further described in §1.2.1.

The maximum flight endurance time of current quadrotor helicopters is in the order of 20 minutes, which may be improved by using a wing for long distance and low maneuverability mission phases.

1.1.2 QTUAV

A quadrotor tail-sitter unmanned aerial vehicle (QTUAV) [1], is proposed to provide endurance, and simplification of the mechanical mechanisms used for control, at the cost of control complexity. The quadrotor tail-sitter has a wing to provide a lift force (and drag force) during forward aeroplane flight, and sufficient static thrust to lift the aircraft in hover. A representation of the QTUAV is shown in Figure 7. Flight time endurance for a QTUAV is expected to be better than the quadrotor helicopter in some flight situations as less thrust is required for a given mass during forward flight on a wing [14]. Control of the angular velocity of the four rotors will provide motion of the craft in forward flight and therefore afford the elimination of shifting aerodynamic surfaces to make the craft construction simple. However, additional mass due to the wing will influence the efficiency of flight because additional lift is required.
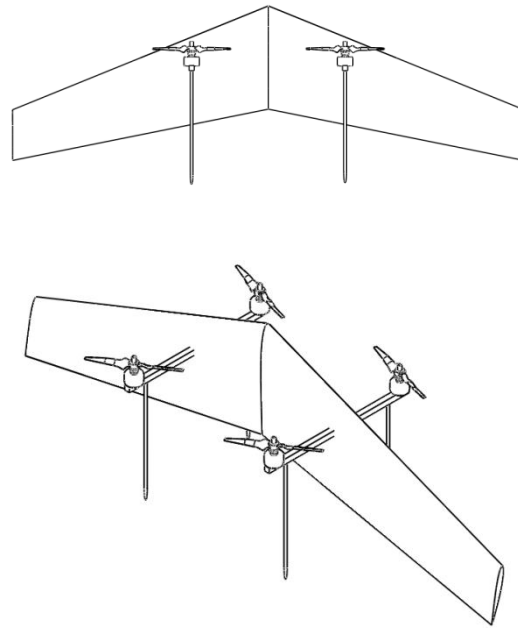
Figure 7: Concept drawings of a QTUAV; front view (top); isometric (bottom)

Several phases of QTUAV flight are shown in Figure 8. The first image illustrates hover, where the lift force is provided by the thrust generated by the QTUAV propellers. Hovering forward flight, where a portion of the thrust is used to move the QTUAV in a forward direction and the aerodynamic forces due to the wing are insignificant. Transitioning forward flight, where a portion of turbulent lift is generated by the lifting surface and a portion by the propeller. Finally, forward flight where the majority of lift generated by the lifting surface and the propellers is primarily used for forward motion during forward flight.

Hover	Hovering Forward Flight	Transitioning Forward Flight	Forward Flight
v=0km/hr; a ≈ 0	v≈5km/hr; a ≈ 0	v≈15km/hr; a ≈ 0	v≈30km/hr; a ≈ 0
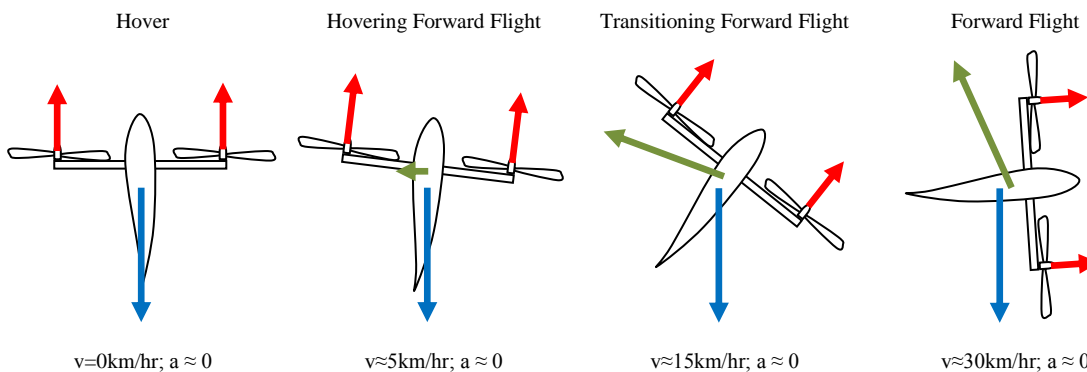
Figure 8: Phases of flight and simplified representation of forces and movement for a horizontally moving QTUAV (red–thrust, blue–weight, green–lift/drag)

At each stage of flight, control inputs have different effects on the translational motion (positional change) of the aircraft. The change in the control input effect is due to the change in the significance of the wing at each orientation. During hover, an increase of

thrust increases the altitude of the craft; in forward flight, an increase of thrust increases both the altitude and the forward/horizontal speed. Additionally, a yaw command in hover corresponds to a roll command in forward/horizontal flight.

A user would preferably control the craft motion directly, although direct control of the motion via control of the QTUAV rotor speeds is complicated. The net force generated is dependent on attitude as the force on the wing depends on the direction and velocity of air flow against the wing. During transition, the QTUAV pilot will then need to know when changes to the command input are required to effect control of the craft, which requires training and practice.

Avoidance of the turbulent flight regime during tail-sitter transition can be achieved. Stone et al avoided the turbulent flight regime by controlling the flight path during transition such that airflow over the wings is laminar [15]. This allows transition capabilities and ensures controllability during hover and forward flight but neglects the desire to control the craft position at all stages.

A QTUAV capable of controlled flight at all orientations between hover and forward flight is desired. Development of a QTUAV will contribute to the aerospace community by providing a rig that is able to take-off and land vertically, have a simple mechanical construction, as well as fly an increased range compared with other helicopter UAVs.

1.1.3 Developmental History

A presentation at the University of Waterloo by students competing in the International Aerial Robotics Competition described the scenario where an aircraft was required to travel to a destination, navigate a building, pick up an object and return the object to the starting point. Due to expected efficiencies during forward flight and manoeuvrability benefits during hover, this meeting inspired Philip and Pinder (University of Waterloo) to undertake development of a QTUAV [16].

Development of the helicopter/airplane hybrid began with the design of the QTUAV configuration. Various structural configurations and components were considered for the quadrotor UAV [16]. Whilst comparing 'X', 'H', and box shaped craft, Phillip suggested an 'H' aircraft configuration due to its larger aerofoils and better balance, and considered tradeoffs due to stability and directionality. A bend in the wing was also suggested to account for a required separation between the aerofoil and propeller. A 3D

sketch of the presented design is shown in Figure 9. A propulsion system was developed by Tremblay [17], and Phillips worked on a dynamic model of the aircraft [18].
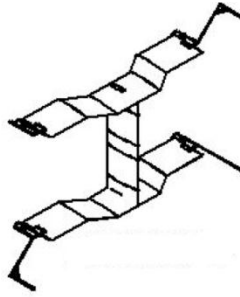
Figure 9: Design of QTUAV, motors/props removed (Reproduced from [16])

A control strategy [19] for a QTUAV was presented by Wilson et al. This Kalman-Filter-based control strategy requires a dynamic model of the QTUAV. A dynamic analysis of momentum [1] was presented by Pinder on the effect of deflections of the QTUAV due to propeller angular momentum on the overall angular momentum. The analysis found that for the 'H' configuration, at constant pitching rates and constantly accelerating pitching rates, the effect of deflection on momentum forces was to contribute to a perceived increase in rotational inertia.

1.1.4 Control Translation

Control of the craft through the four stages (§1.1.2) is dependent on the current state of the craft. Control in hover is unstable which, notwithstanding configuration improvements, prevents direct control of the helicopter. Additionally, changes in motor speeds affect the craft orientation differently at each flight stage. It is ideal that there is no change in the method of command when the aircraft changes from helicopter mode to aircraft mode and that therefore the craft is capable of being commanded using a single concept of the system at all times.

Two terms are defined to ensure reading clarity: 'command' refers to the inputs presented to the control system and the desired states they represent, while 'control' refers to the desired states of the craft and the resulting system to achieve these desired states.

A control interface will need to be created to enable the pilot intuitive command of the QTUAV. The interface will be able to cope with a plant that is dependent on orientation, and allow the user to command the QTUAV using a method that they select. Command methods that may be implemented in the future include airplane

inputs, helicopter inputs, voice inputs, and car inputs. The airplane command method is selected for our development as an experienced airplane pilot is available to test the flight control.

A control translator to convert pilot commands into control outputs for the QTUAV was presented by Pinder [19] as a control strategy (Figure 10). Like a linguistic translator that converts one language to another, a control translator would convert airplane inputs into outputs that would control a helicopter. Once several translation models were developed, a control translator would eventually be capable of translating any input type into any desired output type.
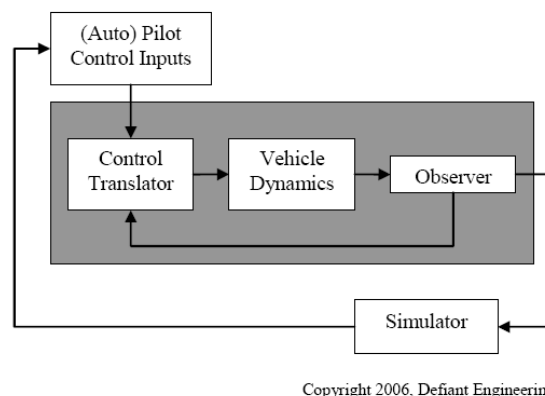
Figure 10: Control strategy block diagram (Reproduced from [1])

The significance of a control translator is the ability to allow users to command a system with which they are unfamiliar, using inputs for a 'supposed plant' with which they are familiar. A user that can drive a car will then be able to control any system which has a previously developed dynamic model (such as a helicopter or aircraft), using inputs that would commonly be used for a car. The user would thus be able to command the new plant without any additional training.

The pilot receives information about the craft orientation from a simulator and the pilot inputs movement commands based on this simulator. Pilot control inputs are translated, sent to the vehicle under control, and an observer watches the subsequent motion. The new state information and pilot control inputs are sent to the translator to generate a better control output for the vehicle [1]. Control in this manner requires inputs from the pilot, and information about the current orientation of the craft. The information output is required to be manipulated so that the control output eventually gives a stable craft and the motion commanded. Additionally, the control strategy requires information

about how control inputs 'map' to control outputs, hence a model relating inputs/outputs is required.

1.1.5 Human Machine Interface

Human centered design is the design of artefacts to allow the co-adaptation of people and technology [20]. The human machine interface (HMI) exists where the human and the machine interact and come in many variations. A selection of HMI variants includes lathe controls, car cockpits, control panels for manufacturing equipment, aircraft cockpits (Figure 11) and computer keyboards. In the design of human machine interfaces, the user desires an interface with which they are familiar, an interface that they can understand and thus an interface that allows the user to command the artefact.

Figure 11: Cockpit of a Cessna 172 (Reproduced from [21])

To command differing plants a user is required to learn to manipulate different interfaces. This can be problematic for novice users of the human machine interface who may wish to command a new machine as they are prone to enact errors during their learning phase.

The traditional method of enabling a user to command a new plant is to provide training to the user so that they may develop a conceptual model of the plant and thereby form an understanding of the plant (§1.1.5 and Figure 12). Training to a standard that allows the user to have a strong understanding of the system can be a lengthy[†] and expensive procedure to perform. A method to allow the user conceptually simple command of a plant will be developed which will eliminate the training process and thus eliminate

---

[†] long in time duration

training resources. The development of the control translator will allow a control method for the QTUAV by separating command and control.

The user will have expectations about the influence that their control input will have on the system. The way the user interacts with the control interface is dependent on the way a user perceives the system, the limitations of the user, and the way the user creates, becomes aware of, and corrects mistakes. This relationship between user inputs and outputs is fully defined by an accurate system model.

Command of any apparatus requires consideration into the interaction between the human user and the aircraft. Development of the true representation of cognition while a user interacts with an apparatus is in majority, the domain of neural science, psychology and philosophy. Generally, applied scientists and engineers seek a representation of these decisions to provide design constraints and parameters. Norman explained the relationship between the user's conceptual model and the controlled system as illustrated in Figure 12. A user interacts with the system, gaining information about how their control inputs relate to the system outputs. The user develops rules and subsequently an understanding of how they should interact with the new system. This understanding is the user's conceptual model. When the user's conceptual model matches the system model, the user is able to fully control the system. A user's conceptual model is separate to the system model, and the user requires as much accurate feedback as possible from the system model to ensure that the user is able to form an accurate conceptual model.

During learning, the user's conceptual model is not likely to be identical to the system model. The system is required to be robust against user control errors yet provide feedback about the error in control to allow improvement of the users conceptual model. The controlled system should be as similar as possible to the user's first conceptual model and this is especially important in the situation where a control error means permanent damage to the system.
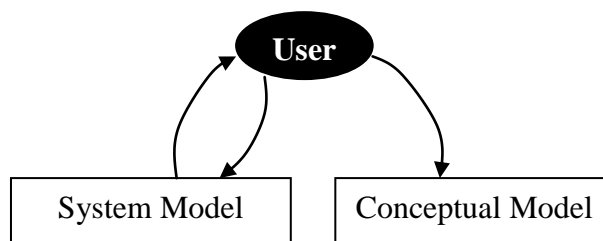
Figure 12: Relationship between user, system model, and the user's conceptual model (Adapted from [22])

A controller that will allow a user to use their preconceived conceptual model would require that all information fed-back to the user is as similar as possible to what they would expect, were the user actually controlling the conceptual craft. Also, without error between what is sensed and what is desired, there will be no change in the mind's representation of the system unless there is an error in what is sensed. A familiar control interface is required to provide an interface that a user is able to use to effectively control a (presumed unfamiliar) QTUAV. We must also ensure that information feedback to the user will represent the motions they expect while using that familiar control interface. The user's conceptual model changes as a result of feedback from the controlled system. Changes to the user's conceptual model during control of a system must be minimised as they will make the control translator less effective.

A more complete representation of the user during interaction with a system was developed by Stengel when he developed systems for intelligent control. Figure 13 illustrates his concept for user-system interactions, which demonstrates that control of the system not only relates to the mind's representation of the system, but also reflexive actions and bodily requirements.
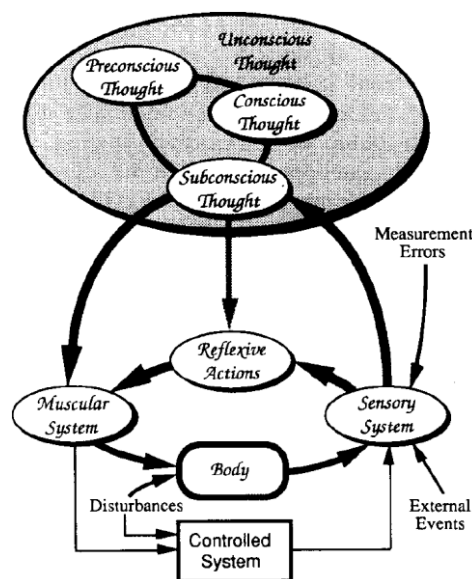
Figure 13: A model of cognitive control behaviour (Reproduced from [23])

The aircraft user interacts with the aircraft which has a dynamic response that is orientation and input dependent. A user forms a conceptual model of the operation of the machine when a user first interacts with a machine. Importantly, it is reinforced that the interface is required to be as similar as possible to the usual interface, as this will alter conceptual models due to its form.

The HMI should present a dynamic response that is within the abilities of the pilot or the control will be unstable. Investigations into the characteristics of a conceptual dynamic model of an aircraft have been completed by researchers of aircraft using the Cooper-Harper scale. Questionnaires were used to determine the dynamic characteristics that make an aircraft easy to control. The information that they have presented show regions where the effort required to control the craft is difficult, moderate, and easy. These regions are constructed so that designers are aware of trade-offs between manoeuvrability and ease of use. Figure 14 shows the design space for designed dynamic models for aircraft.
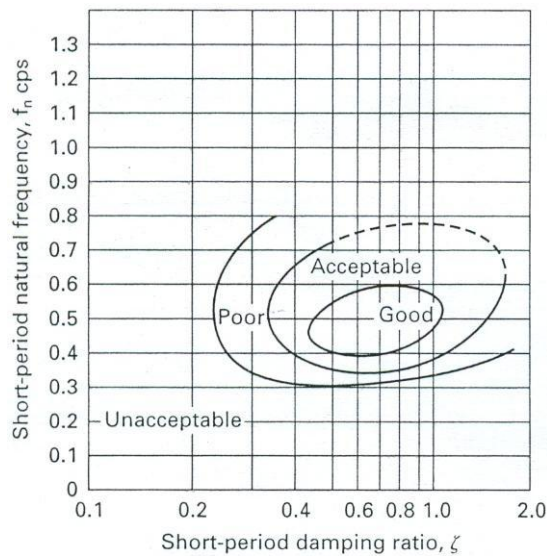
Figure 14: Design space for damping ratio for comfortable to pilot aircraft (Reproduced from [24])

The ideal relationship between roll, thrust, and yaw for airplane flight is at damping ratios within the inner circle shown, thus attempts at a control system for piloted airplanes should attempt to attain these damping characteristics. Therefore, in a simulated environment, experienced pilots generally desire a system damping ratio of approximately 0.7 and a short period natural frequency of 0.5 cycles per second.

Grant and Haycock investigated the effect of acceleration and jerk on the user's perception of motion in the application of simulator design [25]. Visual delays should be designed to ensure no noticeable lag to ensure the provided motion matches sufficiently with the user commands.

1.2 State of the Art

The following is a review of past and current developments in quadrotor unmanned aircraft, tail-sitter aircraft, and control translation.

1.2.1 Quadrotor Unmanned Aerial Vehicles

The first construction of a full scale four-rotor helicopter was the Breguet-Richet quadrotor in 1907. De Bothezat, in 1921 [26], developed a quadrotor and successfully tested it in 1922.
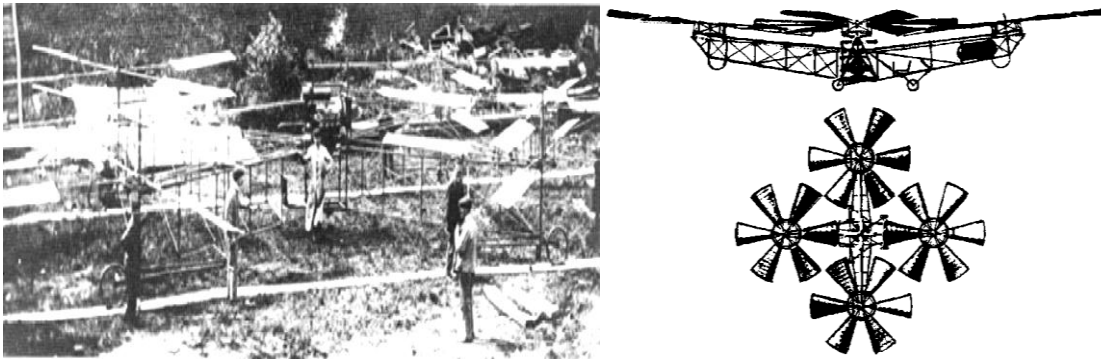
Figure 15: Historic quadrotor aircraft; Breguet-Richet quadrotor (left) [27]; De Bothezat quadrotor (right) [28]

E Oehmichen built and tested several variants of buoyant quadrotor (BQR) aircraft (Figure 16) in an attempt to construct heavy-lift aircraft. In the 1950s, experimental (X series) quadrotor craft were made. The Curtis-Wright X19 and Bell X22 (Figure 16) were tilt rotor aircraft that flew a total of 50 and 500 flights respectively.

Figure 16: Historic quadrotor aircraft; BQR – Oehmichen [29] (left); Curtiss-Wright X-19 [30] (center); Bell X-22 [30] (right)

Development of heavy-lift aircraft renewed in the mid-1960s and multi-rotor craft, the variants of the BQR in particular, were considered to be the solution for heavy lift applications [29, 31]. By 1981, the BQR was deemed to be the best solution to the requirement of heavy lift and became the principal subject of technology development efforts [29]. A buoyant four-rotor aircraft was developed by Nagabhushan who

constructed a dynamic model to assess control characteristics while carrying a sling load [32].

A human powered quadrotor that significantly capitalised on ground effect, YURI I, was developed in 1994 to prove that human powered flight was possible [26]. In 1998, researchers at Stanford University, after developing a micro scale motor, began work on the development of a micro scale quadrotor called the Mesicopter [33]. Their online and published work presented a system, capable of lifting of its own weight, but not yet capable of unsupported flight [3, 34-36].

Draganfly Innovations Inc. developed a quadrotor helicopter in 1999 given the brand name Draganflyer™ [37]. The control system used infra-red to sense the location of the sky and ground relative to the craft, and used this information to orient the craft in space.

Since the release of the Draganflyer™, the quadrotor helicopter has been used by university researchers to test various control methods and sensing technologies. Several research groups began projects on quadrotors, some using the Draganflyer III™ and others developing their own quadrotors.

In 2002, Altug, Ostrowski and Mahony published a paper on the development of a controller using visual feedback [38]. Subsequently, Pounds, Mahony et al [39] have been working toward the development of a quadrotor UAV that, similar to a conventional helicopter, is expected to "exhibit slow unstable dynamics and, [due to the sufficiently slow dynamics], be straight-forward to control by a human or autopilot". This is significant for our development as large helicopter rotational inertia, coupled with fast forward-flight dynamics for the QTUAV and a transition between would provide for a non-sensor-driven QTUAV.

Pounds et al use a purpose-designed inertial measurement unit (IMU) [40] to provide attitude and motion information. Additionally, they have dynamically modelled the quadrotor assuming rigid structure, designed a propeller to optimise for stability [41], and analysed stability using Lyapunov and stability derivatives. A quadrotor with tuned plant dynamics, tethered to allow only pitch and roll, was linearly controlled [42] using a PID controller. Control was successful for rotor speeds less than 450 rads^{-1}, at which point instability was present, presumed to be caused by high-frequency noise from the rotors.

Altug has also been continuing research on control of a quadrotor, but has focused on control methods using vision sensing. He uses two cameras, one on the ground and one on a quadrotor aircraft, to sense the position and orientation of the craft [43, 44]. He also continued research into a PD controller using a single camera to sense a target, and thereby determine position, orientation, and motion [45].

In 2004, Bouabdallah began development of a quadrotor controller [46]. He compared PID and linear quadratic control techniques in the task of quadrotor control [47]. His results indicated PID control to be superior, citing the weakness as simplifications in the LQ controller model. Final results for his PhD research were presented where he achieved position, altitude and attitude control of a quadrotor in 2007 [48].

Tayebi and McGilvray developed a quadrotor controller using a PD^2 feedback system and utilised partial quaternion representation for attitude representation due to processing benefits [49, 50]. Tayebi continued to develop their craft by focusing on low cost sensing [51] and further reducing processing time via purely quaternion craft orientation representation [52].

Darafa developed a dynamic model and PID controller for a quadrotor aircraft that incorporated gyroscopic effects and motor dynamics. Constants defining the quadrotor were experimentally determined. Constrained to altitude and yaw movements, the developed control system was validated [53].

Bouchoucha developed a nonlinear PI controller to stabilise the attitude of a quadrotor [54]. He also worked with Bouadi to develop a sliding mode control strategy based on a backstepping approach [55].

Dunfield et al attempted to control a quadrotor using neural networks [56]. They had successful pitch and roll control but problems identifying drift in their yaw control due to noisy gyro measurements. Coza compared adaptive, sliding mode, neural network (NN) control methods and developed an adaptive fuzzy controller [57]. Adding to Coza's work, a NN controller was developed by Nicol et al that aimed to cope with large disturbance gusts. Simulations by Nicol et al show promising results [58].

In 2006 a group of students at Malaysia Universiti Teknologi began development of quadrotor aircraft as testbed for control [59]. They identified magnetic interference of

gyro measurements to be the cause of yaw control problems. The source of magnetic interference is likely the motors.

Since 2004, a team under Hoffmann at Stanford University have been working on development of the Stanford test-bed of autonomous rotorcraft for multi-agent control (STARMAC) [60, 61], where the main objective is the development of a control system to control multiple craft with collision and obstacle avoidance. They have developed a dynamic model for the quadrotor and incorporated changes in thrust due to free stream and vehicle velocity, and moments caused by the difference in incident air velocity of retreating and advancing propellers [61]. In control system design for STARMAC, Waslander used both the integral sliding mode and reinforcement learning to design a more stable altitude controller [62]. Earl, whilst working on the Cornel AFV (Autonomous Flying Vehicle), determined the aircraft state using gyros and three orthogonal cameras to sense four red light emitting diodes. A Kalman Filter was used to combine the orientation and position information [63]. This craft is also intended to be used as a test bed for control of groups of UAVs [64].

Gurdan et al developed a 350g quadrotor and control system optimised at 1kHz. This system used two infrared cameras to attain position data. Altitude control was attained through PD control and an accumulator (to provide integration of altitude errors). Horizontal motion was controlled by regulating/controlling speed which used velocity and acceleration inputs. They also set up a UDP (user datagram protocol) client to control the aircraft over the internet [65].

An embedded controller has successfully been implemented to control a four-rotor helicopter [66]. A simplified dynamic model using momentum theory and neglecting gyroscopic effects and air friction has been used in the design of a quad rotor control system [67]. Madani controlled a quadrotor using the 'full state backstepping technique' in 2006 [68].

Berbra developed an observer capable of detecting a failed rotor, and providing control to compensate for the lost rotor. This system used several observers, each sensitive to failure of a different motor and a fault tolerant switching control law to select the controlling observer [69]. This method was successful for a simulation using a Matlab/Simulink model of a quadrotor. Development of quadrotor UAVs have also featured as an undergraduate constructed solution to USAR/WSAR scenarios [70].

Ng, who had previously worked on the development of a mUAV [71], recognised the difficulty of selecting optimal components for a quadrotor. He developed a program that would select optimal components for a quadrotor using genetic algorithms [72].

Considering the previous work, decisions that need to be made in the development of quadrotor helicopters include selection of coordinate systems, model assumptions, method of control, frequency of operation, method of state measurement, human consideration of control interfaces, and design of experiments.

The coordinate systems considered are the direction cosines matrix and the unit quaternion. The direction cosines matrix (Appendix E) has a space-dependent singularity, the quaternion coordinate representation has a rate-dependent singularity. The most complete rotation representation and fastest computation efficiency is provided by the quaternion coordinate system where several commercially available IMU have quaternion and Euler angle measurements available.

The system model might assume the QTUAV frame as rigid. All physical models have used rigid frames, and dynamic models have assumed a rigid body. Pounds et al implemented aerodynamic modelling of propeller deflection and airflow changes. All quadrotor helicopter designs have used an X-shaped frame as it can be considered symmetrical about the pitch and roll axes. Resultantly, this configuration provides simplification in modelling constants.

Orientation and motion sensing provide feedback to the pilot. The method of sensing has been diverse. The commonality is that there has always been the inclusion of some method to measure orientation and positional change. Variations include IMU (3x gyro, 3x accelerometers), GPS, compass sensing, dual and single camera visual sensing.

The methods implemented in quadrotor control includes Neural Networks, PI, PD, PD^2 and optimal methods. Controllers have also been augmented to enhance stability using back-stepping methods and the integral sliding mode. A quadrotor control system has been optimised at a frequency of 1kHz which provides a reduction in power consumption and increase in control resolution.

While the control commands have been mentioned, the control interface has not been a principle aim in quadrotor literature. The principle concern in the literature has been the development of a type of controller for an unstable system.

1.2.2 Tailsitter UAV

Tailsitter UAVs provide a balance between the manoeuvrability of helicopters and the comparative endurance of aeroplanes. A bi-wing quadrotor tail-sitter UAV has been developed at the American Institute of Aeronautics and Astronautics (AIAA) Ames research center (Figure 17). Their QTUAV was able to successfully achieve VTOL and low-speed forward flight [73] though they have had issues with sustained forward flight. Success with sustained forward flight has yet to be published for this quadrotor tail-sitter.

Figure 17: AIAA Ames four-rotor tail-sitter [73] (left); Brigham-Young university tail-sitter [74] (right)

An aircraft in forward flight can be made stable through the use of a tail, which will provide a moment to stabilise the QTUAV in level flight. However, the stabilising moment may conflict with the propulsion control of the propellers. Tailless aircraft require a directionally stable craft configuration. Directional stability is often provided by high wing aspect ratios (25-35 deg) which allow trailing edge control surfaces to be effective as pitch axis controls [75]. A wing and tail design that is not mechanically designed for stability will need to be forced to be stable by a sufficiently fast control system.

A tail-sitter aircraft using a single propeller and four control vanes was under development by the Naval Postgraduate School in Monterey, California. The craft was originally developed as a hovering vehicle, but would be capable of forward flight by the attachment of a wing.

Several single-rotor and double rotor tail-sitter aircraft and tail-sitter control systems have been developed by researchers at Brigham Young University, MIT, and the University of Sydney. Knoebel at Brigham Young University has developed a control system for a tail-sitter using a quaternion representation of the aircraft. The control

architecture includes a back-stepping controller with a recursive least squares observation of the aircraft dynamics [74].

A control system developed for the control of a single rotor, mono-wing aeroplane capable of prop-hanging was tested at the MIT real-time indoor autonomous vehicle test environment. They separated the control of the aircraft into hover, transition to level flight, transition to hover, level flight, landing, and takeoff. Additionally, they have used a quaternion helicopter model, and an Euler aeroplane model to represent the aeroplane dynamics. Orientation control was achieved through vision sensing of several infrared LEDs.

K. C. Wong et al developed a PD controller for roll, pitch and yaw control of a twin-rotor mono-wing tail-sitter with variable pitch propellers called the Bidule-CSyRx [5] (Figure 1). He also did another project with Stone for the T-wing tail sitter (Figure 18). The orientation of the craft was determined using three different coordinate systems including a non-standard Euler axis for hovering flight, a zyx Euler axis for horizontal flight and quaternion for transitions. The aircraft went through four flight modes including, vertical, transition to horizontal, horizontal, and transition to vertical. Mode selection was automatic in the case of transition [76]. The control through transitions was automated.

This image has been removed by the Author of this thesis due to copyright reasons

Figure 18: Tail-sitter unmanned aircraft; T-wing [15] (left); T-wing flight stages [15] (right)

Several issues in flight control of tail-sitters due to flight and transition include attitude representation, design for stability and measurement of state. Each is presented below.

Measurements of the aircraft motion, orientation and environment are used to provide an estimate of the orientation of the aircraft. Position information can be provided by GPS, vision sensing, or integration of velocity and acceleration measurement. Orientation and acceleration information is commonly provided by the fusion of

information from gyroscopes, and accelerometers. This fusion can be achieved through the use of an optimal estimator.

There are several coordinate systems often used to model the orientation where the most common include Euler angle, Euler axis rotation, direction cosines, and Euler-Rodrigues quaternion [77]. The zyx Euler coordinate system is inadequate for the representation of aircraft due to the singularity present for excessive pitch angles (a pitch angle larger than $\pi/2$). As a result, several researchers have opted to use quaternion representation for tail-sitter aircraft. With the correct modifications, the DCM (which is derived from the Euler coordinate system) is adequate for the attitude representation; although, the quaternion representation has been shown to be a more computationally efficient method of attitude representation and control [77]. Quaternions provide a universal representation of orientation provided that the rate of change of rotation between measurements does not exceed 180 degrees.

The control inputs provided to the quadrotor must provide stable command of the quadrotor helicopter. Stability can be ensured using Lyapunov's stability criteria which, provided that Lyapunov's function is satisfied, guarantees asymptotic stability of a craft. This method is used for a range of unstable systems to ensure bounded control inputs and system stability.

The configuration of tail-sitters ranges from aeroplanes, whose control method has been changed to allow for a 'prop-hang', to flying wings and aircraft that have been designed with the VTOL condition in mind. Variations exist in the number of propellers, number of wings, number and location of control surfaces, craft rigidity, method of control, overall size and weight, method of state measurement, and method of control input. Considerations in the design of the craft originate with the craft design objectives.

Wing elasticity increases the information required to fully define the state of the aircraft and thus introduces the requirement for more sensing ability, refinement of the observer, or a perceived increase in variation of the thrust vector. A more elastic wing also reduces the resonant frequency of the wing structure and provides greater potential for catastrophic vibration.

Three major methods of orientation and position measurement use a combination of GPS and either a micro inertial guidance system, infrared radiation sensing, or vision sensing [78]. These measurements are translated into information about the state of the

aircraft through state estimation using the Kalman Filter or directly controlled using strategies including NN, PID and fuzzy logic [79]. Data from an IMU can be transformed into attitude data by manipulating the kinematic equations, using the relationships between measured data and 'desired to be measured states', putting this data through a Kalman filter to determine average representations of state (ARS). A low-cost nonlinear observer has been designed to measure attitude and heading [80].

Within the reviewed literature, there has been no observation of a successfully forward flying and hovering four propeller craft (QTUAV). Although there are potential improvements on the NASA Ames configuration including wing design for stable forward flight, and conceptually easy user interaction with the controlled system.

1.2.3 Control Translation

The conversion of user inputs into propeller velocities depends on the desired craft state (command), and the required input to achieve that state (control). Direct control of a system entails the user commanding a motion using an input with which he is familiar. Control translation in this sense is the determination of control directives in order to realise the user's desired motion.
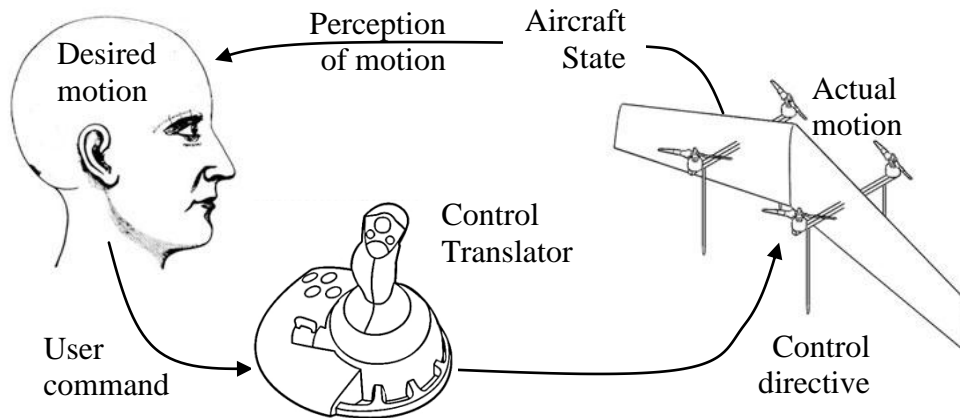
Figure 19: Identifying the difference between desired motion, commands, control, and actual motion

In the following work, we seek to develop a system that will allow a user to pilot a QTUAV as if it is an aeroplane. The advantage of this control method is the user will not require knowledge of the control requirements for a quadrotor, and they will be able to use prior aeroplane piloting knowledge to provide commands. The user will perceive the motion of the QTUAV to match that of the motion of an aeroplane. Figure 20 shows the users interpretation of the system for the control of an aeroplane.
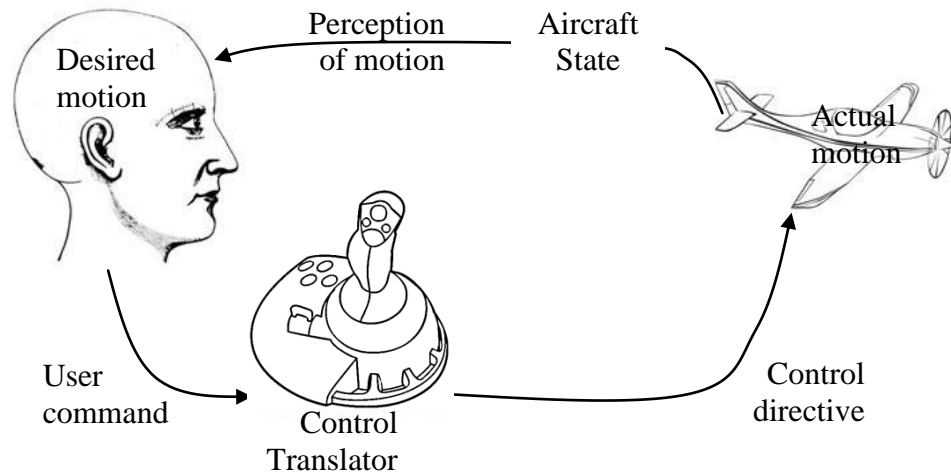
Figure 20: Users interpretation of system

An adjustment to the output of the control translator in Figure 19 is required to provide a conceptual model identical to Figure 20. Figure 21 shows the addition of a translator to Figure 19. The translator will convert control directives from the joystick into control directives for the aircraft using aircraft state measurements. The purpose of the translation box is to convert control 'directives' (commands) for an airplane into control directives for a QTUAV. The ideal result is that the system within the dotted box represents the motion of the air-plane in Figure 20.
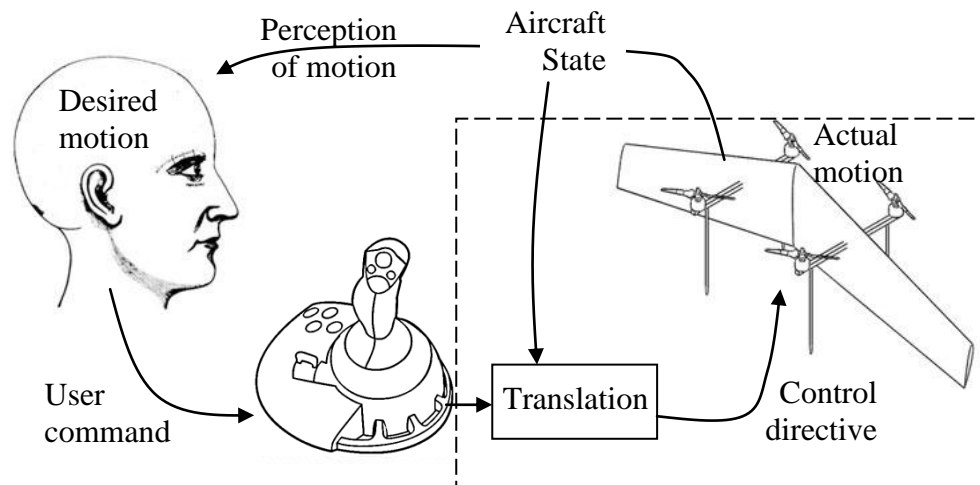
Figure 21: Purpose of the control translator (system within dotted box to resemble aircraft in Fig. 20)

The commands issued by the user are dependent on the user's concept of the system which changes as the user interacts with the system based on the feedback returned to them.

To determine the control directive, an inverted representation of the user's concept of the system is replicated in the control translator to determine the user's desired state. Provided that the controller is able to maintain the states at a rate that is an order of magnitude faster than the human user, a controller would seek to achieve the user's desired state.

The challenges with this control method are threefold. Firstly, the user's concept of the system can be estimated, but a perfect model is not available which means we cannot exactly determine the user's desired state. Good models are available, but their accuracy depends on the degree of model specialisation. The second is the system may not be able to achieve the state due to functional constraints, such as stalling angles or rates of turn, which determine boundaries of the flight envelope. This influences the third challenge, that the controlled system must follow the path desired by the user lest his conceptual model be changed. The control method would be required to provide control limitations, whilst providing a minimum of effect to the user's conceptual model of the system.

The parameters that have the greatest effect on perception of motion in simulators are the control interface (control systems, methods, and surfaces) and the control feedback (simulator motion, instrument readings, audio and visual feedback). Maintaining these parameters will ensure the conceptual model of the system does not change.

A summary of control translation methods are presented below to provide a background in various methods of control.

Literature in control translation includes the development of a knowledge based system to cope with system upgrades in an industrial process [81]. Literature regarding the tail-sitter aircraft control used a hierarchical control architecture (§1.2.2), where different phases of flight were defined, and control mapping and inputs were defined for each flight phase. Highly complex systems are commonly handled by means of a hierarchical decomposition of the activities to be performed by the autonomous vehicles, and the implementation of a hierarchy of control and decision layers [82]. The use of inverted nonlinear dynamic models is unsuitable as an accurate dynamic model is too slow for control.

Standards for the translation of data in computing are designed to allow similar software to use the same data file. Translation of inputs to outputs could follow from

developments in data translation. A particular data translation standard has been under development since 1999 by ISO (ISO 10303) to enable the exchange of product data between various computer design software. Historically, each software package had to provide translation capability for each file format that it supported. This meant that for a software package, a translation method was developed to be functional with other software packages.

Development of the standard enabled all software dealing with product data, a common (neutral) file format in which to communicate. The alternative to utilising a neutral format is the direct translation from one format to the other. Direct translation poses potential problems once a large number of systems exist on either side of the translator.

The two methods are illustrated in Figure 22.
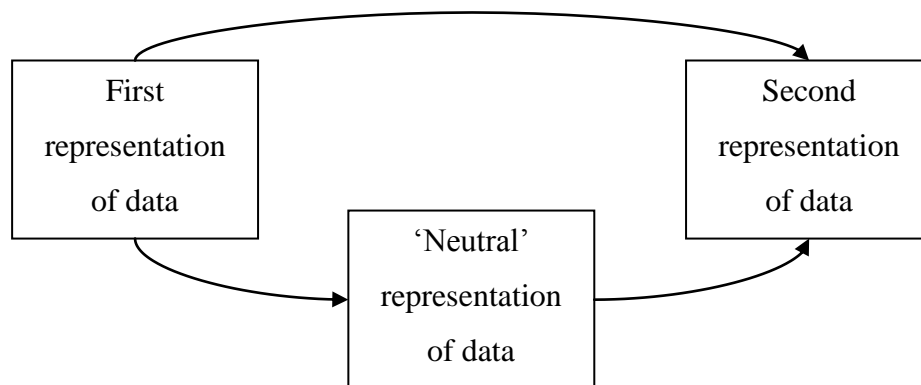
Figure 22: Comparing direct translation (upper path) to translation through a neutral representation of data (lower path)

Neutral representation of data is advantageous once the number of systems becomes large as the number of dynamic models required for conversion smaller. The advantage of using a direct translation of data as compared to neutral representation is that the processing speed between translation methods is reduced.

The eventual control translator will be capable of translating between various control inputs and systems. The current prototype translator is being developed for one control input type (aircraft) and several output types (changing aircraft model).

To convert user inputs into control commands, a translator requires information about;

Method 1:

1. How the user inputs relate to their desired command (adaptive control).
2. Information to determine the control command that would reach the desired state (optimal control/PID).

Method 2:

1. How user inputs relate to control inputs for the new system (optimal control).
2. Control method for new system (optimal control).

Where both methods attempt to determine the user's desired state. The relationship between user commands and their desired state is dependent on the user, more specifically the user's interpretation of the system they are familiar with manipulating (§1.1.5). To produce an effective control translator, the first stage of the translation would act as an inverse model of the user's system concept, and would subsequently produce either the user's desired state or translation of control inputs as its outputs. The actual state is driven by the user's conceptual model of the craft.

The second stage of translation would act as a normal feedback system and seek to control the craft so that it is at the user's desired state. The control of the system state would need to be an order of magnitude faster than the user's dynamics to ensure that the user's concept of the system does not change. If the user's concept of the system does change, the first state of the translation would need to cope with this change.

1.3 Contribution of Thesis

The eventual quadrotor tail-sitter unmanned aerial vehicle (QTUAV) will be a purely propulsion-controlled UAV capable of transitional flight. The thesis is to *design and test a control translator for a quadrotor tail-sitter unmanned aerial vehicle to enable a pilot experienced in the control of a normal aircraft to control a quadrotor tail-sitter unmanned aerial vehicle from hovering flight to forward flight using normal aircraft inputs.*

The objectives of the thesis are:

- Development of a dynamic model for a quadrotor tail-sitter unmanned aerial vehicle.
- Development of MATLAB software to enable communication between the computer and controller.
- Design and build a quadrotor unmanned aerial vehicle.
- Testing to determine discharging rates and thrust coefficients.

Contributions made in parallel work:

- A design for a wing for the current configuration of craft was presented by Joseph Robinson [83].

1.4 Structure of Thesis

Development of the dynamic model for the control system for a quadrotor aircraft first required a prototype. Chapter 2 presents the development of a prototype quadrotor aircraft. Chapter 3 presents testing used to determine propeller thrust relationships and speed controller capabilities. Chapter 4 presents the development of a dynamic model to determine the relationship among QTUAV states. It includes the development of a unique quadrotor dynamic model which is modified to suit a QTUAV. The final section presents an expression to be optimised to allow zero angular momentum. Chapter 5 presents the development of the program architecture and programs required to enable joystick inputs to be converted into a PPM waveform for a radio controller. Chapter 6 is a critical assessment of the work presented herein. Chapter 7 presents the conclusions of the current work and future work required in the development of the QTUAV.

Chapter 2 Prototype Construction

A prototype was constructed to test the control translator. The following outlines the requirements and limitations accounted for in the design, and the selection of the craft components. A prototype was created at a design weight of 1kg and flight time of 15 minutes. Motors, batteries, propellers, and speed controllers were chosen based on these requirements.

2.1 Goal

It is desired to select the components, and configuration for a manoeuvrable, electrically powered, brushless motor driven, QTUAV.

2.2 Requirements and Limitations

The following tables summarise the performance objectives, and the limitations due to propeller flight. Safety, manoeuvrability and forward speed are optimised in the following design iteration.

The objectives are listed in order of importance for the development of the quadrotor prototype in Table 1. Propeller diameter is to be minimised to ensure safety to the user and to minimise the load applied to the motor. The ratio of static thrust to weight should be maximised to ensure that the craft is manoeuvrable. The aerofoil should be optimised for cruise at the design forward pitch speed. The location of the selected components will influence the center of gravity which will influence the stability of the craft. The remaining objectives investigate range maximisation through improvements in flight time and efficiency. The optimisation of range is left for subsequent design iterations.

The limitations for the quadrotor prototype are presented in Table 2. The range limitations are due to the radio equipment. During testing of the control method the line of sight range is sufficient. A minimum payload of 300gm is desired to allow for GPS equipment. The rotational speed is limited to Mach 0.7, this is due to compressibility effects during rotation. Additionally, the rotational speed is limited by centrifugal forces that may damage the propeller. APC provide propeller limitations to ensure that yield is

not experienced. The budget is considered to be adequate for purchased components. A design weight of 1kg is selected as this approach is suggested by aircraft design texts.

Table 1: Objectives for quadrotor prototype

Particular	Objective
Propeller Diameter	Minimise
Static Thrust : Weight	Maximise
Pitch Speed (Forward Speed)	Maximise
Aerofoil	Optimise
Range (Flight distance)	Maximise
Flight Time	Maximise
Altitude	Maximise

Table 2: Limitations for quadrotor prototype

Particular	Limitation
Size (Overall)	700x700mm (fit through door)
Size (Prop)	Prevent harm to user
Rotational speed (Prop)	Mach 0.7
Rotational speed (Prop)	Mechanical limit
Weight	1kg (artificial limitation)
Range (Radio)	Line of sight (10km)
Payload	>300gm
Cost	$5000

An optimised aerofoil is required to allow slow flight, high angle of attack, and stable forward flight at a speed maximised within these constraints. A wing designed to meet the pitch speed, lift and stability requirements was developed and successfully tested by Robinson [84]. Design criteria for an ideal aerofoil for this type of aircraft include:

- Sufficient lift to carry weight of craft at pitch speed of (40km/hr)
- Minimum weight
- Known model for force due to air-flow at all angles of attack
- Moderately low lift at high angles of attack
- Drag that does not exceed that which provides cruising velocity of (40km/hr)
- Accommodate wiring and support structure of motor
- Able to accomplish high lift high drag for short landings (if we are to land as airplane)
- Accommodate space for attachment/housing of landing gear

An optimal combination of components will have the smallest propeller diameter, the largest thrust to weight ratio, and a large maximum pitch speed, where the thrust to weight ratio is dependent on the mass of each component and the structure supporting it. Selection of components requires the selection of an initial design mass (MAUW). A mass of 1kg will be selected and the author will seek to maximise thrust given this mass.

Individual components also have requirements as well. A review of components and information to aide in their selection is discussed in the next section.

2.3 Components

The following is a brief review of the components selected. A brushless electronically commutated DC motor was chosen based on the decision matrix provided by Tremblay [17]. Reduction of propeller velocity through a gearbox was not implemented as to avoid frictional losses and conserve energy.

2.3.1 Voltage Supply

Energy is supplied to the aircraft through the battery (Figure 23). The voltage and the capacity characteristics are to be chosen for the battery. The mass of the battery has a considerable effect on the overall mass. Additionally an increase in capacity will increase the maximum current draw. Lithium polymer (LiPo) batteries currently have the best storage to mass ratio.

Figure 23: Hyperion LiteStorm™ CX 2100mAh lithium polymer battery

The maximum rate of current draw from the battery is related and expressed relative to the capacity (C) of the battery considered. Electric current limitations are illustrated in Appendix F.

The capacity per mass is constant for a given cell combination (ie Li/Po, NiCd, NMH) as this is a measureable characteristic of electric cells called electro cell potential. Variations of Li/Po batteries were plotted to analyse the storage and weight relationship to ensure the relationship was the case for as supplied batteries and aid in the battery selection process and the results shown in Figure 24 (data retrieved from Hyperion battery data sheet).

A line of best fit yields battery capacity,

$$C = 0.0423 \times m_{battery} - 0.6843 \qquad\qquad 1$$

where $m_{battery}$ is the mass of the battery. Figure 24 also shows the capacity associated voltage available. The line of best fit provides information to trade off between storage capacity and mass.
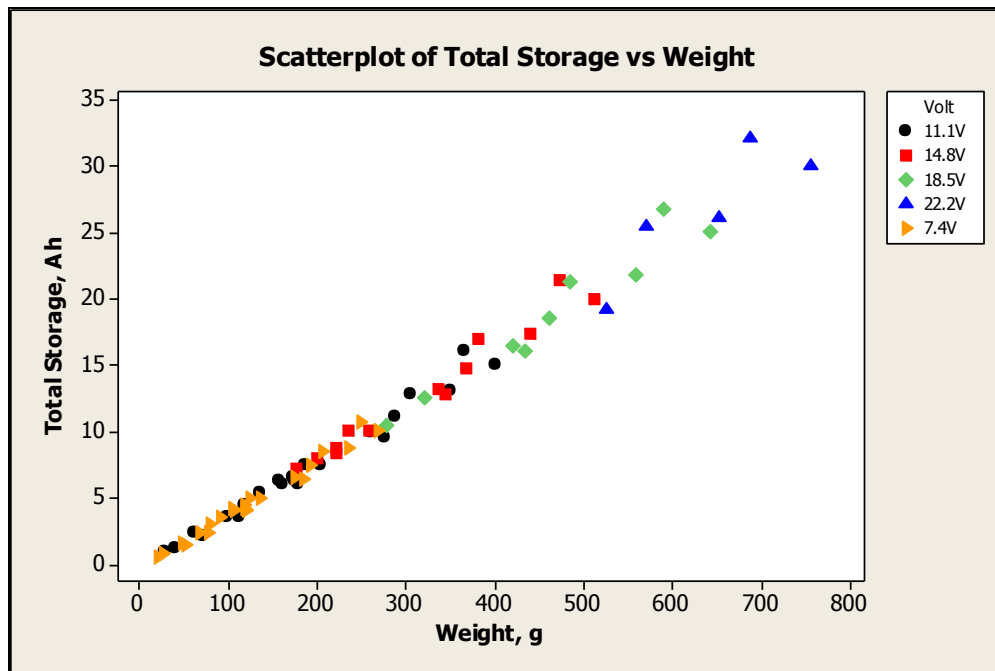
Figure 24: Battery storage vs weight for Hyperion LiPo batteries

There are three 'series' of Hyperion batteries cx, vx and vz. Comparison of these three series of batteries shows the cx series is marginally better than the others followed by vx, then vz. The difference in storage density can be regarded as negligible.
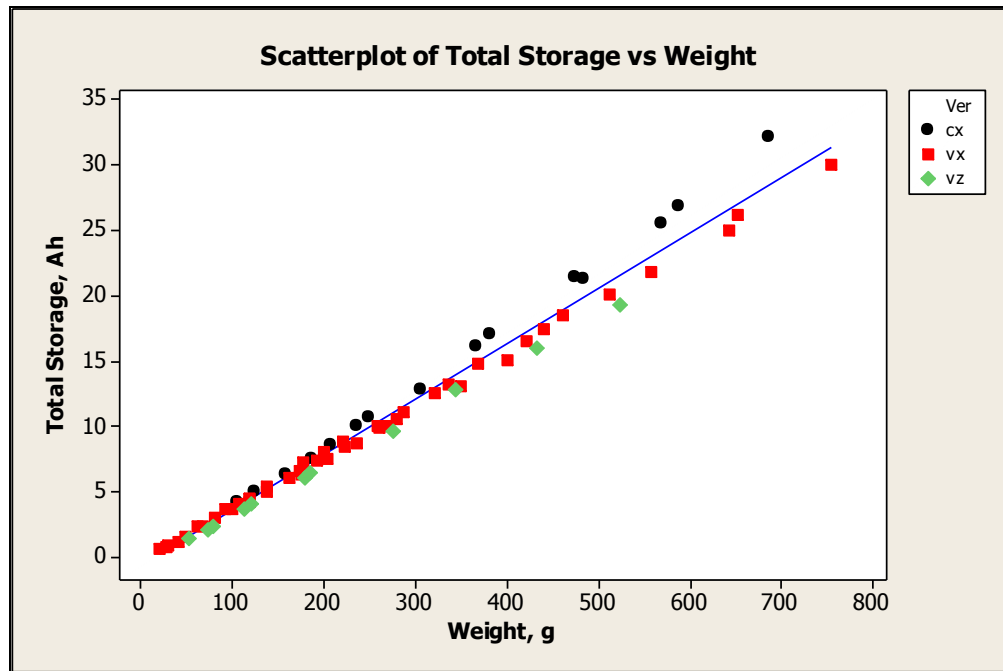
Figure 25: Total storage vs weight, CX/VX/VZ battery variants

2.3.2 Electronic Commutation

Electronic speed controllers (ESC) convert *control inputs* into the switching required for a network of field effect transistors. A Hyperion electronic speed controller is shown below in Figure 26.

Figure 26: Align 10A electronic speed controller

ESCs are sized according to the maximum applied current. The input to an ESC is a pulse-width-modulated (PWM) signal between 1ms and 2ms, where a 1ms pulse is off, 2ms is constantly on, 1.5ms is 50% and linear variation between. The weight of an ESC is small compared with other components so the suggested ESC for the motor chosen should be used.

2.3.3 Brushless Motor

The motor rotates at the speed that the ESC provides, provided that adequate power is provided to the motor, and the motor is able to dissipate the heat. The motor requires more energy to rotate the load for a larger motor load.

The motor is rated according to the number of cells it can support (voltage) and the current that it can support continuously (continuous current rating). There are several other current ratings but we are concerned with the continuous current rating due to the expected continuous high speed operation of the motor.

Figure 27: Hyperion Z2205-38 motor

There is experimental information on some engines and the current draw of attached propellers at set voltages. The 'propeller motor voltage' combination is not recommended if the current draw exceeds the rating. Information about the combination of components was obtained from the AlleRC website (Appendix G).

The motor contributes more mass than the ESC and, in quadrotor configuration, is located at the extremities of the craft. The brushless motor is required to be of a sufficient voltage, current rating and max speed to allow the rotation of a suitable propeller. The next section investigates the characteristics of a suitable propeller.

2.3.4 Propeller

A propeller is shown Figure 28. The propeller thrust and propeller drag are each dependent on the properties of the air surrounding the propeller and the motion of the propeller relative to the air. The relationship between the propulsive force of propellers and various parameters,

$$M_{prop} = \frac{1}{2} C_M \rho A_{prop} \left(\omega R_{prop}\right)^2 R_{prop} \qquad\qquad 2$$

$$T_{prop} = \frac{1}{2} C_T \rho A (\omega)^2 \qquad\qquad 3$$

where C_M and C_T are functions that depend on the angle of attack (AOA_{prop}) and Mach number; ρ is the density of air, which is a function of humidity, temperature and altitude; A is a reference area which is often selected to be the area of the propeller and its selection is dependent on the area used to determine C_T and C_M; and ω is the rotational speed of the propeller. The AOA_{prop} mentioned here is different to the craft AOA, and can vary across the propeller due to incident airflow. It is the velocity of air relative to the propeller and is the vector sum of the free stream air velocity, velocity of the body origin, rotation of the propeller center about that origin, and rotation of the propeller about its body center. A discussion of the effect of airflow on propeller lift is shown in Appendix E.

Figure 28: APC-E 7x5 propeller (left); attachment hub assembly (right)

The relationships in equation 2 and 3 are often reduced to the form of equation 4 and 5 to determine 'static thrust' and 'static torque' respectively. These tests determine the propulsive force and torque for constant conditions and are used to estimate the propulsive force of the propeller for controllers.

$$M_{static} = d(\omega)^2 \qquad\qquad 4$$

$$T_{static} = b(\omega)^2 \qquad\qquad 5$$

Where 'd' and 'b' are proportionality constants.

The maximum forward speed at which the propeller generates thrust is determined by the propeller geometry. The pitch speed is the distance the propeller moves in one revolution times the RPM the motor is spinning and a constant to correct the units. The propeller provides thrust to the craft which has an inverse relationship to the pitch speed. The reduction in thrust is due to a reduction in the propeller angle of attack (AOA_{prop}). A larger pitch speed results in a larger maximum forward flight speed. Larger static thrust means more maneuverability and payload. (see equation 3)

APC propellers are popular in hobbyist forums and stores. Although, several researchers have created their own propellers [85] and several have based their designs on the Draganflyer. APC have propellers designed for slow flight, rotational speeds or minimum load which have a maximum rotational speed dependent on the manufacturing specifications and dimensions. Equations are provided by APC which identify the maximum rotational velocity and are shown below for reference. There are commercially available pusher varieties (APC-EP) that are mirror images of APC-E propellers. This is significant as the quadrotor helicopter requires mirror imaged propellers for the counter-rotating propeller and is the basis of the brand selection.

The APC-E propellers are their lightest and have a larger maximum rpm [APC website].

Glow engine & Thin Electric (E)

$$rpm_{max\_prop} = \frac{190000}{\emptyset_{prop}} \qquad\qquad 6$$

Slow flyer (SF)

$$rpm_{max\_prop} = \frac{65000}{\emptyset_{prop}} \qquad\qquad 7$$

Racing (8.75N, W and 8.8 series 40 pylon props)

$$rpm_{max\_prop} = \frac{225000}{\emptyset_{prop}} \qquad\qquad 8$$

It is unknown if the E type props will be able to support the weight of the vehicle, the SF propellers are expected to be capable of supporting weight in this direction due to a larger cross sectional area of the blade. However, the unavailability of pusher propellers (or equivalent) requires the selection of E type.

Propeller attachment is dependent on the propeller and motor used. Hyperion provides attachment hubs for APC propellers. The hub selected is shown in Figure 28.

2.3.5 Radio Controller

Communication between the model and the helicopter is to be completed wirelessly. A total of at least four control signals are required to be sent to the QTUAV. The radio controller and receiver combination is required to have a minimum of four controller signals, and line of sight range.

Figure 29: Receiver (left) and radio controller (right)

2.3.6 Supporting Structure

The supporting structure is required to perform several functions including:

- Provide attachment points for;
  - Motor/ESC/battery/receiver/sensing equipment (GPS/IMU)/wing.
  - Four motors in a symmetrical, in-plane configuration.
- Optimise parasite drag for stability control requirements.
- Minimise parasite (skin) drag for forward velocity.
- Attachment or provision of at least one lifting surface for forward flight.
- Positioning of components to enable a stable craft in forward flight, and large rotational inertia in helicopter flight.
- Provide landing surfaces.
- Maximise thrust.

The mass of the supporting structure at the selection stage is unknown, but is constrained to be within the designed mass of 1kg.

The material used for the supporting structure should be light and strong. Materials which possess this trait are some varieties of wood, carbon fibre reinforced plastic (CFRP) and glass fibre reinforced plastic (GFRP). A commonly selected material in RC manufacture is balsa wood as it is cheaper although other developers have used carbon fibre. During the developmental stage, balsa wood will be used to allow rapid changes to the craft configuration during testing.

Several considered configurations are presented below in Figure 30. The first configuration (Figure 30-a) can reduce wingtip vortices. However a disadvantage is likely instability of the air due to the propeller torque. A significant reduction of stability is expected during forward flight due to the large lever arm of forces on the wing tip due to air vortices.

(a)   (b)   (c)
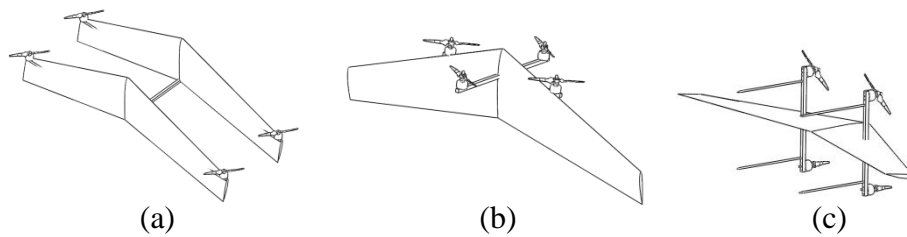
Figure 30: Concepts for aircraft configuration

The second configuration (Figure 30-b) is expected to modify flow over the wing lifting surface significantly. The effect can be modelled by introducing the effect of the propeller on the airflow over the wing surface directly behind the propeller. The majority of quadrotor helicopters currently use the X-frame. The benefit of this configuration for helicopters is the symmetry of angular inertia about the quadrotor roll and pitch axis.

An X-shaped TQUAV wing will be difficult to control and model as they are not commonly utilised for air craft, therefore the standard wing shape shown in Figure 30-b will simplify initial development. However, the addition of the wing eliminates the symmetry of the craft, and therefore eliminates the control simplification. The TQUAV quadrotor components can be located about the craft to achieve inertial symmetry.

The third configuration (Figure 30-c) uses the H configuration implemented for previous design concepts for the QTUAV. The configuration avoids lift variation

caused by changes in the propeller air-velocity. No presented mathematical model developed for this orientation exists.

2.4 Component Selection

A selection procedure suggested during the design of aircraft is presented in Raymer, 2006. The following presents a selection of the components for the quadrotor helicopter. For different combinations of motor, prop, battery, and ESC, it seeks to determine which combination gives the smallest propeller diameter whilst maximising *thrust/weight* ratio and giving adequate *flight time*. Selection of propulsion components is focused around the selection of a propeller that can accomplish these tasks. Genetic algorithms [72] have been used to optimise the selection of components but is not implemented due to unavailability of the code.

The propeller selected is required to provide sufficient static thrust to lift the aircraft. Software[‡] which included a database of propeller coefficients and motor data was used to find a propeller that provided thrust in excess of 250gm (2.45N). Sufficient propulsion magnitudes were obtained with the APC-E 6x4, and APC-E 7x5 propellers. Fixed (non flapping/non lagging) propellers were chosen for simplicity of attachment.

A motor was selected to maximise the motor RPM, and thereby maximise propeller thrust. Capability of the motor to rotate the propeller load was measured through the software. Whilst ensuring sufficient provision of torque, motors with less windings were desired as this would maximise the motor RPM through increases in the kV value (rpm/V). The motors available which maximised the motor RPM for each diameter size were the Z1705, Z2205-38 and Z3007-28 where diameters are 17mm, 22mm, and 30mm respectively. The Z1705 was not capable of rotating either the 6x4 or 7x5 propellers. The Z 2205-38 motor was simulated as being sufficient to rotate both APC-E propellers. The calculator provides information that presents that the selected motor will be within its voltage and current specifications during operation.

The current draw required for the Z2205-38 motor to rotate the propeller at an optimum speed was determined. This is related to the capacity of the battery, Hyperion specify the maximum continuous rate of current draw is 12C-15C (ie where C is capacity), as specified by Hyperion. A maximum current draw of 6.9A for a single motor was predicted by the calculator. Over four motors, this draw rate becomes approximately

---

[‡] Available at www.drivecalc.com

28A. The minimum capacity of battery required that will allow the discharge of the battery within desired operating current is,

$$I_{allowable} = 12 \cdot C \Rightarrow C = \frac{I_{max}}{12h^{-1}} = 2333mAh \qquad\qquad 9$$

$$I_{allowable} = 15 \cdot C \Rightarrow C = \frac{I_{max}}{15h^{-1}} = 1867mAh \qquad\qquad 10$$

where $I_{allowable}$ is measured in amperes. The end code selected is CX as these batteries have a slightly larger energy density. A lighter battery is chosen for flight conditions to reduce the payload. Therefore, a battery sufficient to allow constant current operation, at 13.3C, is a 2100mAh battery. The battery selected is the 'Hyperion LCX 2100 mAh 3S 18C lithium polymer battery pack'. This battery provides a maximum continuous current of 37.8A as shown in Appendix G.3, which is sufficient for the Z2205-38 motor.

A radio controller was store purchased along with a receiver; this was expected to simplify the development of the communication between the computer interface and the physical model. The receiver includes a binding procedure, which programs the receiver output in the event of loss of connection. This was selected to be controls low (and is possible with the purchase of additional attachments). The radio controller communicates with the receiver using digitised PWM (pulse width modulation) carried on a 2.4GHz signal. The receiver also communicates with the speed controller using PWM.

The ideal configuration of the helicopter will accomplish all of the requirements outlined in §2.3.6. The H configurations are selected to provide a structure that will enable testing of the dynamic response expected by Pinder et al. A pusher configuration is desired as otherwise a reduction in thrust would be caused by the resistance to air flow due to the rear surface. The resistance may be minimised by designing nacelles to reduce turbulent flow over the rear surface. The effect of the flow induced (or imposed) by the propeller is to increase the lift of the section of wing, which can be beneficial but can vary significantly. Propellers should not be attached to the tips of the wings as this section of the craft has a significant effect on stability due to its moment arm from the mass center. A representation of the configuration chosen is shown in Figure 7. Initial testing of the QTUAV dynamic model will be completed using a quadrotor construction. A quadrotor helicopter prototype was constructed and is depicted (with the 4270mAh battery) in Figure 31. Individual selected components are shown in Figure 23

to Figure 28. Electrical wiring was attached to the frame with cable ties where required. The quadrotor frame was constructed from three 10x10mm balsa wood sections and the four motor assemblies were fastened to the frame using 13mm screws.
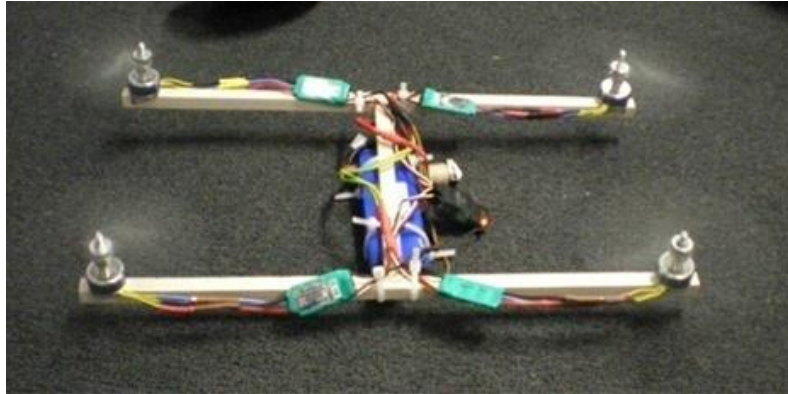
Figure 31: Quadrotor helicopter

2.5 Summary

A prototype quadrotor helicopter was desired to test the control strategy. Requirements and specifications for the quadrotor tail-sitter unmanned aircraft were presented and prioritised. Components for a 1kg quadrotor helicopter prototype with minimal propeller diameter, optimised thrust and flight time were selected. The components selected were;

- Hyperion Z2205-38 brushless motor
- Align 10A electronic speed controller
- 3.5mm Hyperion hub
- 7x5 APC-E propeller
- 2100mAh lithium polymer battery
- Balsa wood

Chapter 3 Testing

The following are experiments undertaken to determine propeller constants, and determine control issues. The following experiments were necessary to ensure the equipment selected was capable of providing adequate control of propulsive forces. Three tests were performed. Firstly, relationships were determined between thrust and rpm to obtain control constants, and with control setting to ensure equipment performance. Secondly, the rpm was measured as the battery discharged to ensure the speed controller was capable of maintaining speed requirements despite the depletion of the voltage source. The final test was conducted to ensure the current draw of the system was below specifications.

3.1 Thrust, RPM, and Control Setting Relationships

The following is an investigation into the effect of changes in electronic speed controllers (ESC), motors, propellers and hub components. RPM measurements are obtained for combinations of components. Historic tests show that thrust is consistently related to rpm, rpm drops as the test progresses, and slight variation between components. These relationships will be provided to the controller should propeller rpm be measured. It is also to test the hypothesis that the ESC provides linear control of the rotational speed with negligible nonlinearities or errors.

3.1.1 Equipment

2 x APC-E 7x5 Propeller, 2 x Hyperion Z2205-38 brushless motor, 2 x Align 10A ESC, 2 x attachment hub, 1 x 4270mAh LiPo battery, 1 x 10A switch, 1 x attachment frame, 1 x digital balance (max 1000gm), 1 x DX7 2.4 GHz radio controller, 1 x AR70000 2.4 GHz receiver, 1 x digital tachometer (Standard, ST-6234B), 2 x sections of reflective tape, 1 x 4S 3A balancing charger, 1 x 12V power supply, stopwatch

3.1.2 Experimental Setup

Figure 33 shows a representation of the simultaneous measurement of thrust and rotational speed at given time intervals (note: during measurement, the experimenters hand was a minimum of 1.0 meters away from the spinning propeller).
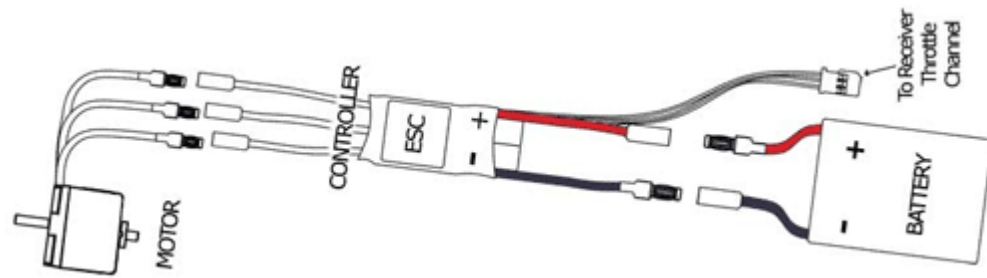
Figure 32: Connection of electronic components

Figure 33: Representation of thrust vs RPM and time measurement

3.1.3 Method

The following assumes that the ESC is bound to the correct settings of hard brake/low timing/low discharge. The ESC should be programmed via the procedure included (Appendix H).

1) Fully charge 4270mAh battery at a rate of 1.5A (up to 2hrs required).
2) Number each ESC, motor, hub, and propeller arbitrarily as 1 and 2.
3) Attach reflector tape to top surface of propeller 1 and 2.
4) Ensure controller is off.
5) Order of connection is[§];
   a. Motor to test rig top (2 x screws).
   b. ESC to motor.
   c. ESC to throttle channel of the receiver.
   d. ESC to battery (one lead).

[§] guide for wiring connection at http://www.allerc.com/motorwiring.htm

      e. ESC to switch (one lead).

      f. Ensure switch is off.

      g. Switch to battery.

      h. Test rig top to test rig case (4 x screws).

6) Place the assembled test rig on top of the mass balance.

7) Turn on the mass balance. The value on the digital display should read 0.00 gm.

8) Switch on the controller, wait 5 seconds.

9) Configure controller;

      a. Ensure that the thrust control setting is at zero.

      b. Open menu to observe control setting value.

10) Switch on the transmitter.

11) Wait for confirmation tones.

12) Ensure propeller is rotating in the correct direction, if not disassemble test rig and switch two of the ESC-Motor connections.

13) Begin test;

      a. Beginning at control setting zero, start stopwatch.

      b. At 30 seconds, increase the control setting by four, to 4.

      c. At 60 seconds, increase the control setting by four, to 8 (propeller will rotate).

      d. Continue, at 30 second intervals, to increase the control settings to 12, 16, 20… 96, 100.

      e. Repeat until battery discharges.

14) Repeat for trial 2, 3, 4, and 5 (Table 3).

Table 3: Components and associated trial number

Trial No	ESC	Motor	Hub	Propeller
1	ESC 1	Motor 1	Hub 1	Prop 1
2	ESC 2	Motor 1	Hub 1	Prop 1
3	ESC 2	Motor 2	Hub 1	Prop 1
4	ESC 2	Motor 2	Hub 2	Prop 1
5	ESC 2	Motor 2	Hub 2	Prop 2

3.1.4 Results and Discussion

The results are presented below where; RPM 1, RPM 2, and RPM 3 represent the trial repeat 1, 2, and 3 respectively.

Where, in reference to Table 3: M.ESC.P.Hub 1 represents the components used in trial 1; ESC 2 – M.Hub.P 1 represent the components used in trial 2; M.ESC 2 – P.Hub 1 represent the components used in trial 3; M.ESC.Hub 2 – P 1 represent the components used in trial 4; and M.ESC.Hub.P 2 represent the components used in trial 5.

During the trial, an amendment was made to the method where a thrust and rpm measurement was made at a control setting of 7. Thrust and rpm values measured at this control setting were consistently 0g and 0rpm respectively.

Figure 34 below shows that the relationship between static thrust and RPM is consistent for variations in motor, ESC, propeller and hub. Some outliers exist for trial 4 and are either due to variations because of the propeller or measurement error. Values attained for trial 4.1 were consistently in-line with the trend which suggest the outliers are due to initial measurement inaccuracies.
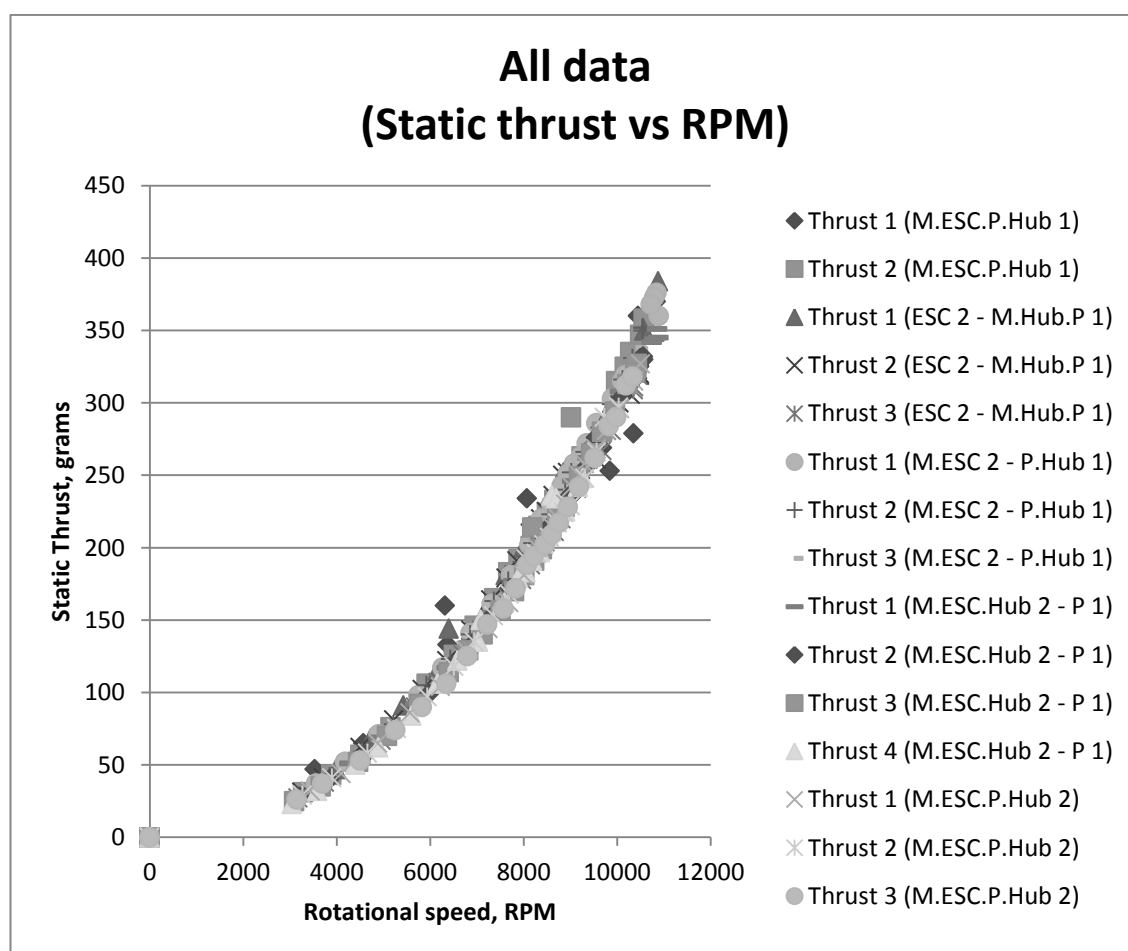
Figure 34: All data; thrust vs RPM for an APC-E 7x5 propeller

There is a proportional relationship between static thrust and the square of rotational speed, under the assumptions of constant air density, propeller shape, moisture content and static free air. Formulaically,

$$T = b\omega^2 \qquad\qquad 11$$

A similar relationship between propeller drag torque and the square of rotational speed also exists (with a different proportionality constant) which was not tested. Thrust was measured for combinations of hub, motor, ESC and propellers. The power law is used for least squares fitting to fit the thrust relationship above and yields a proportionality constant ('b') of 2.9402 x 10^{-6} N/rpm^2 for gravity = 9.81ms^{-2}.

The maximum rotational velocity measured was 10892rpm. It is confirmed below that the rotational speeds achieved in thrust testing are well below Mach0.7, which approximately is the speed at which compressibility effects are significant [86].

$$v_{proptip} = \omega_{prop} r_{prop} \qquad\qquad 12$$

$$v_{proptip} = \left(10892rpm \cdot \frac{2\pi}{60}\right) \cdot (3.5" \cdot 0.0254) = 101.4ms^{-1} \qquad 13$$

$$Mach = \frac{v_{proptip}}{v_{soundair}} = \frac{101.4}{331.5} = 0.31 \qquad\qquad 14$$

Additionally, the specifications for the propulsion speed were not exceeded.

$$rpm_{max\_prop} = \frac{190000}{7"} = 27142rpm \qquad\qquad 15$$

$$10892rpm < 27142rpm \qquad\qquad 16$$

The data collected to present the relationship between thrust and rpm was used to plot relationships between controller setting and RPM, as well as, controller setting and thrust. The combined results are shown below in Figure 35 and Figure 36. There was variation in the measurement of rotational speed against values of controller setting. Figure 34 has established the relationship between thrust and rpm for our setup.
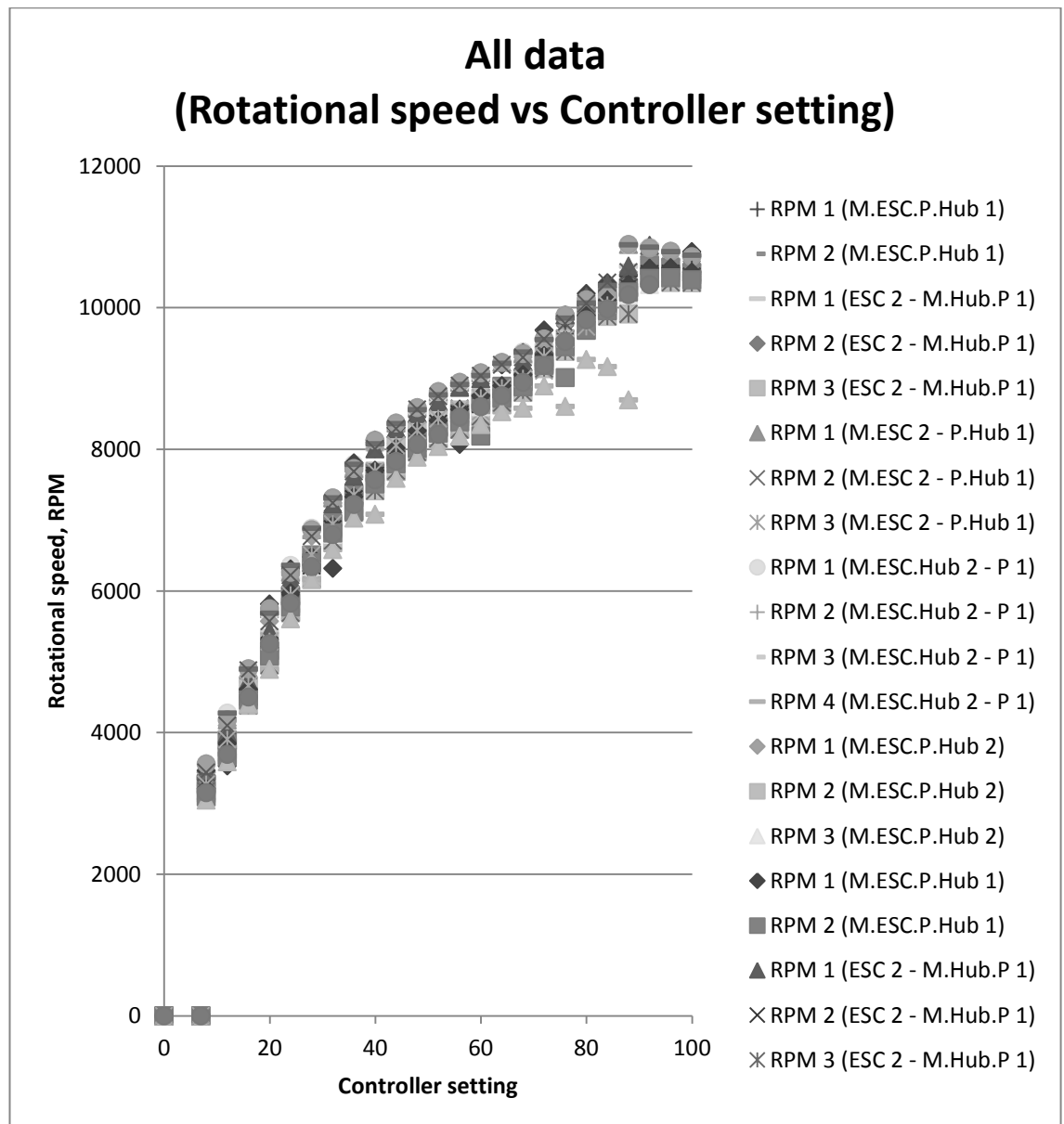
Figure 35: All data; controller setting versus rotational speed

All data
(Static Thrust vs Controller setting)

Legend:
- Thrust 1 (M.ESC.P.Hub 1)
- Thrust 2 (M.ESC.P.Hub 1)
- Thrust 1 (ESC 2 - M.Hub.P 1)
- Thrust 2 (ESC 2 - M.Hub.P 1)
- Thrust 3 (ESC 2 - M.Hub.P 1)
- Thrust 1 (M.ESC 2 - P.Hub 1)
- Thrust 2 (M.ESC 2 - P.Hub 1)
- Thrust 3 (M.ESC 2 - P.Hub 1)
- Thrust 1 (M.ESC.Hub 2 - P 1)
- Thrust 2 (M.ESC.Hub 2 - P 1)
- Thrust 3 (M.ESC.Hub 2 - P 1)
- Thrust 4 (M.ESC.Hub 2 - P 1)
- Thrust 1 (M.ESC.P.Hub 2)
- Thrust 2 (M.ESC.P.Hub 2)
- Thrust 3 (M.ESC.P.Hub 2)
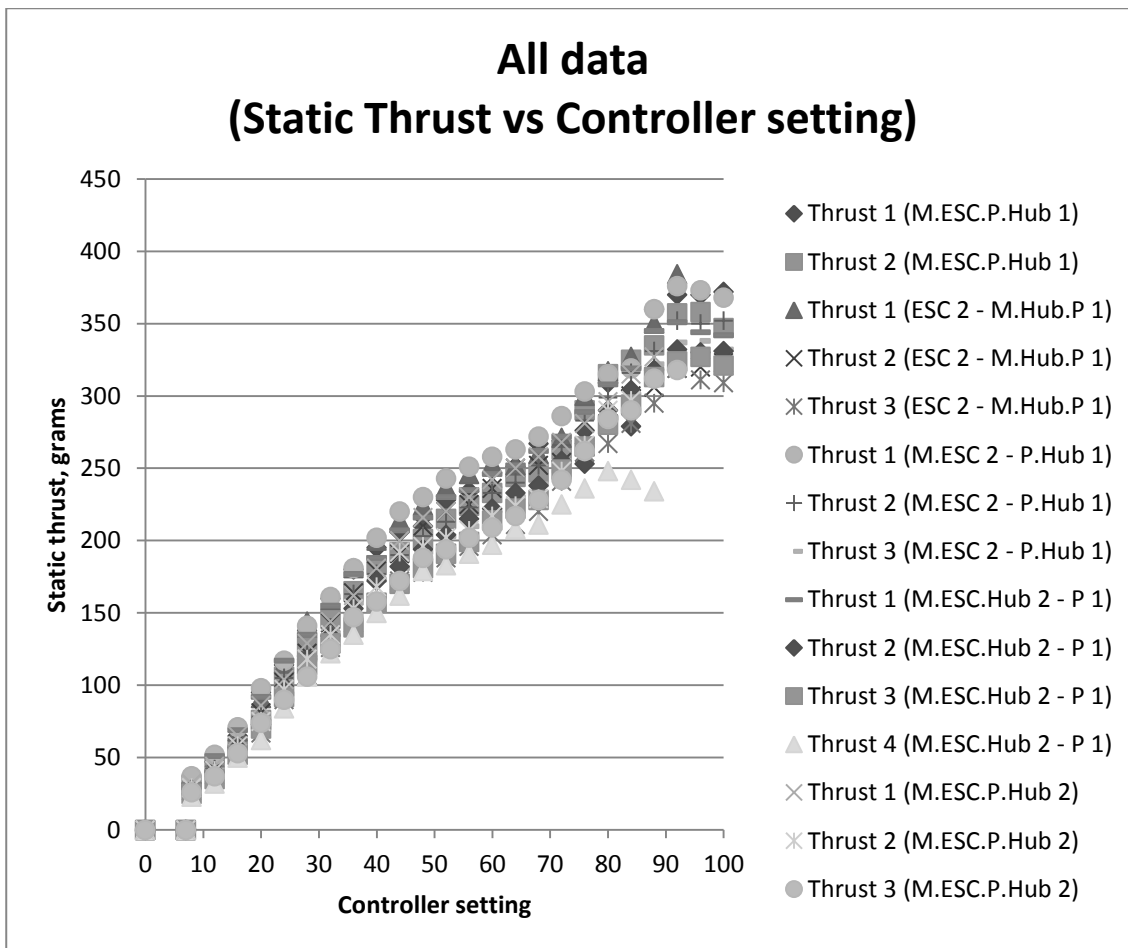
Figure 36: All data; controller setting versus static thrust

The variation of the RPM and thrust vs controller setting is illustrated using statistical control limits which are determined by averaging the values attained for each control setting, and determining the standard deviation for each control setting. The two sigma and one sigma control limits for thrust vs controller setting and rpm vs controller setting are presented in Figure 37.

A large variation (greater than 5% full scale) of rotational speed, and more significantly, thrust, is present at each measured control setting. Additionally a large variation at a controller setting of 90 is observed. This is likely attributed to the drop off in thrust during trial 4.4. Furthermore, there is a non-linear relationship between control setting and rotational speed.

However, Figure 37 shows an almost linear region exists between 8000 RPM (controller setting 40) and 9000 RPM (at controller setting 60). The mass of the quadrotor prototype has been measured as 450gm, and with a desired payload of 300gm, 750 grams of lift is desired. Figure 36 indicates that a controller setting of 40 gives 150

grams of thrust per motor, 600 total, and controller setting 60 gives over 800 grams total thrust. The propulsive components selected for the current prototype are adequate for the range of QTUAV propulsive forces required during hovering flight.
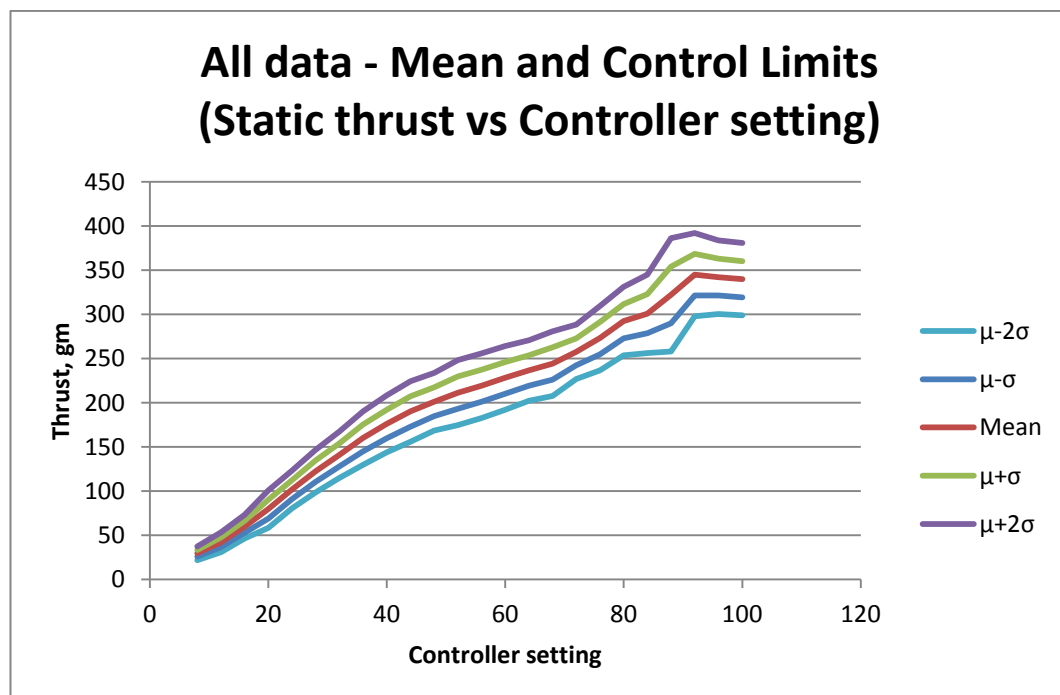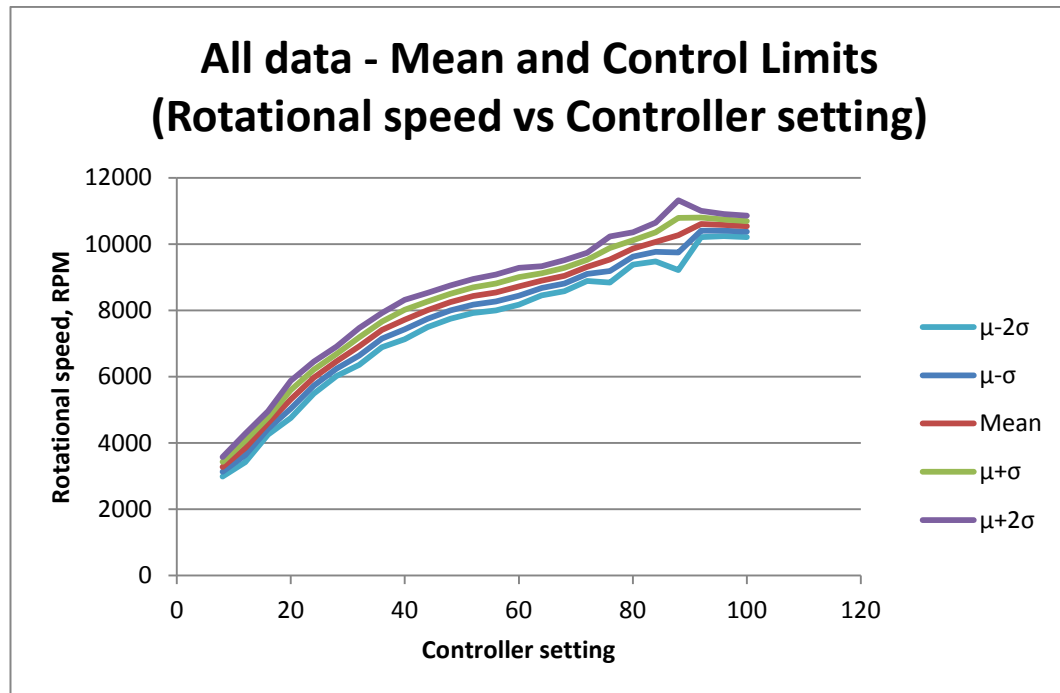
Figure 37: Mean and control limits for rotational speed vs controller setting (top); mean and control limits for thrust vs controller setting (bottom)

Comparison is also made between changes of propellers. For consistency and clarity, only the first data set is used in the analysis. There is negligible difference in the

rotational speed as plotted against controller setting for all cases except for changes in ESC; Figure 38 (top). The difference may be attributed to the trial being the first for the set of experiments, otherwise there is an inconsistency between ESCs.
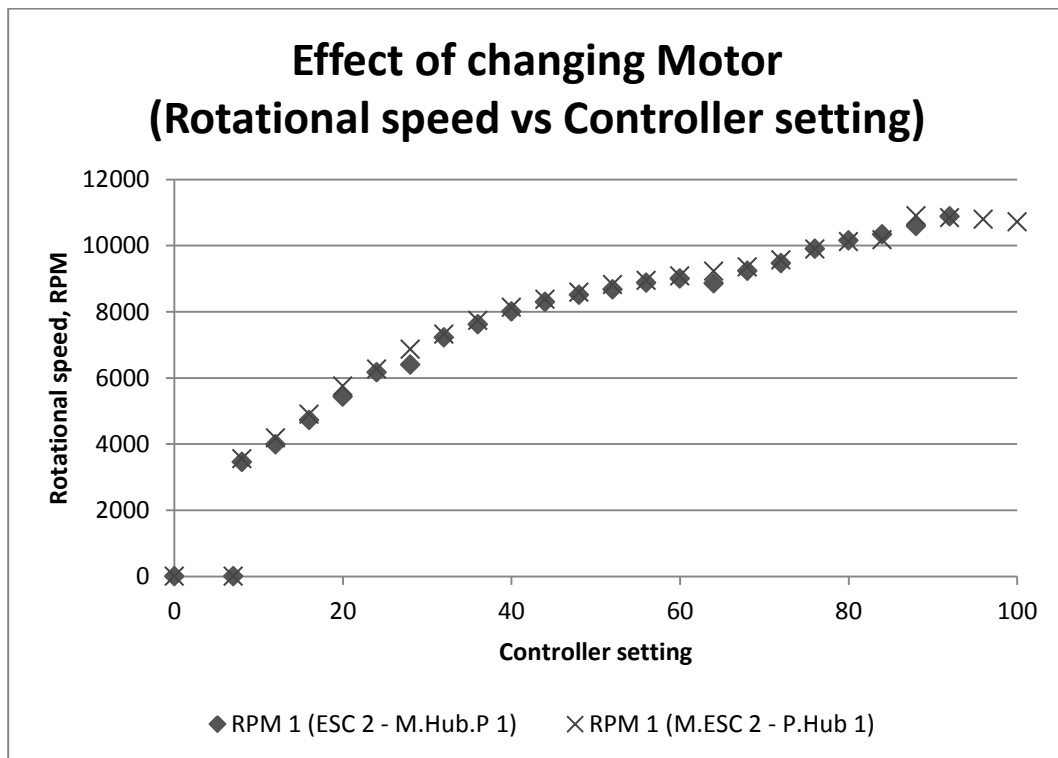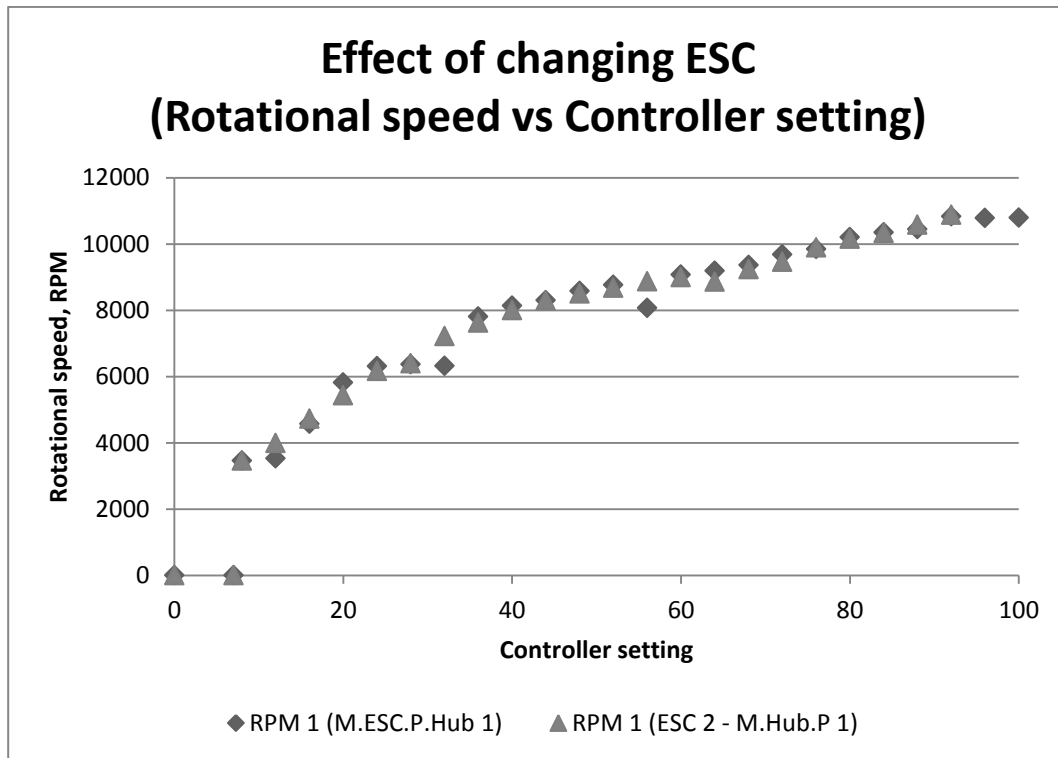
Figure 38: Effect of changing ESC on rotational speed (top); effect of changing motor on rotational speed (bottom)

Effect of changing Hub
(Rotational speed vs Controller setting)

Rotational speed, RPM

Controller setting

◆ RPM 1 (M.ESC 2 - P.Hub 1)   ✕ RPM 1 (M.ESC.Hub 2 - P 1)

Effect of changing Prop
(Rotational speed vs Controller setting)

Rotational speed, RPM

Controller setting

◆ RPM 1 (M.ESC.Hub 2 - P 1)   ✶ RPM 1 (M.ESC.P.Hub 2)
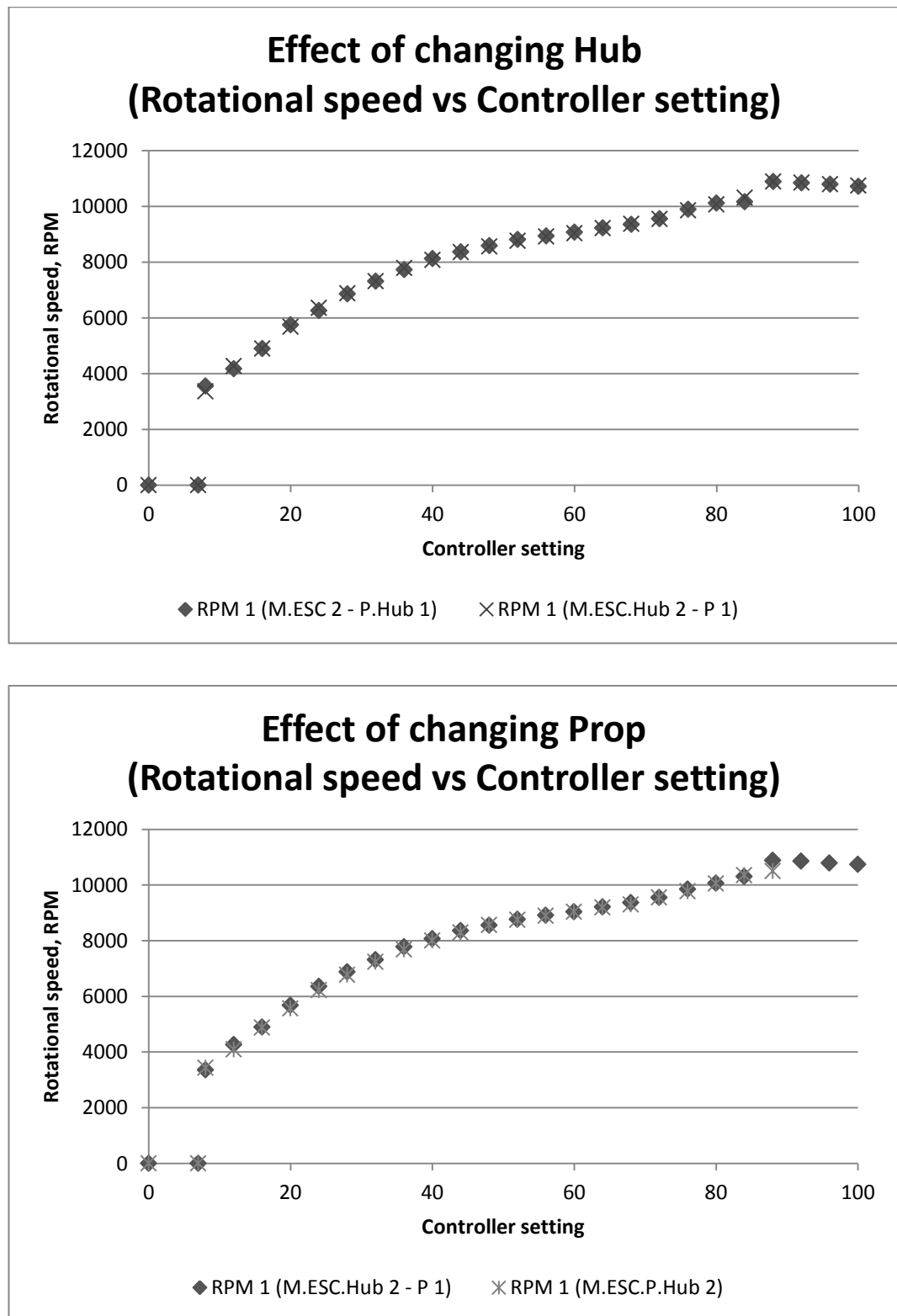
Figure 39: Effect of changing hub (top); effect of changing propeller (bottom)

3.1.5 Conclusions and Recommendations

Conclusions

- Propeller speed for static conditions reaches a Mach number of 0.31.
- A reduction of static thrust is seen for sequential measurements of static thrust at given control settings.
- The controller does not maintain the rotational speed independent of battery power supply.
- Static thrust is related to the square of rotational speed. The proportionality constant is equal to 2.9402×10^{-6} N/rpm^2.
- The investigation has not determined the static torque.

Recommendations

- Air may be assumed compressible for all operable control settings and a supply voltage of 12V.
- It is recommended that a constant control setting test is performed to determine the relationship between control setting and static thrust.
- It is recommended that the a controller is developed to maintain the rotational speed of the propeller, or that a new ESC is selected and tested to ensure adequate performance as the battery voltage reduces.
- That the static thrust constant is used for the dynamic model.
- That a method to measure static torque is developed and used for the dynamic model.

3.2 Battery Discharge Rate

The following investigates the reduction in propulsion speed as the battery discharges. This is to confirm that the propeller speed was reducing over time for a given setting. Confirmation of this hypothesis will mean that a thrust/propeller speed control system independent of battery supply will need to be developed.

3.2.1 Equipment

1 x APC-E 7x5 Propeller, 1 x Hyperion Z2205-38 brushless motor, 1 x Align 10A ESC, 1 x attachment hub, 1 x 2100mAh LiPo battery, 1 x 4270mAh LiPo battery 1 x 10A switch, 1 x attachment frame, 1 x DX7 2.4 GHz controller, 1 x AR70000 2.4 GHz receiver, 1 x digital tachometer (Standard, ST-6234B), 1 x section of reflective tape, 1 x 4S 3A balancing charger, 1 x 12V power supply, stopwatch.

3.2.2 Experimental Setup

Figure 40 shows a representation of the setup used to determine the rotational velocity of the propeller over time (note: during measurement, the experimenters hand was a minimum of 1.0 meters away from the spinning propeller).

Figure 40: Representation of RPM vs time test (Battery/ESC are located inside covering)

3.2.3 Method

ESC settings are set to Hard Brake/Low timing/Low discharge

1) Charge fully, the 2100mAh and 4270mAh LiPo battery.

2) Connect the circuit and test rig. Order of connection is[**];

    a. Motor to test rig top (2 x screws).

    b. ESC to motor.

    c. ESC to throttle channel of the receiver.

    d. ESC to battery (one lead).

    e. ESC to switch (one lead).

    f. Ensure switch is off.

    g. Switch to battery.

    h. Test rig top to test rig case (4 x screws).

3) Switch on the controller, wait 5 seconds.

4) Configure controller;

    i. Ensure that the thrust control setting is at zero.

    j. Open menu to observe control setting value.

5) Switch on the transmitter.

6) Wait for confirmation tones.

7) Ensure propeller is rotating in the correct direction, if not disassemble the test rig and switch two of the ESC-Motor connections.

8) Begin test 1;

    a) (test uses 2100mAh battery).

    b) Shift controller to controller setting 80.

    c) Record RPM using Tachometer.

    d) Start stopwatch as soon as reasonable.

    e) Record RPM at intervals of 30 seconds.

9) Begin test 2;

    a) (test uses 4270mAh battery).

    b) Shift controller to controller setting 50.

    c) Record RPM using Tachometer.

    d) Start stopwatch as soon as reasonable.

    e) Record RPM at intervals of 30 seconds.

[**] Guide for wiring connection is located at http://www.allerc.com/motorwiring.htm

3.2.4 Results and Discussion

Test 1 was completed with;

- Motor 2.
- APC-E 7x5 Prop 2.
- ESC 2.
- Battery 2100mAh.

Figure 41 below shows a reduction of propulsion speed over time of approximately 10% at which point the motor cuts out due to overheating of the motor. Overheating is known to be the cause as the motor was seen to pulse at the end of the test. The information attained from the test shows a greater than 10% reduction in propeller speed as the battery discharges.

The experiment has shown that the ESC does not maintain a constant rotational speed when the battery storage is reduced. Control of the propeller rotational velocity will need to be independent of the voltage supply and will require measurement of the rotor speed, propulsive torque, or measurement of the battery voltage. Measurement of the rotor speed will provide feedback control of the rotor speed, measurement of propulsive torque can be used to indicate rotor speed, and voltage regulation will provide control of the power input and will give battery discharge warnings.
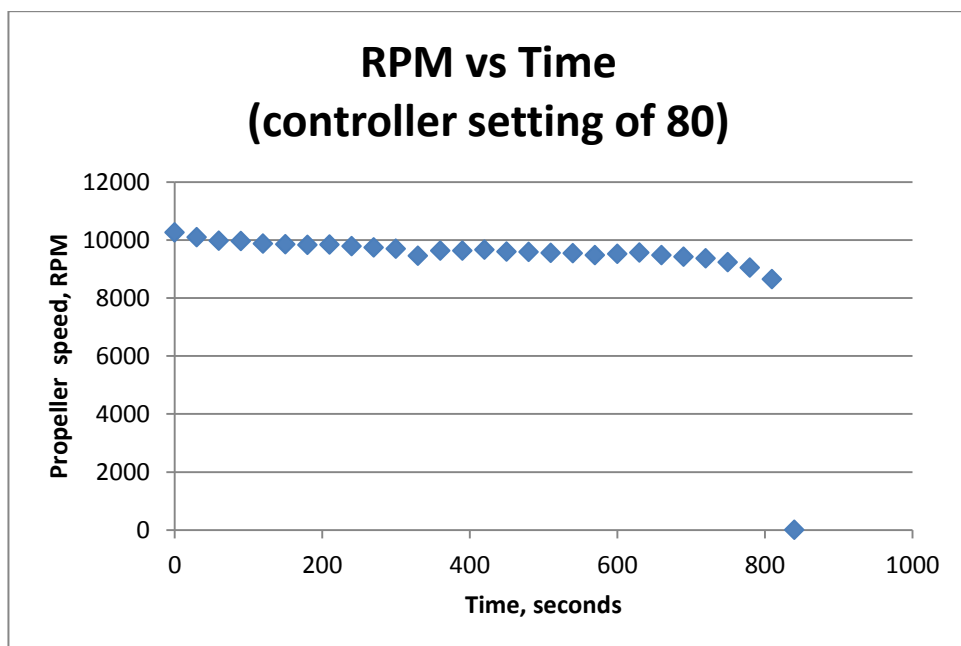
Figure 41: RPM vs time – controller setting of 80

Test 2 was completed with;

- Motor 2.
- APC-E 7x5 Prop 2.
- ESC 3.
- Battery 4270mAh.

A larger battery capacity improves the current rating of the battery, and a lower control setting reduces the power used by the motor during the test thus reducing the temperature. A second test at a lower control setting and larger capacity battery was performed at a control setting within the motor continuous operating limits. A similar drop in propeller velocity is observed for a larger capacity battery at a lower controller setting.
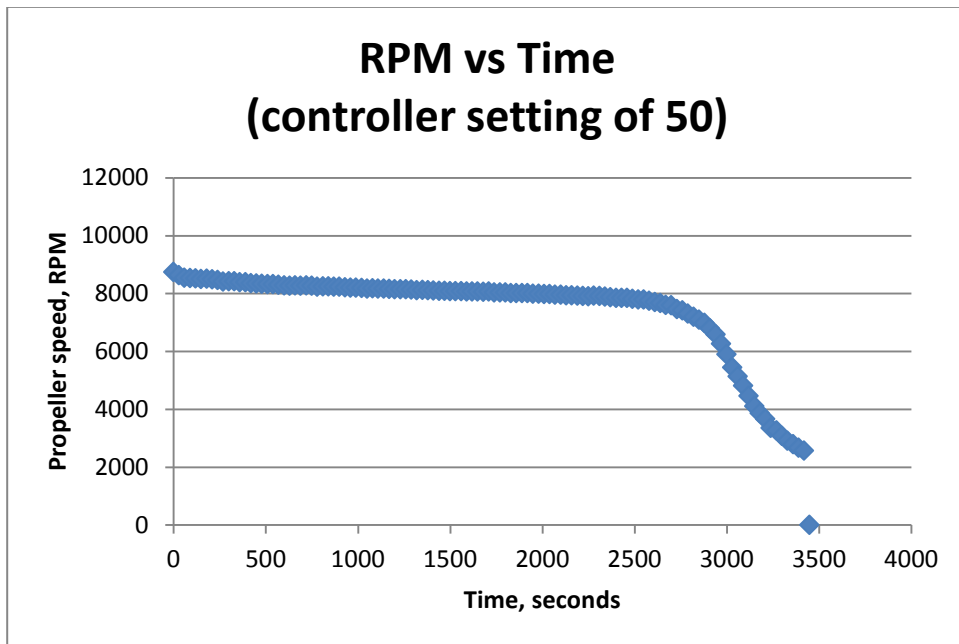
Figure 42: RPM vs time – controller setting of 50

3.2.5 Conclusions and Recommendations

Conclusions

- The propeller speed reduces as the battery discharges.
- The information attained for test 1 may have been due to overheating of the motor due to excessive current, the current variable was not measured.

- An additional test to determine the response for a controller setting (50) known to be within the rated continuous current inputs observes a similar reduction in propeller RPM.

Recommendations

- A developed control system will need to account for a changing battery voltage.
- A speed controller is purchased/designed that is invariable to supply voltage or supply is regulated to ensure constant supply.
- A future test to ensure thermal effects are not the cause – a larger motor may be required.
- That current drawn at this controller setting is measured to be certain of the assumed within specification current.

3.3 Battery Discharge Rate – Current and Rotation Speed

The following is an investigation into the reduction of the propulsive speed during discharging of the battery. The experiment is conducted at a control setting of 70. The test is used to ensure that the current drawn by the ESC is within battery specifications, the current is measured simultaneously with propulsion RPM.

3.3.1 Equipment

1 x APC-E 7x5 propeller, 1 x Hyperion Z2205-38 brushless motor, 1 x Align 10A ESC, 1 x attachment hub, 1 x 2100mAh LiPo battery, 1 x 10A switch, 1 x attachment frame, 1 x DX7 2.4 GHz controller, 1 x AR70000 2.4 GHz receiver, 1 x digital tachometer (standard, ST-6234B), 1 x sections of reflective tape, 1 x 4S 3A balancing charger, 1 x 12V power supply, stopwatch.

3.3.2 Experimental Setup
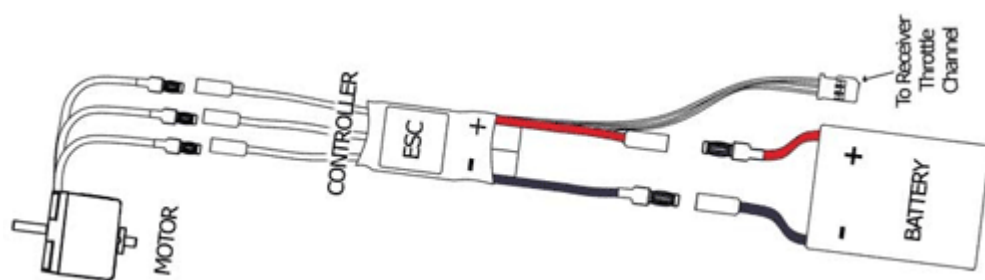
Figure 43: Experimental setup to measure current

3.3.3 Method

The experimental setup is similar to previous section except an Ammeter is inserted between switch and battery. The ESC settings are set to hard brake, low timing, and low discharge.

1) Charge fully, the 2100mAh LiPo battery.

2) Record the charge voltage reading from the LiPo balancer.

3) Connect the circuit and test rig. Order of connection is[††];

    a. motor to test rig top (2 x screws).

    b. ESC to motor.

    c. ESC to throttle channel of the receiver.

    d. ESC to battery (one lead).

    e. ESC to switch (one lead).

    f. Ensure switch is off.

    g. Switch to Ammeter.

    h. Battery to Ammeter.

    i. Test rig top to test rig case (4 x screws).

4) Switch on the controller, wait 5 seconds.

5) Configure controller;

    a. Ensure that the thrust control setting is at zero.

    b. Open menu to observe control setting value.

6) Switch on the transmitter.

7) Wait for confirmation tones.

8) Ensure propeller is rotating in the correct direction, if not disassemble test rig and switch two of the ESC-Motor connections.

9) Begin test 1;

    a) (test uses 2100mAh battery).

    b) Shift controller to controller setting 80.

    c) Record RPM using Tachometer.

    d) Start stopwatch as soon as reasonable.

    e) Record RPM at intervals of 30sec.

10) Record final voltage.

[††] Wiring connection guide provided at http://www.allerc.com/motorwiring.htm

3.3.4 Results and Discussion

Over the duration of the experiment, RPM is seen to correlate to the measured current. At a controller setting of 70, the current measured is 6.76A. This is above the rated continuous current of the motor of 4A (Appendix G), but below the maximum continuous current rating of the battery of 37.8A .
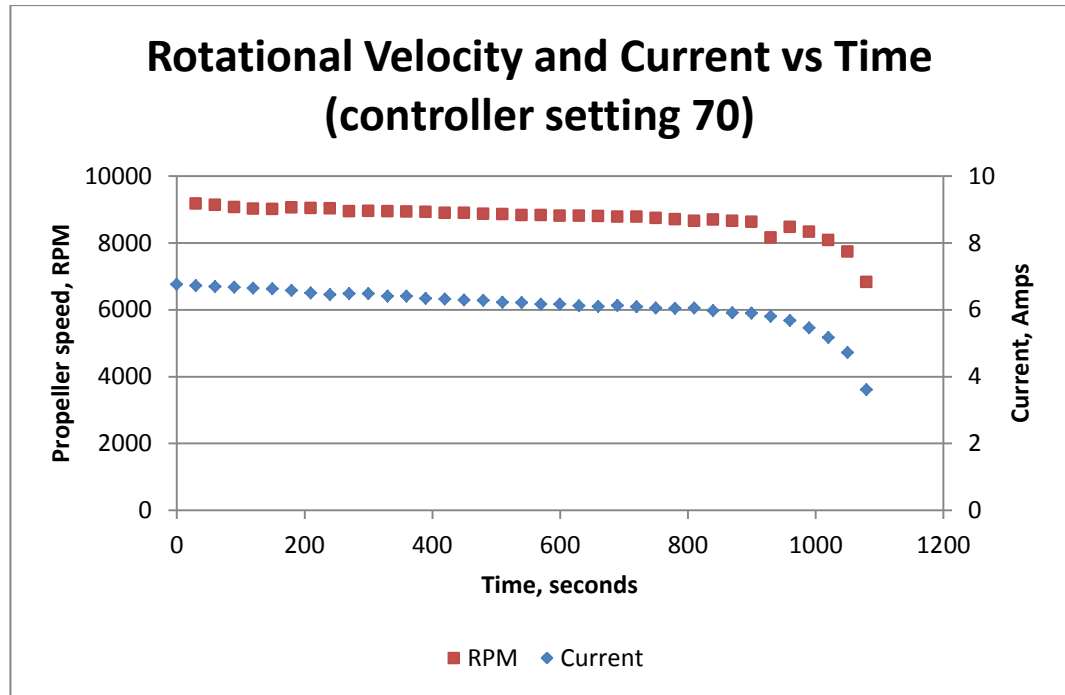
Figure 44: Rotational velocity and current vs time

3.3.5 Conclusions and Recommendations

Conclusions

- The current draw at a controller setting of 70 is below the rated current draw for the battery.
- A drop in current supplied to the ESC is observed as the trial progresses.
- The drop in current supplied to the ESC is observed simultaneously with a drop in rotational speed.
- The voltage of the supply drops during the experiment as observed by the beginning of trial and end of trial supply voltages.

Recommendations

- Battery has a sufficient capacity for current draw rates the expected control settings.

- The reduction in rotational speed is due to a reduction in the battery voltage as the battery discharges.

- The controller setting set-point must consider the reduction of the propeller speed as the battery discharges.

3.4 Measurement of Moment of Inertia

The following determines the moment of inertia experimentally by implementing the knife-edge method. The knife-edge method is used for three different orientations to determine the mass moment inertia about the x, y and z body axes. The principle assumptions made for this method are that the oscillation angle is approximately zero, friction is approximately zero, the rig is rigid, the resultant SHM motion is planar and the measurement errors are negligible.

3.4.1 Equipment

QTUAV (fully assembled), mass balance, test rig, stopwatch.

3.4.2 Experimental Setup

The orientation of suspension for each of the three tests is depicted in Figure 45 below. The axis used to calculate the mass moment of inertia about the x, y, and z axes were provided by two skewers which penetrated the supporting member.
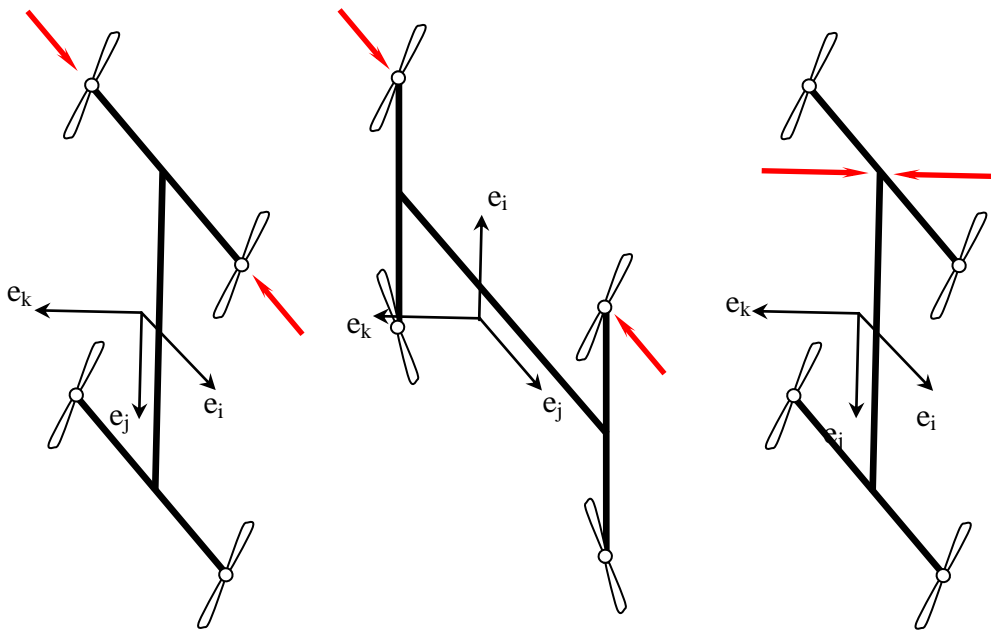
Figure 45: Configuration used to suspend the craft to calculate inertia constants; a) x-axis mass moment of inertia configuration; b) y-axis mass moment of inertia configuration; c) z-axis mass moment of inertia configuration

3.4.3 Methodology

The mass of the quadrotor helicopter was determined by weighing on laboratory mass balance. The center of mass was determined by suspending the quadrotor by two ropes, the intersection of lines that continue the line of action of the rope support provide the quadrotor center of mass.

The following relationship between oscillation period from an axis away from the center of mass was derived. Where this relationship is commonly used in the 'knife edge method'.

$$I_G = m_{total} r \left[g \left(\frac{t_{osc}^2}{4\pi^2} \right) - r \right] \qquad\qquad 17$$

The QTUAV was lifted to approximately 5 degrees from the equilibrium point, the period required to perform 20 oscillations about an axis offset from the x-axis was measured and the average period taken for a single oscillation determined. Additionally, the distance from the suspension axis to the center of mass was measured with a ruler. A representation of the set up is shown in Figure 46 where the axis was provided by two wires centrally skewered into the support frame. This test was performed three times to ensure experimental consistency.

Figure 46: Experimental configuration for x-axis mass moment of inertia measurement

The values obtained were then used to calculate the mass moment of inertia about the x-axis using equation 17 modified for the x-axis. The period for 30 oscillations was then obtained for an axis parallel to the y-axis, and z-axis where the experimental setup is shown in Figure 47 (left) and Figure 47 (right) respectively. The axis for the y-axis and z-axis measurement is provided by skewers mounted to an adjustable support.

Figure 47: Experimental configuration for inertia measurement of; a) y-axis; b) z-axis;

3.4.4 Results and Discussion

The overall mass was measured using a mass balance. The overall mass is 0.450 kg ± 0.001 kg.

Measured values of the oscillation period measured for each test are presented in Table 4. The number of oscillations was different for the x axis measurement as the amplitude of oscillations diminished beyond visual limits of measurement. The number of oscillations for the y and z-axis remained at 30 in order to ensure the minimisation of stop watch synchronisation errors.

Table 4: Moment of inertia about x-axis (n = no. of oscillations)

Axis	Trial No.	N	$t_{osc,tot}$
x-axis	1	20	16.75 s
	2	20	16.89 s
	3	20	16.86 s
y-axis	1	30	32.16 s
	2	30	32.18 s
	3	30	32.20 s
z-axis	1	30	31.99 s
	2	30	32.55 s
	3	30	32.28 s

The distance from the suspension axis to the center of mass, average oscillation time and mass of the quadrotor were then used to determine the mass moment of inertia about the x, y and z axis. The values obtained are summarised in Table 5, where the estimation of inertia uncertainty is presented in Appendix I.

Table 5: Mass moment of inertia about x, y, and z axis (m = 0.450kg)

Particular	x axis	y axis	z axis	Uncertainty (+/-)
r	119 mm	212 mm	161 mm	2 mm
$t_{osc, av}$	0.84 s	1.07 s	1.08 s	0.02 s
I_G (x 10^{-3})	3.0 kg.m^2	6.9 kg.m^2	9.3 kg.m^2	

The values of mass moment of inertia are reasonably accurate estimates. The error margin does not include errors due to the linearisation of sine. Improvements can be made to the experimental procedure by improving the measurement of time as error analysis has shown that this has contributed the most to the experimental uncertainty.

3.4.5 Conclusions and Recommendations

Conclusions

- The mass moment of inertia about the x, y, and z axes are 3.0g/m, 6.9g/m and 9.3g/m respectively.

Recommendations

- The values are utilised as initial estimates of the QTUAV mass moment of inertia.

3.5 Summary

Three experiments were presented. The first investigated the relationship between thrust, rotational speed and controller setting. This experiment determined the proportionality constant between rotational speeds and thrust, and observed that rpm was not consistent for a given controller setting, over time. The second experiment observed a reduction in rotational velocity as the battery discharged, proving that for a given controller setting the rotational speed did not remain constant. The third experiment observed a drop in current draw and battery voltage supplied to the ESC. Future developments of the control system will require a steady consistent supply of energy or a modification of the speed controller to ensure consistent propulsion speeds for a varying supply. The final experiment provides an experimental estimate of the mass moment of inertia for the current iteration of QTUAV.

Chapter 4 Dynamic Modelling

The design of any control system can take one of three paths of development: control requirements and specifications are defined; measurements of an existing model are used to determine the model; or a mathematical model is developed from known physical principles [87].

The form and functions of the QTUAV are known and a plant which we would like to control has been developed in Chapter 2. The approach implemented in the development of our control system uses a mathematical model developed from known physical principles. The required propeller speeds at given control inputs and states are to be determined using an optimising control translator. Dynamic models for the QTUAV under development and an airplane which represent these relationships are developed in the following section.

4.1 Dynamic Model for the Quadrotor

Several researchers have developed dynamic models for the quadrotor in an 'X' configuration and tail sitter aircraft. A dynamic model is developed for the 'H' configuration QTUAV. The system modelled is a frame, with four propellers that have controlled rotational speed. Two propellers spin clockwise, two propellers spin anticlockwise. The propellers provide thrust and torque to control the system. Gyroscopic forces due to the propeller introduce moments that impede rotations of the craft. Propeller rotational speed reduces as the battery discharges (§3.2 and §3.3). Static thrust and static torque are related to the square of rotational speed through proportionality constants (§3.1). An image of the current configuration of the VTOL QUAV is shown Figure 48.
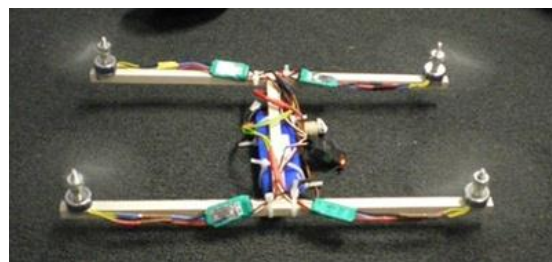
Figure 48: Quadrotor helicopter

A summary of the selection method for the construction of the craft is shown in Chapter 2. Its main structure is manufactured from balsa wood. The components selected are: Align 10A electronic speed controller (ESC); APC-E 7x5 propellers, Hyperion Z2205-38 motor, 4270mAh battery. A 2.4GHz receiver and transmitter/controller are used to communicate wirelessly with the QTUAV.

Gyroscopic forces are modelled in quadrotor control literature, although the deflection of the frame required to provide the associated gyroscopic reaction force is not modelled. The Newton-Euler model developed will account for frame deflections and hence will provide a more complete representation of the system. Quaternion attitude representation will account for singularities that would be problematic for the SP-quadrotor.

4.1.1 Previous Work

Several researchers have published dynamic models for the four-rotor system. A model developed, and applied to a mini scale quadrotor was presented by Altuğ et al in the development of a control system using vision sensing [38]. This model ignored gyroscopic effects and used the xyz Euler representation for angles.

Quaternion representation was used [88] to avoid singularities present, in the Euler representation. A singularity is also present in quaternion representations, which corresponds to a 180° rotation change. The quaternion singularity is avoided by increasing the frequency of rotation measurements. Attitude representations using quaternion coordinate values are not intuitively understood to a user accustomed to roll, pitch and yaw representations. Quaternion angles can be converted to Euler angles provided that the representation is a unit magnitude quaternion. The processing time for quaternion representation (with conversion between quaternion and Euler) is shorter than purely Euler representation [77].

Gyroscopic forces were modelled by Tayebi and McGavlray, a rigid body assumption was made which ignores the provider of gyroscopic torque. The model developed below is adapted from the Newton-Euler model presented by Bouchoucha [54].

Differences between the quadrotor literatures have been observed for the definition of body co-ordinate system orientation, attitude nomenclature and attitude representations. Tayebi et al, Hoffman et al, Bouchoucha et al, Erginer and Bouabdallah et al use a coordinate system with the z-axis toward earth, where Pounds, Altug use a coordinate

system with the z-axis toward the sky. Additionally Pounds, Altug have used differing nomenclature for helicopter attitude. In general, the convention is for a 'z-down' coordinate system to allow positive pitch values for increases in pitch. The aforementioned literatures all assume a rigid body supporting frame.

Euler xyz representation is the most common rotation matrix used for quadrotor helicopters although quaternion attitude representation is becoming more popular. A summary of the DCM is attached in Appendix B. The xyz representation provides for a direct relation between the attitude measurements and the coordinate expressions for pitch and roll. The convention for airplanes is the zyx rotation, which correspond to heading, pitch then roll.

A summary of the unit quaternion and the direction cosines matrix (DCM) for aerospace can be found in [89] and [77]. Quaternion representation has been shown to be more computationally efficient than the DCM [77]. The present work utilises the quaternion formulation of the dynamic model developed by Tayebi and McGilvray [49]. Researchers in the surveyed literature have positioned the coordinate system so that each rotor is located on a coordinate system axis as shown in Figure 49 (an exception is Altug et al). The QTUAV will use the body coordinate system shown in Figure 50 as it will allow substitution of lift and drag force expressions for the (coincident to axis) wing loading to relate to the body. Modifications (including a change in coordinate system, same as Altug, and implementation of gyroscopic forces, which make the model different to Altug) to existing published models are required due to our unique quadrotor frame and desire to allow an ease of modification to incorporate lift due to an aerofoil.
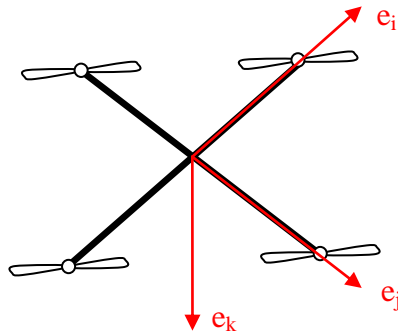
Figure 49: Body coordinate system used by other quadrotor researchers

The body coordinate system will be defined at the center of mass of the quadrotor. The craft is assumed to have a symmetric mass moment of inertia about its body centered coordinate system to allow simplification in the expression for applied moments.
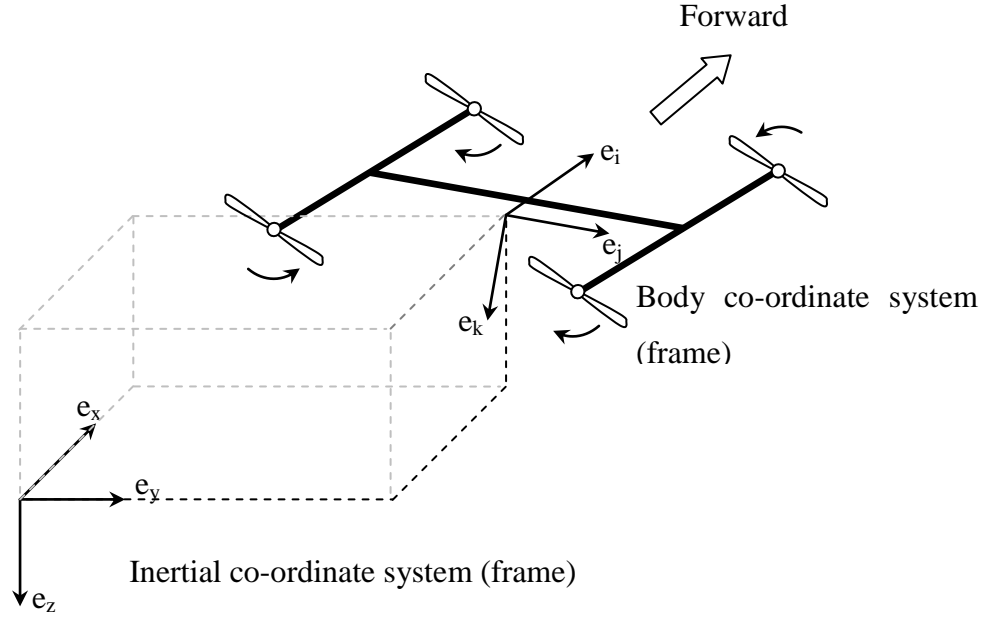
Figure 50: Coordinate system showing inertial (x,y,z) and body (i,j,k) coordinates

4.1.2 Preliminaries

The quadrotor is split into five systems: the four propulsion plants which each consist of the motor, propeller hub, and propeller; and the frame which rigidly holds the four propellers, control system, energy source, and payload. Each system will be analysed using the Newton-Euler formulation. However, the translational analysis investigates the entire quadrotor as a single system.

The unit quaternion is implemented to represent the coordinate frame computationally due to a reduction in the number of control calculations, but the Euler body coordinate system will be used to represent the orientation as it better represents the direction of applied forces. The Euler body and space coordinate systems used to represent the craft orientation are shown in Figure 50. The locations of the motors attached to the frame are symbolically defined with respect to the body axis in Figure 51.
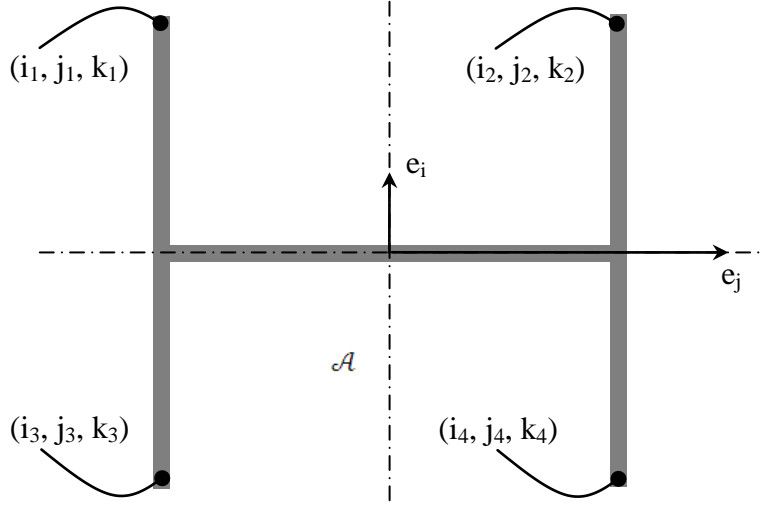
Figure 51: Coordinates of motor attachment points

It is assumed that the craft is symmetrical about the origin of the body coordinate system (which coincident with vehicle mass center), therefore the motor locations can be defined equal.

$$(-i_1 \approx i_2 \approx -i_3 \approx i_4) = i$$

$$(j_1 \approx j_2 \approx -j_3 \approx -j_4) = j$$

$$(k_1 \approx k_2 \approx k_3 \approx k_4) = k \qquad\qquad 18$$

A xyz Euler rotation matrix (direction cosines matrix, DCM) will be used to rotate body coordinates to space coordinates. Derivations for the xyz and zyx DCM can be found in Appendix B.

The model assumes the following:

- Earth is supposed flat and stationary in inertial space (no inertia effects due to earth rotation).
- The mini-aircraft is seen as a single rigid body (depends on propeller model representation).
- The center of mass and the body fixed frame origin are assumed to coincide (simplify gravity vector, significant assumption).
- The ground effect is neglected (simplify thrust).
- The structure is supposed rigid and symmetric (diagonal inertia matrix).
- Thrust is defined as the component of force axial to the propeller assembly, variation of thrust across propeller due to non constant relative velocity of air, is ignored.

A summary of constants that describe the physical quadrotor presented in Table 6, where constants that have been determined are listed. The thrust coefficient for the quadrotor is as determined as in §3.1. The mass moment of inertia for each axis is as determined in §3.4. The lever arms, i and j, are directly measured from the quadrotor.

Table 6: Constants for TQUAV

Description	Symbol	Value	Units
Body axis inertia about $\hat{e}_i$	I_{ii}	3.0	$g.m^2$
Body axis inertia about $\hat{e}_j$	I_{jj}	6.9	$g.m^2$
Body axis inertia about $\hat{e}_k$	I_{kk}	9.3	$g.m^2$
Rotor inertia about rotor axis	I_r	-	
Mass	m	0.45	kg
Thrust coefficient	b	2.9402 x 10^{-6}	gm/rpm^2
Rotational drag coefficient	d	-	
Lever arm in $\hat{e}_1$ direction	i	210	mm
Lever arm in $\hat{e}_2$ direction	j	108	mm

4.1.3 Analysis of Rotation and Translation – Propeller

Propeller n rotates at a velocity ω_n with mass moment of inertia I_R. The moving propeller interacts with the air and creates an axial thrust force, T_n, and drag moment, M_n. A free body diagram is presented below in Figure 52. A reaction moment, τ_n, and force, T_{nR} is provided at the base of the motor where the gravity force vector points down in the inertial frame and the remaining forces are described with reference to the body frame.
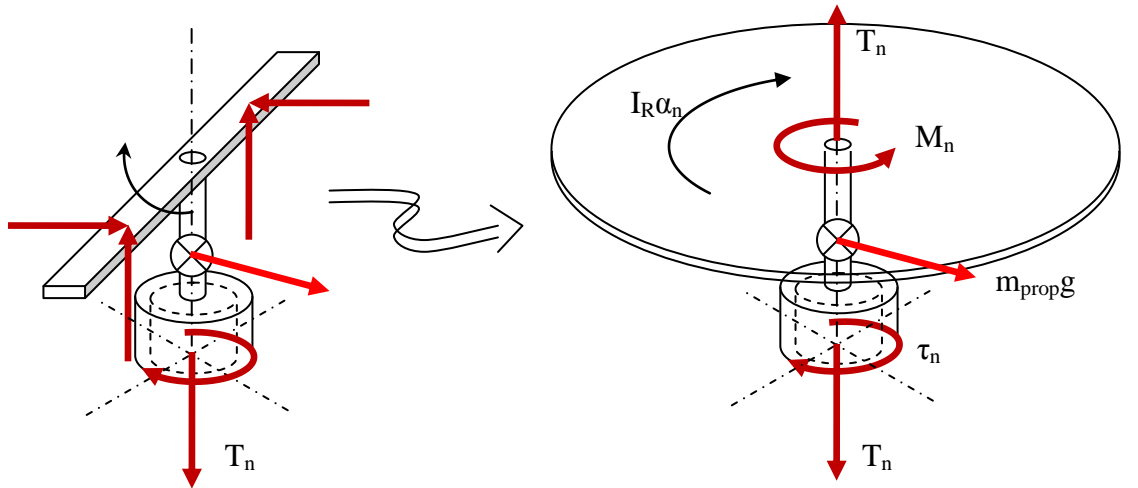
Figure 52: Free body diagram for propeller n

Eulers law for the conservation of momentum

$$\sum F = \frac{d(mv)}{dt} \qquad\qquad 19$$

$$\boldsymbol{T_n} - \boldsymbol{T_{nR}} + m_{prop}g\widehat{\boldsymbol{e_z}} = m_{prop}\dot{\boldsymbol{v}}_{\boldsymbol{prop,i}} \qquad n\epsilon\{1,2,3,4\} \qquad 20$$

Rotational force balance

$$\sum \boldsymbol{M_R} = \frac{d}{dt}(I_R\boldsymbol{\omega_n}) \qquad\qquad 21$$

$$\tau_n - M_n = I_R\dot{\boldsymbol{\omega}}_n \qquad n\epsilon\{1,2,3,4\} \qquad 22$$

An experimentally determined relationship [86] for the moment of drag force applied to the rotor is presented below. Assuming constant AOA, air density, blade area and Mach number, we obtain an expression for static moment showing M_{static} proportional to the square of rotational velocity.

$$M = C_M\rho A\big(\omega R_{prop}\big)^2 R_{prop} \qquad\qquad 23$$

$$M_{static} = d\omega^2 \qquad\qquad 24$$

Experimental bench testing is used to determine 'd' for an APC-E 7x5 propeller.

The coefficient, C_M, has been experimentally determined to have a parabolic relationship with respect to the AOA until the angle at which it stalls [86]. Propeller specifications state the maximum pitch the propeller may travel per revolution; maximum pitch for an 'APC-E 7x5' propeller is five inches. We can take a linear approximation of the parabolic relationship and modify C_M to account for changes in propeller AOA in the $\hat{e}_k$ direction by assuming zero moment at the pitch rate and a maximum moment given by M_{static}. Nice performed this assumption in his dynamic model [90].

The static thrust is linearly related to the pitch

$$M_n = M_{static}\left(1 - \frac{1}{pitch_{max}}pitch\right) \qquad\qquad 25$$

Propeller pitch is the distance travelled by the propeller in one revolution, the distance is determined from the propeller speed and air velocity seen by the propeller.

$$pitch = \frac{v_{n/air}}{t_{rev}} = \frac{v_{n/air}}{\omega_n} \qquad\qquad 26$$

The relative wind velocity is the air velocity minus quadrotor body motion relative to the airflow.

$$v_{n/air} = v_{n/origin} - v_{air/origin} \qquad\qquad 27$$

$$v_{n/air}\hat{e}_k = \begin{bmatrix} i_n & j_n & k_n \end{bmatrix} \times \begin{bmatrix} \Omega_i \\ \Omega_j \\ \Omega_k \end{bmatrix} \hat{e}_k + \begin{bmatrix} v_{air,i} \\ v_{air,j} \\ v_{air,k} \end{bmatrix} \hat{e}_k \qquad\qquad 28$$

$$v_{n/air}\hat{e}_k = \left(i_n\Omega_j - j_n\Omega_i \right) + v_{air/body,k} \qquad\qquad 29$$

The expression for drag torque in relation to the body fixed frame is then

$$M_n = M_{static}\left(1 - \frac{(i_n\Omega_j - j_n\Omega_i) + v_{air/body,k}}{\omega_n \cdot pitch_{max}} \right) \qquad\qquad 30$$

The above equation ignores effects due to lateral airflow. The effect of lateral airflow would be to provide cyclic variations of M_n, where the magnitude of the oscillations would have a proportional dependence on lateral airflow. The drag torque M_n approaches the static torque M_{static} as free air velocity and body motions tend to zero (conditions for hover).

4.1.4 Analysis of Rotation – Frame

The quadrotor system is defined as all non-fluid components of the quadrotor, less the motor assembly. The FBD for this system is shown in Figure 53.
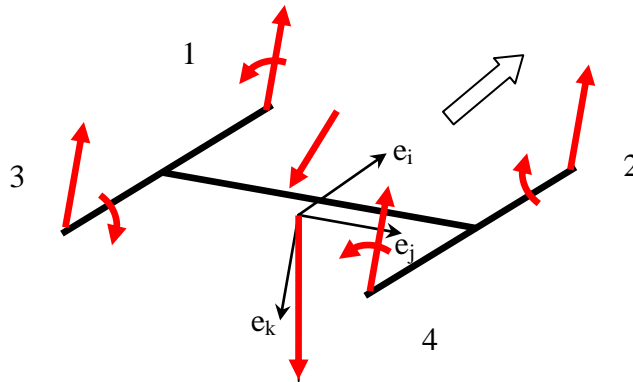
Figure 53: FBD of quadrotor

Eulers law for the conservation of angular momentum

$$\sum M = \frac{d(I\Omega)}{dt} \qquad\qquad 31$$

$$M_{rotor} + M_{gyro} + M_{drag} = I\dot{\Omega} + \Omega\frac{d(I)}{dt} \qquad\qquad 32$$

Due to the rigid body assumption, the rotating propellers move at an angular velocity, Ω. A gyroscopic torque is generated by the rotation of the momentum vector for each propeller.

$$M_{gyro,n} = I_r(\Omega \times \omega_n\hat{e}_k) \xrightarrow{yields} I_r\omega_n\left(\Omega_j\hat{e}_i - \Omega_i\hat{e}_j\right) \qquad\qquad 33$$

Moments are generated by the torque and the thrust generated by the motor, for moments that are not compensated for axial airflow. Assuming symmetry about the coordinate origin

$$i = i_1 = i_2 = i_3 = i_4$$

$$j = j_1 = j_2 = j_3 = j_4$$

$$k = k_1 = k_2 = k_3 = k_4 \qquad\qquad 34$$

The following expressions are obtained for body moments due to the rotors.

$$\begin{bmatrix} M_{rotor,i} \\ M_{rotor,j} \\ M_{rotor,k} \end{bmatrix} = \begin{bmatrix} bj & -bj & bj & -bj \\ bi & bi & -bi & -bi \\ -d & d & d & -d \end{bmatrix} \begin{bmatrix} \omega_1{}^2 \\ \omega_2{}^2 \\ \omega_3{}^2 \\ \omega_4{}^2 \end{bmatrix} \qquad\qquad 35$$

Rearranging equation 32 and substituting and expression relating $\frac{d(I)}{dt}$ to Ω (shown in Appendix D)

$$I\dot{\Omega} = -\Omega \times I\Omega + M_{rotor} + M_{gyro} \qquad\qquad 36$$

The Euler rotation matrix is mathematically related to the angular rotation. An overview of the derivation is included in Levine's summary of control principles [91]. A full derivation has been included in Appendix C where the final relationship is show below. sk( ) is a skew symmetric matrix.

$$\dot{R} = Rsk(\Omega) \qquad\qquad 37$$

4.1.5 Analysis of Translation – Frame

The translational motion of the frame is also analysed using Newton's law for the conservation of momentum in the body frame.

$$\sum \boldsymbol{F} = \frac{d(m\boldsymbol{v})}{dt} \qquad\qquad 38$$

The forces that influence quadrotor translation are thrust due to each propeller in the $\hat{e}_k$ direction and the gravity force vector in the $\hat{e}_z$ direction.

$$m_{total}[\ddot{x} \quad \ddot{y} \quad \ddot{z}]^T = F_{weight}\hat{\boldsymbol{e}}_{\boldsymbol{z}} - T_{rotor}\hat{\boldsymbol{e}}_{\boldsymbol{k}} \qquad\qquad 39$$

Then using the DCM, where **R** is the roll-pitch-yaw rotation matrix, a relationship to maintain QUAV altitude is attained.

$$m_{total}\ddot{\boldsymbol{\xi}} = F_{weight}\hat{\boldsymbol{e}}_{\boldsymbol{z}} - \boldsymbol{T_{rotor}}R\hat{\boldsymbol{e}}_{\boldsymbol{z}} \qquad\qquad 40$$

4.1.6 Summary of Newton-Euler Equations

Overall equations

$$m_{total}\ddot{\boldsymbol{\xi}} = F_{weight}\hat{\boldsymbol{e}}_z - T_{rotor}\boldsymbol{R}\hat{\boldsymbol{e}}_z$$

$$\dot{\boldsymbol{R}} = \boldsymbol{R}sk(\boldsymbol{\Omega})$$

$$\boldsymbol{I}\dot{\boldsymbol{\Omega}} = -\boldsymbol{\Omega} \times \boldsymbol{I}\boldsymbol{\Omega} + M_{rotor} + M_{gyro}$$

$$\tau_n - M_n = I_R\dot{\boldsymbol{\omega}}_n \qquad n\epsilon\{1,2,3,4\}$$

$$\boldsymbol{T_n} - \boldsymbol{T_{nR}} + m_{prop}g\hat{\boldsymbol{e}}_z = m_{prop}\boldsymbol{v_{prop,n}} \qquad n\epsilon\{1,2,3,4\}$$

Component equations

$$sk(\boldsymbol{\Omega}) = \begin{bmatrix} 0 & \Omega_z & -\Omega_y \\ -\Omega_z & 0 & \Omega_x \\ \Omega_y & -\Omega_x & 0 \end{bmatrix}$$

$$\boldsymbol{M_{rotor}} = \begin{bmatrix} M_{rotor,i} \\ M_{rotor,j} \\ M_{rotor,k} \end{bmatrix} = \begin{bmatrix} bj & -bj & bj & -bj \\ bi & bi & -bi & -bi \\ -d & d & d & -d \end{bmatrix} \begin{bmatrix} \omega_1{}^2 \\ \omega_2{}^2 \\ \omega_3{}^2 \\ \omega_4{}^2 \end{bmatrix}$$

$$M_{gyro,n} = I_r\omega_n(\Omega_2\hat{\boldsymbol{e}}_i - \Omega_1\hat{\boldsymbol{e}}_j)$$

$$M_n = M_{static}\left(1 - \frac{(i_n\Omega_j - j_n\Omega_i) + v_{air/body,k}}{\omega_n \cdot pitch_{max}}\right)$$

$$T_n = T_{static}\left(1 - \frac{(i_n\Omega_j - j_n\Omega_i) + v_{air/body,k}}{\omega_n \cdot pitch_{max}}\right)$$

$$\boldsymbol{\Omega} = [\Omega_i \quad \Omega_j \quad \Omega_k]^T$$

Where the equations above are similar to those developed in literature, the difference being the alteration of M_{rotor}, and the addition of a wing lift and drag term.

4.2 Dynamic Model for QTUAV

The dynamic model for the QTUAV differs to the quadrotor helicopter due to the lift and drag forces generated by the aircraft wing. Lift and drag forces for two dimensional

profiles are directly related to the inward air velocity by the empirical relationships shown in equation 42 and 43.

$$L_{2d} = \frac{1}{2}C_{L,2d}\rho A_{wing}\left(v_{air/body}\right)^2 \hspace{3cm} 41$$

$$D_{2d} = \frac{1}{2}C_{D,2d}\rho A_{wing}\left(v_{air/body}\right)^2 \hspace{3cm} 42$$

Where the coefficient of lift and coefficient of drag are determined experimentally. Additionally, the location of the lift and drag force varies. Thus an additional expression for moment is introduced.

$$M_{2d} = \frac{1}{2}C_{M,2d}\rho A_{wing}\left(v_{air/body}\right)^2 \hspace{3cm} 43$$

Where the coefficient of pitching moment is also determined experimentally. The forces mentioned in equation 42 – 43 above are orthogonal components of the overall reaction forces on a wing element.
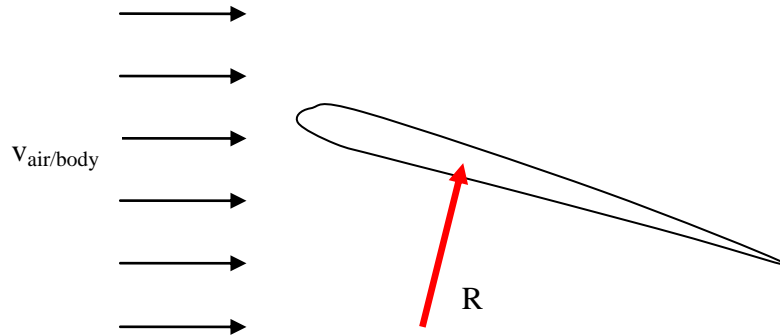
Figure 54: Reaction force due to air relative to body

A resource on the empirical results is available [86]. Additionally, two texts that identify calculative techniques in aerodynamics are available [92, 93]. Stengel presents a comprehensive text in aerodynamics and is recommended for future dynamic modeling work incorporating aerodynamics [92]. Bramwells helicopter dynamics is a recommended reference for developments where propeller deformation is significant [93].

The following formulation leaves the formulation of forces due to inward airflow (which will vary across the airfoil), and experimental analysis to determine coefficients for future work. It will also assume that lift force, drag force, and pitching moment on

the wing are all functions of angle of attack and wind velocity. It is assumed that density, and wing area remains constant.

The quadrotor helicopter dynamic model is modified to allow the insertion of the measured wing lift constants. The wing developed has dihedral, longitudinal twist, is manufactured out of polystyrene, and a constant tapering profile shape.

Given experimental data obtained from experimental testing, lift and drag due to the wing can be determined at various angles of attack and various airflow speeds.

4.2.1 Modifications for Wing Forces

The expressions modelling the translation and the rotation of the body in §4.1 are to be modified to include the wing forces provided by a QTUAV. These equations are restated below for convenient comparison.

$$m_{total}\ddot{\boldsymbol{\xi}} = F_{weight}\hat{\boldsymbol{e}}_z - T_{rotor}\boldsymbol{R}\hat{\boldsymbol{e}}_z \qquad\qquad 44$$

$$\boldsymbol{I}\dot{\boldsymbol{\Omega}} = -\boldsymbol{\Omega} \times \boldsymbol{I}\boldsymbol{\Omega} + \boldsymbol{M}_{rotor} + \boldsymbol{M}_{gyro} \qquad\qquad 45$$

A new free body diagram is constructed for the frame analysis below. Figure 56 shows a free body diagram for a QTUAV frame, where wing forces due to impinging air velocity are represented in blue, non wing forces due to impinging air velocity (parasite drag) are represented in green, weight force due to the mass of the frame and its attached components are represented in orange, and thrusts and torques due to the motors and propellers are represented in red.
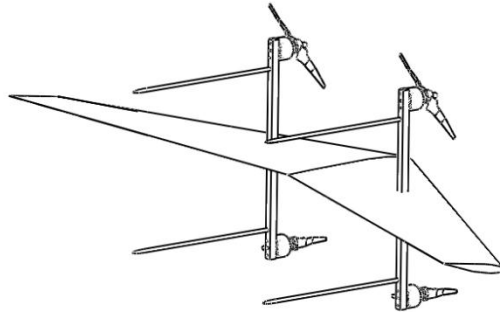
Figure 55: QTUAV configuration in forward flight
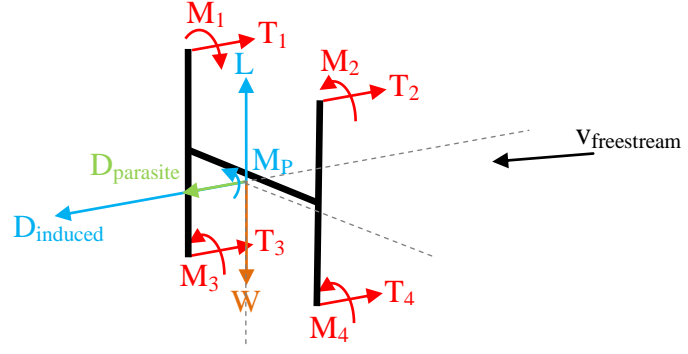
Figure 56: Free body diagram of QTUAV; wing forces (blue); motor forces (red); body drag (green); weight (orange)

The directions of $D_{induced}$, $D_{parasite}$, and L are dependent on the free-stream velocity vector. Lift is the component of the wing force perpendicular to the free stream air, and induced drag is the component of the wing force parallel to the free stream air.

Firstly the rotational motion of the craft is analysed. Eulers law for the conservation of angular momentum;

$$\sum M = \frac{d(I\Omega)}{dt} \qquad\qquad 46$$

The forces acting on the QTUAV include the originally modelled forces due to the rotor and parasite drag. Additionally, there are additional moments due to the induced drag component and lift.

$$M_{rotor} + M_{gyro} + M_{drag-para} + M_{drag-ind} + M_{lift} = I\dot{\Omega} + \Omega\frac{d(I)}{dt} \qquad 47$$

Additionally, conservation of translational forces (assuming a wing mounted perpendicular to frame as shown in Figure 55.

$$m_{total}\ddot{\xi} = F_{weight}\hat{e}_z - T_{rotor}\hat{e}_k - L\hat{e}_i + D\hat{e}_k \qquad\qquad 48$$

Substitution of the DCM yields a representation with an inability to represent its orientation in level flight, due to the singularity present at pitch angles of 90 degrees;

$$m_{total}\ddot{\xi} = F_{weight}\hat{e}_z - T_{rotor}\hat{e}_k - L\hat{e}_i + D\hat{e}_k \qquad\qquad 49$$

$$m_{total}\ddot{\xi} = F_{weight}\hat{e}_z - T_{rotor}R\hat{e}_z - LR\hat{e}_x + DR\hat{e}_z \qquad\qquad 50$$

The formulation above is insufficient to represent the orientation of a TQUAV due to 'gimbal lock' which occurs at a pitch angle of 90 degrees for the xyz Euler angles representation. The unit quaternion will provide a universal representation of attitude.

Additionally, expressions for lift and drag become turbulent for large angles of attack. A potential limitation is the angles at which a representation of the coefficients of lift, thrust, and pitching moment are not measureable due to the turbulence. Limitations for the flight envelope for a fixed wing tail sitter will exist which is problematic due to the potential to change the user's conceptual model.

4.2.2 Modification for Orientation Representation.

A singularity in orientation representation exists for the roll-pitch-yaw representation where a pitch of 90 degrees will cause terms in the derivative of the R matrix to tend towards zero (Appendix C).

Changes in the rotation matrix need to be described as they will be required to implement control of the rotation angle. Quaternion representation offers a solution to the orientation representation issue.

4.3 Model for Angular Momentum

A dynamic model to determine angular momentum is developed below. This is required in order to enable control of ZAM (in particular) to make it equal to zero.

The previously developed dynamic model for a QTUAV is represented below;

$$M_{rotor} + M_{gyro} + M_{drag-para} + M_{drag-ind} + M_{lift} = I\dot{\Omega} - \Omega \times I\Omega \quad 51$$

The expression for angular moment is then;

$$M_{rotor} + M_{gyro} + M_{drag-para} + M_{drag-ind} + M_{lift} = I\dot{\Omega} - \Omega \times I\Omega \quad 52$$

The function that relates vehicle states and craft motion when momentum is equal to zero is therefore;

$$M_{rotor} + M_{gyro} + M_{drag-para} + M_{drag-ind} + M_{lift} = 0 \quad 53$$

Where the above are functions of propeller velocity, orientation, free stream velocity, ambient conditions, and craft geometry.

The model above can be modified used to estimate the angular momentum given QTUAV states but requires the coefficient of lift and drag profiles for the wing. ZAM may be achieved using the optimal controller with the desired value of the angular momentum set equal to zero. This is developed in the control translator development section.

4.4 Summary

A dynamic model for a four-rotor helicopter was presented. Initial development of a QTUAV dynamic model was also presented.

Future work will require the;

- Tests to determine the coefficient of lift, drag and pitching torque of the wing.
- Tests to determine the coefficient of drag for the propeller.

Chapter 5 Control Translator Development

An introduction into the control translation concept was presented in §1.1.4. The purpose of the translator is to calculate control inputs using user command inputs. The following chapter outlines the development of the control translator block (shown in Figure 57), which transforms airplane commands provided by the user, into control outputs for the QTUAV vehicle. The vehicle dynamics for the QTUAV was developed in the previous section, and is used to create a computer dynamic model of the quadrotor.
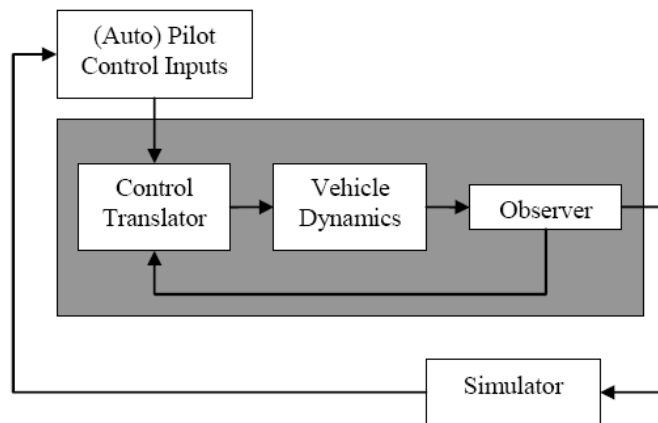
Figure 57: Control translator (Reproduced from [1])

The purpose of the control translator is the conversion of inputs for one vehicle type into outputs for another output type. The developed translator will need to account for inaccuracies of the translation algorithm and boundaries of operation for the output type (§1.2.3). The control translator may limit the flight envelope, subsequently affecting the user's system concept (§1.1.5), and therefore cause control issues.

Optimising functions to achieve the required control conditions are developed, and the control architecture defined. The optimal control of control outputs to a QTUAV is developed, where the desired optimised characteristics are;

1. Achieving the user's/autopilots desired state.
2. Maintaining the ZAM condition.

Additionally, control inputs from the autopilot must be converted into controllable states. Flight simulator has a database of simulink aircraft models that have been tested by several users. The models provide a relationship between pilot joystick inputs and expected craft motions/states. A simulink model for the Cessna 172 is chosen to convert joystick inputs into desired states. The values of the desired state (position, orientation, position rates, and orientation rates) are provided by passing joystick inputs through the flight simulator model.

The pilot commands are transformed into 'expected' desired states by placing the control inputs through a Cessna 172 aircraft model. The attained desired states are presented to the control translator.

Figure 58: Airplane model control translator – inputs and outputs

The inputs and outputs of the control translator are displayed below. Desired states and vehicle states are presented to an optimal controller where the optimising functions seek to maintain zero angular momentum and to achieve desired vehicle states (whilst being constrained by the allowable flight envelope : optional).

Figure 59: Control translator – inputs and outputs

Dynamic models which represent the relationship between propeller rotation, current states and expected future states were determined in the previous section. The current and future expected states (ZAM, orientation, motion, position) are estimated using the dynamic models, and propeller velocities are chosen to minimise ZAM and achieve desired states. An application of optimal control is available in Pinder's thesis [94] and a good reference for optimal control is available in Ogata [95].

The control translation will look like Figure 60 where pilot joystick inputs are put through an aircraft model to determine desired states and then into a quadrotor model to

determine propulsion (speeds/thrusts) that achieve ZAM and approach desired states. Additionally, measured states are provided to both the aircraft model and the quadrotor model.
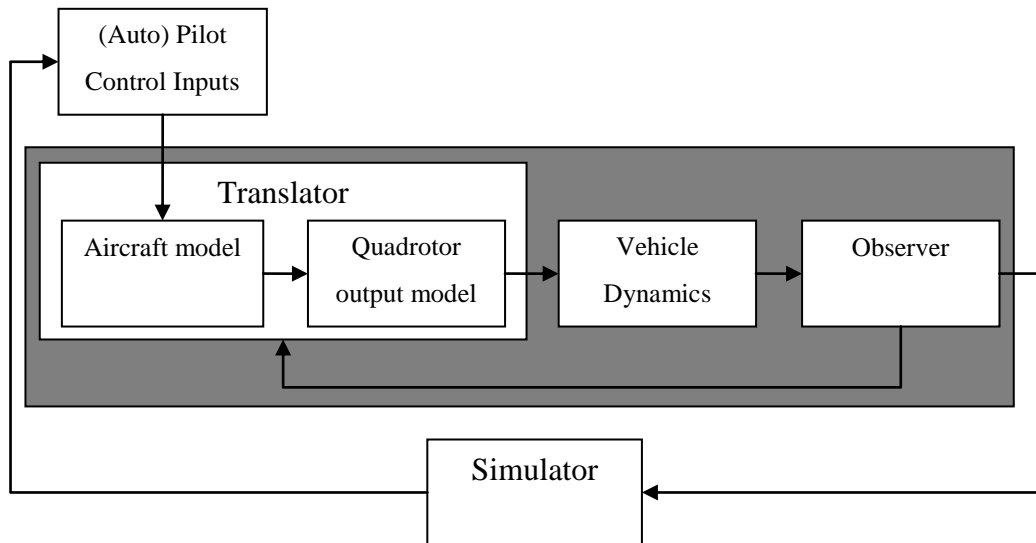
Figure 60: Control diagram for aircraft to quadrotor control translation

5.1 Program Architecture

The control translator is separated into four sections: the first acquires joystick inputs and determines desired states (§5.2); the second acquires state measurements from a (future developed) state estimator (§5.3); the third uses state measurements and desired states to determine propeller speeds using optimal cost functions (§5.4); finally, the fourth uses the sound port to send the desired states to the controller (§5.5). The following sections present each sub-module of the control module. In addition, a quadrotor helicopter simulink dynamic model was created to provide for virtual testing of control developments (§5.6).
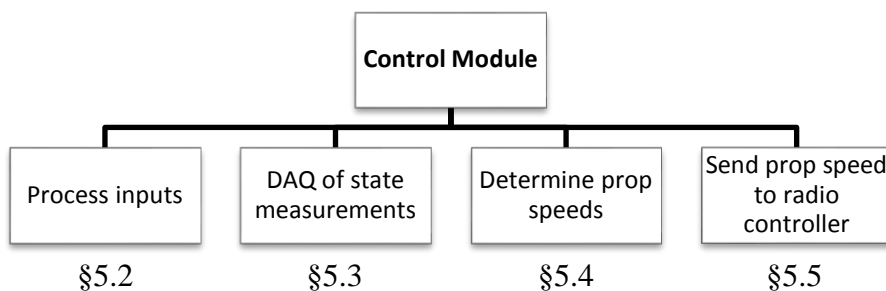
Figure 61: Control translator program architecture

5.2 Acquisition and Processing of Joystick Inputs

The purpose of this module is to acquire control inputs and determine desired command states. Two methods of processing joystick inputs were used: the first was proportional mapping of joystick motions and propeller motions; the second was the transformation of remote controller inputs using a simple dynamic model. These are each presented in the following sub-sections.

5.2.1 Direct Mapping

The relationship between roll, pitch, yaw and thrust commands via the joystick were related to the angular velocity via the relationship presented in Table 7, where positive motions are defined as per positive motion for the joystick. Please see chapter 5 for motor nomenclature.

Table 7: Map of relationships between motor inputs and control outputs

	Motor 1	*Motor 2*	*Motor 3*	*Motor 4*
Thrust	1	1	1	1
Pitch	1	1	-1	-1
Yaw	-1	1	1	-1
Roll	1	-1	1	-1

Using the above relationships, MATLAB™ code to enable computer to quadrotor communication was developed. This is included in Appendix C. Control of the helicopter using the relationships shown in Table 7 above was unstable. This confirmed that a dynamic model and subsequent control method development is required.

5.2.2 Cessna 172 Model

Joystick inputs are processed through a simplified mathematical model for a Cessna 172. Several aircraft simulators utilise flight dynamics models developed by various groups including JSBSim, YASim, and the applied aerodynamics group at the University of Illinois (UIUC).

There are two main dynamic model types used for aircraft control simultors. The first is a parametric model, which uses pilot inputs, dynamic parameters of the craft, and the current state to calculate future states. The second is a geometric model, which uses

pilot inputs, the current state and a geometric model of the craft surface to calculate future states.

A C program with the Cessna 172 dynamic model is presented by Jackson from Langley research center [96]. The dynamic models are developed using LaRCsim, a dynamic model developed by NASA to provide a simplified dynamic model for simulators [96]. This model may be useful in the future when the project aims to improve computational time.

Airlib, is a library of MATLAB aircraft models to be used with simulink and requires the aerosim blockset, aerospace blockset, and flight dynamics and control (FDC) toolbox. A Cessna 172 dynamic model has been developed in MATLAB Airlib by Giampiero Campa and is presented in Figure 62.
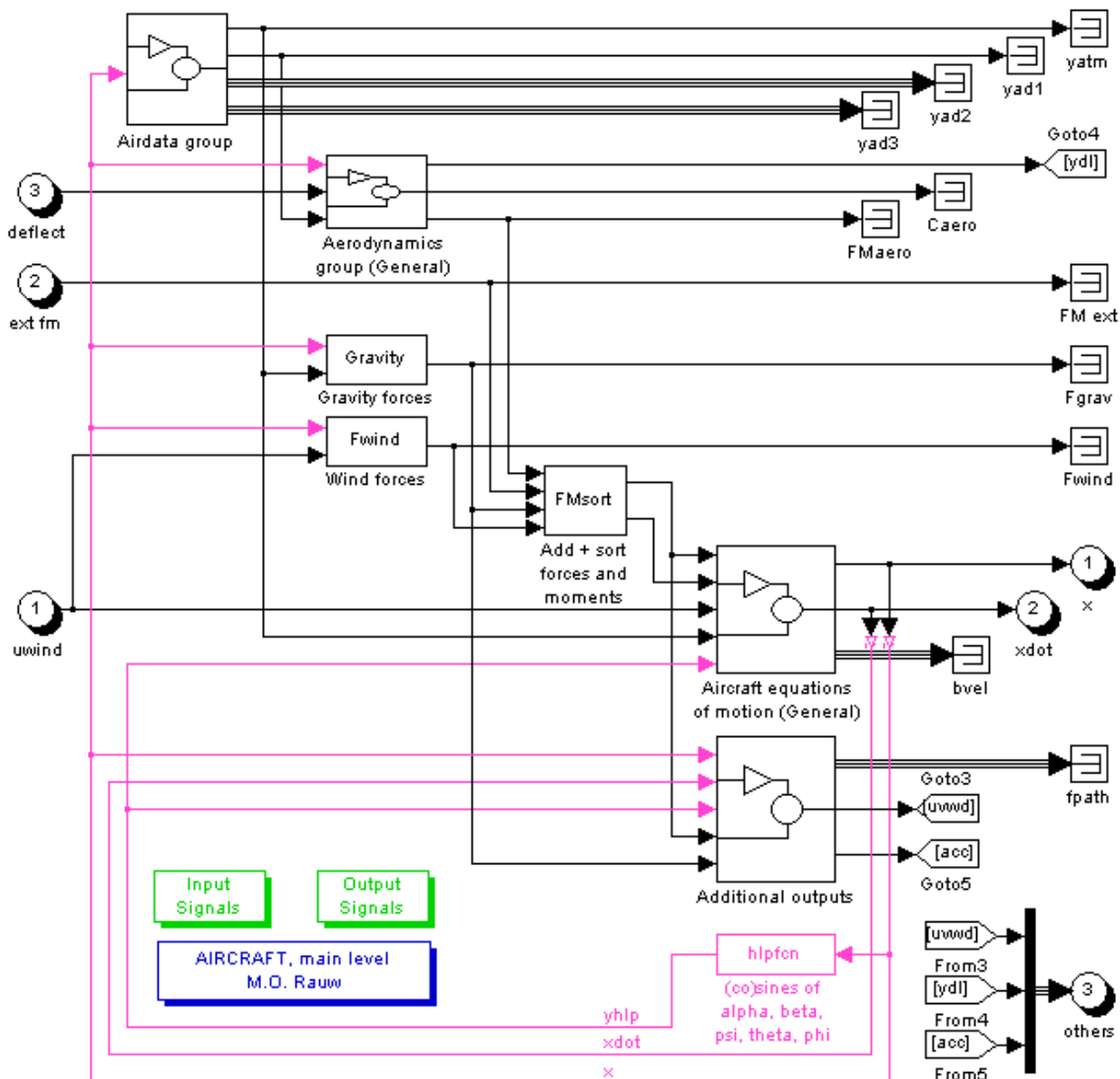
Figure 62: Cessna 172 MATLAB Simulink Model [97]

5.3 Acquisition and Processing of State Measurements

Adequate state information is required to be provided to the pilot and the controller. The states that are required to be estimated include:

- Attitude
- Altitude
- Position
- Motion

The most common method for orientation measurement uses the measurement of acceleration components and angular rates using accelerometers and gyros respectively. The measurements are subsequently modified to account for the gravity vector. Equipment must be selected that provides adequate measurement frequency and measurement domain. The development of a state measurement system is left to future work.

5.4 Optimal Control of Controller Speeds

The rotational speeds of each motor are to be determined by optimising desired states and attempting to maintain ZAM. The dynamic model developed in Chapter 4 is to be modified to determine the control outputs which optimise the quadrotor orientation and ZAM condition.

The development of the function that optimises propulsive speeds whilst subject to motion constraints is left to future work.

5.5 Computer/Controller Communications via MATLAB

A MATLAB™ function is developed that is used to accept joystick inputs and provide outputs to a controller (transmitter). The controller (transmitter) used has the function to both act as a master controller, and as a slave controller. The communication to the transmitter takes advantage of the controller's (transmitters) trainer function. The designed purpose of this functionality is to allow an experienced RC pilot to fly a RC plane, and then switch to allow a novice RC pilot to control the aircraft, then to switch back in an event where the novice makes a mistake.

The signal transmitted by a trainer is determined by activating the controller 'trainer mode' function, using an audio plug to extract the signal, and connecting the audio plug

to an oscilloscope. The image attained from the oscilloscope was then used to determine the format of the controller signal. A representation of the pulse waveform attained with the ground wire of the oscilloscope attached to the central connection point of the sound cable and the measurement probe attached to the outer most connection point of the sound cable is shown in Figure 63.
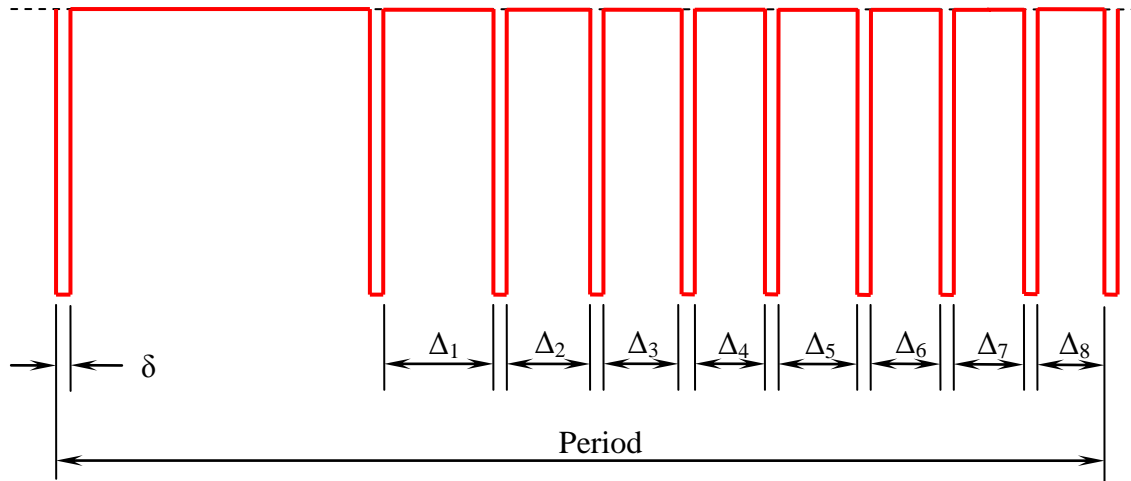
Figure 63: Signal transmitted by controller in trainer mode

The signal transmitted is pulse period modulated (PPM), where the period of each pulse is δ, and the duration between each pulse is equal to Δ. The overall period is 22ms where a 100% control setting maps to a Δ of 1500µs; 50% control setting maps to a Δ of 1100µs; and 0% control setting maps to a Δ of 700µs. Additionally, mapping between the duration between each pulse and the control input is determined by manipulating the controller controls (Table 8).

Table 8: Mapping between signal dimension and control input

Signal definition	Control input
Δ_1	Throttle
Δ_2	Rudder
Δ_3	Elevator
Δ_4	Aileron
Δ_5	Gear
Δ_6	Aux1
Δ_7	Aux2
Δ_8	-

5.6 Vehicle Dynamics – MATLAB Model for QUAV

The dynamic model was simulated using MATLAB Simulink. A block diagram of this is available on the included CD. The model coefficients used for the model are available in Appendix J. The behaviour of this model appeared reasonable, and can be used to make sensible detailed design choices in the future.

5.7 Summary

A program architecture is proposed and MATLAB code to send desired control settings for the aircraft to the controller was developed. A Cessna 172 dynamic model is presented that provides translation of control inputs into desired states.

A large quantity of future work is presented in the development of a control translator including:

- Calculation of state transition matrix for the optimal controller.
- Development of embedded hardware to measure craft states.
- Acquisition and processing of state measurements.

Chapter 6 Discussion

The following presents the author's critical evaluation of the work presented. It also presents the development of conclusions and recognises future improvements to the development of a quadrotor tail-sitter unmanned aerial vehicle.

6.1 Prototype Development

A quantity of work was reviewed on the development of quadrotor helicopter control and dynamic modelling where a commonly presented piece of information was that the quadrotor helicopter was intrinsically unstable (§1.1.2). A prototype quadrotor helicopter was developed (Chapter 2) and MATLAB code developed to enable joystick inputs to be converted into commands for the four rotors (§5.2.1). The developed code provided a linear direct mapping of motion where changes in the controller input were linearly varied according to the joystick input, and provision of trimming was afforded by keyboard inputs (Appendix A). A rudimentary test of control of the prototype confirmed the statements of other authors that the quadrotor UAV (with non flapping/lagging propellers) is unstable, and that a control system is required to enable stable hover.

Development of the first quadrotor helicopter prototype required selection of components that were able to provide sufficient static thrust to carry the quadrotor and additional excess for attitude and motion control. A propeller type was selected which (when combining the four propellers) provided a total of 400g more thrust that the design weight of 1000g when operating at the selected motors maximum speed (i.e. 4 x 350g = 1400g). This was expected to provide sufficient manoeuvrability for initial quadrotor testing and is expected to be sufficient as 400gms of payload is still available.

The propulsion system includes an electronic speed controller (ESC) used to regulate the rotational speed of the brushless motor. During the development of the propulsive system, it was expected that the ESC would be capable of maintaining the rotational speed of the brushless motor despite changes in the supplied voltage. Experimental testing saw this not to be the case. As a result, rotational speed, and of more concern, the related thrust of the propeller is a function of the supplied voltage, which introduces

a drift in the actual control thrust of the propeller for a given control setting. Compensation for the speed change may be applied by modelling a bias that decreases as the battery discharges, or the voltage of the supply provided to the ESC can be maintained. Although, this assumes that the ESC speed is dependent on the voltage. Alternatively, the rotational speed (through microphone, tachometer etc) or the thrust (through measurement of frame stresses) can be measured and an embedded control system developed to control the propulsive thrust. Measurement of rotational speed is possible through an encoder. This will be problematic as a further model will be required to determine the relationship between thrust and rotational speed. In static situations, this is fortunately consistent as presented in chapter 3. However, in conditions where the free stream velocity is not equal to zero, there are variations to the thrust generated by the propulsions system that will need to be accounted for as described in Appendix F.

Sensing of the quadrotor attitude and orientation will be required for the quadrotor helicopter. Possible methods of providing this sensing include the use of an inertial measurement system (IMS) which will enable the system to work outdoors. Alternatively, cameras may be used to sense other artifacts and allow orientation control using other artifacts as a reference. The second method is suited to operation around a given artifact (as a following drone or in a room).

Additional information may be required to provide feedback to the user and includes measurements such as airspeed and altitude. Also an onboard camera will provide more information to allow the user greater conceptual control.

Currently, the mass of the quadrotor is below the designed mass, although as a result of the suggested improvements, future development of the quadrotor will increase the mass of the quadrotor. A new propulsive system may be required if the additional components result in a quadrotor that approaches the 1kg design mass.

A wing to allow stable forward flight was developed and tested concurrently to the project which allows stable forward flight at speeds up to 50km/hr. It is a traditional wing, with taper, twist, and dihedral angles, that is capable of providing lift until an unknown lower limit at which the free air speed is insufficient to provide laminar flow. Development of a wing should investigate the lower limit of the developed wing and developments in slow flight.

The location of the propulsive system with respect to the lifting surfaces will alter the lift and stability characteristics of the plane. Aircraft with a propulsive system in Tractor configuration (which have the propulsive system fore of the wing) pull the craft through the air and increase the free stream velocity of the air over the wing section directly behind the propeller. This improves the lift of the wing section but can reduce the thrust force due to the air resistance of the wing cross section. Pusher aircraft push the craft through the air, the aft position can make tailed aircraft unstable. Wing design may consider tailless stability.

The criteria used to select the aircraft components should be re-ranked to allow maximisation of the flight envelope through an increase thrust-to-weight ratio and increased range of operation (AOA & v_∞) for the attached wing. Diameter of the propeller should be limited by overall craft size constraints, operation conditions, and compressibility effects rather than by the minimisation of radius. Minimising the radius does influence the load, which influences the size of the motor and battery used, which alters the thrust to weight ratio. An improved thrust to weight ratio may be obtained through the minimisation of diameter.

6.2 Dynamic Translation Models

Several stages were involved in the development of the dynamic translation models and translation method. The input interface used for the prototype is a joystick, the input dynamic model identified is a Cessna 172 dynamic model used in flight simulator and the 'output dynamic model' is formulated from dynamic relationships expected in the QTUAV. State observation is required in order to provide state estimates to the user and the translator.

The interaction between the user and the craft including situations where the user's conceptual model of control exceeds the craft capability affect the user's command capability. The resolution of the control is influenced by the computational speeds and model accuracy. Each aspect of the development of the dynamic translation models are discussed in turn below.

The input interface presented to the user of the control system should be representative of the interface that the user expects. In the development of this control translator, this means that the interface should provide all the control ability and all the data that would be available to a pilot controlling a Cessna 172. Development of the user interface

should then allow presented data of airspeed (vertical and horizontal), attitude, heading, airspeed, and slip. A trade-off must be made between the measurement of these values and the mass of the controlled system. The user's relationship to the control interface is related to the likeness of the interface displays and response to the developed conceptual model. Throttles, control sticks, and displays should be purchased to allow the interface to be as similar as possible to the user's conceptual model.

Inputs from the input interface are to be translated into desired states from control inputs. Two methods were identified, the first seeks to cancel the user's concept of control of the system by acquiring data relating user inputs to user outputs, and then generating an inverse model. The second uses an approximate dynamic model that relates expected pilot inputs to pilot outputs. Models for a variety of aircraft types and helicopters are available in flight simulator 2004 within the aircraft folder. Selection of the dynamic model provided by flight simulator is sufficient for initial development because it has been tested by several users and has as its purpose a desire to simulate the aircraft movement. More complex dynamic models used in commercial aircraft simulators will provide a modestly accurate conversion of user states into user outputs should further accuracy be required. Alternatively, dynamic models are available in several papers on the development of control systems for airplane UAV [98] and helicopter UAV [99, 100]. Future work should implement the flight simulator simplified dynamic model, or the airlib dynamic model, as a first run through control translation. Obtaining the dynamic model from flight simulator 2004 proved to be a difficult task although several references were presented. An alternative dynamic model is presented by Flight Gear, whom utilise LaRCsim [96], a model developed for simulators by NASA Langley. A Cessna 172 dynamic model was selected as it is a common aircraft, and thus ensures a greater availability of pilots to eventually test the controller. Selection of the input model dynamics may be provided for by choosing parameters within the good region of Figure 14. The user's concept of the system can be ensured by selecting an input method that is not limited by non-allowable states. Alternative models may be more capable of allowing conceptually accurate control.

The dynamic model developed has a range of empirical relationships and experimentally determined constants. These provide a more accurate model, but as a result make the model suitable only for the particular model with its own measured system parameters. Development in mass production will allow the standardisation of components and improvements in the constancy and modelling accuracy of the

QTUAV. This will result in the elimination of aerodynamic and inertial constant measurement. During the development stages, the measurement of aerodynamic and structural constants is accepted. The dynamic model developed in Chapter 4 assumes a linear relationship between zero thrust at the pitch speed and a maximum thrust at zero axial speed (static thrust). This relationship remains to be confirmed. Additionally, the pitch speed is assumed as being correct to the supplier specifications and has also not been confirmed.

Several improvements to the dynamic model are required including the calculation of the torque coefficient for the APC-E 7x5 propeller which will require the development of a device to allow torque and thrust measurement. Wind tunnel testing will then be required to determine the lift and drag coefficients for various wing attitudes which will provide average expected values of lift and drag, variation about these mean values is expected. Dynamic model can be further developed to allow incorporation of effects of structural elasticity. A text on the development of the empirical relationship between aerofoils and various states is available [86].

The aircraft must have a valid attitude representation at all attitudes. The control system must also be capable of providing 'defined' control at all attitudes. A singularity present in the representation of the dynamic model when the craft is tail sitting (if zyx Euler angles are used) and in forward flight (if xyz Euler angles are used) requires the use of unit quaternions for the representation of attitude. The unit quaternion is a currently popular method for 'complete' attitude representation. Investigation into the quaternion coordinate system was made although additional work is required to allow the production of a quaternion based dynamic model for the QTUAV. Previous work in the control of tail-sitter aircraft has used a combination of the aforementioned xyz Euler angles, zyx Euler angles and unit quaternions [15]. Tayebi et al have developed a quaternion controller for a quadrotor and future work can focus on development here to allow a more universal representation of attitude.

Many other control systems for quadrotor helicopters and unstable hovering systems have used a Lyapunov function to ensure stability. This method of bounding control signals may offer solutions should future developments of the control translator induce problems in controllability.

The dynamic model includes gyroscopic forces that are caused by the precession of the rotating propellers. The moment induced on the frame due to the precession is provided

by a deflection of the frame which is not modelled in the 'as-developed' model. Further development of the dynamic model to include elasticity of the aircraft will provide for the inclusion of gyroscopic forces.

Designing the QTUAV to have a large rotational inertia will improve the controllability of the quadrotor helicopter. Pounds, Mahony et al have been working towards design to allow sufficiently large rotational inertia. A sluggish quadrotor is provided by large moment arms, large propeller rotational speed, and large propellers.

In the computation of the control translation, a trade off will be required between model precision and computation speed. Initial development focused on a general model as a full representation of the aircraft dynamics can eventually be developed and split into individual models. Models can be switched between depending on orientation. Berbra presented a method of switching between multiple optimal observers [69]. Usage of the dynamic models will consist of using an optimal controller to determine control settings which optimally attain estimations of future user inputs and maintain zero angular momentum.

The user's conceptual model of the system can be maintained by ensuring that the input dynamic model has a state space that is smaller than the output dynamic model (Figure 64 - left). In the case where the input dynamic model exceeds the boundary of the output dynamic model (Figure 64 - right), a compromise between maintaining the user's conceptual model of control of the aircraft, and control translation is required.
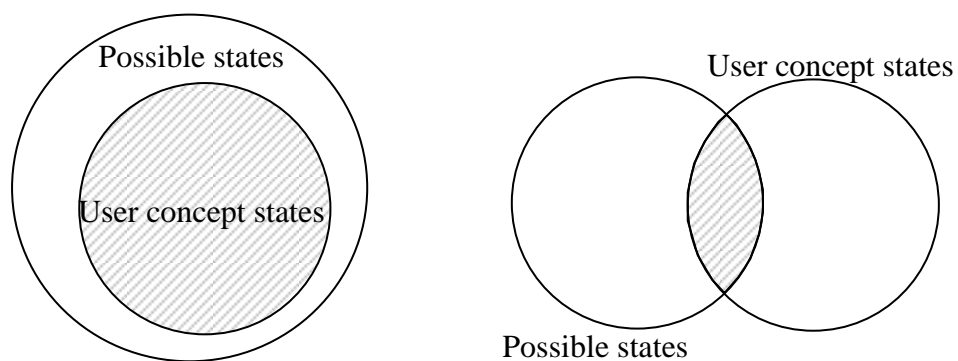
Figure 64: Range of operation vs concept of control; possible states for dynamic input model within possible state for craft (left); possible states for dynamic input model outside possible state for craft (right)

A constraint to the control limit could be implemented which would provide flight envelopes that the user is unable to exceed. The advantage of constraining control is the craft will not exceed the designed flight envelope. The disadvantage is that the flight

envelope and therefore the manoeuvrability will be constrained by an artificial barrier within the code. This limits the flight envelope and alters the user's concept of flight envelope. Alternatively the user can be left to set desired points as they please using an aircraft concept of control. The advantage is that the user will have possible implementation of controlled flight at all phases where the craft is controllable, although it is highly probable that the user will fly outside the 'flight envelope' and the craft will crash. This will both likely damage the craft and the user's concept of control. It is ideal that any increase in the flight envelope will maintain the users' conceptual model of control.

Chapter 7 Conclusions and Future Work

This chapter summarises all important findings in this thesis and proposes recommendations for future work.

7.1 Conclusions

As a result of this study on the ZAM Quadrotor VTOL UAV, a QUAV was developed, a dynamic model for a QUAV was developed, human factors involved during control were discussed, and a suitable control translator was developed. The masters transcript has provided a foundation to design and test a control translator for a quadrotor tail-sitter unmanned aerial vehicle which will enable a pilot experienced in the control of a normal aircraft to control a quadrotor tail-sitter unmanned aerial vehicle, from hovering flight to forward flight, using normal aircraft inputs. The following section provides a summary of the conclusions reached from the investigation of the thesis.

7.1.1 TQUAV Prototype Development

A quadrotor helicopter prototype was developed to provide a physical model to test quadrotor control routines. Parallel work has also included development of a wing suitable for the TQUAV. The quadrotor prototype was used to test the plausibility of a user directly controlling motor speed using a (remote) controller. The test found that direct control of motor speed was difficult as the QUAV would rapidly rotate and translate into nearby objects. Improved control would be provided by increased vehicle inertia, increased control sensitivity, and a control interface that is familiar to the user.

7.1.2 Control

MATLAB code was developed to enable conversion of joystick inputs to an output for the (remote) controller. The motor speed control setting is presently computer controllable. However, joystick control of the motor speed is insufficient to allow control of the quadrotor UAV. Improved control would be provided by orientation measurement, and a suitably programmed controller to orient the craft to commanded setpoints.

The method of control translation by Pinder [1], was further developed to separate command and control aspects of the control translator. The method utilises two dynamic models to convert control inputs into commands, and control the craft to the command set-point. The separation of command and control allows any input model to be used to command the QTUAV. However it may involve more computation than directly translating inputs to outputs. The increase in complexity is required because different flight phases exist for the QTUAV. Hierarchical control is a commonly applied method for the control of tail-sitters and is an alternative that offers linearisation of the dynamic model and complete dynamic representation. The separation of command and control could improve controllability as the user could fly using a single conceptual model, and multiple output models could be used during the various flight phases presented in Figure 8.

The electronic speed controller does not provide rotational speed control that is independent of voltage. This was investigated by measuring rpm as the battery discharged. It was found that at a constant control setting, the rotational speed of the motor reduced as the battery was discharged. A suitable linear region exists for control of the QUAV. However, the linear region is not large enough to include the slow motor speeds used during forward flight for the TQUAV.

7.1.3 Dynamic Modelling

A dynamic model was presented that estimates the expected motion of the craft given propeller rotational speeds. Additionally, several prototype parameters were obtained as summarised in Table 6. The static thrust coefficient for the APC-E 7x5 propeller is empirically estimated as $2.94\mu gm/rpm^2$. The coefficient can be modified by including relative airspeed in the empirical calculations. Mass moment of inertia for the principal axes are $30kgm^2$, $6.9kgm^2$, and $9.3\ kgm^2$ for I_{xx}, I_{yy}, and I_{zz} respectively. The error analysis shows large error/uncertainty that may be significan during control. Torque test equipment is required to allow measurement of the torque coefficient. A suitable test would measure torque for a range of propeller speeds, and provide a plot of torque against propeller speed.

7.2 Future Work

The transcript has provided a foundation to continue development of a TQUAV. The following works are recommended for future study to improved the prototype, control system, and control interface of the TQUAV.

7.2.1 HMI Considerations

A HMI similar to the interface expected in a Cessna 172 is obtained. A suitable interface should be as similar as possible to flight in a Cessna 172, where an existing Cessna 172 simulator is preferred. Important components include a joystick, rudder pedals, gauges, and display.

Investigate the ability of the Cessna 172 dynamic model to be bounded by the dynamic model for the QTUAV. If it is not bounded, investigate alternative input dynamic models that are bounded. The investigation of disparities between command models and control models will provide a check to ensure the users concept does not change significantly, and that the controlled system will suitably move.

7.2.2 TQUAV Prototype Development

A quadrotor prototype with a single wing as shown in Figure 7 is developed with necessary modifications to allow equipment storage. The initial TQUAV prototype should use the wing designed in Robinsons work as this design has considered the motor and propeller operating limits [84].

Component selection should maximise flight envelope as it will ensure a greater ability to allow various input control models to be used for the controlled system. Developments include selection of components to match the maxiumum-all-up-weight of the vehicle prototype, attachment and inclusion of sensing equipment, and development of the geometry of the craft surface. The wing and body should be developed to allow slow flight and minimise the transition phase. Minimising the transition phase will provide orientation relationships that can be modelled for a greater domain of command and control states.

7.2.3 Dynamic Modelling and Control Algorithms

A torque measurement rig to allow the measurement of torque for the propeller is required in order to determine the torque constant in equation 4. The rotational inertia of the propeller (and motor assembly), I_R, is also required for the dynamic model. The

dynamic model will need to be verified by applying known forces, observing the response, and comparing the response with expected modelled results. The dynamic model should then be used to develop a ZAM optimal controller in order to improve control of the quadrotor.

Investigate the validity of the negative linear variation of thrust against pitch speed. Variation of thrust will be significant when the propellers each experience differing pitch speeds, such as during rapid rotation. This test is required because all the thrust-rpm relationships have been obtained for static airflow. Cross-winds and high acceleration turning are expected to change the relationship between thrust and torque due to non-axial ($\hat{e}_k$) rotor torques

7.2.4 Development of Sensing System

Accurate measurement of the current state of the craft is necessary to provide estimates of error between desired and required states. It is recommended that an observer is developed to allow measurement of the craft rotation, altitude, airspeed, and acceleration in order to provide information for the user, and to provide measurements to the control translator. A wireless camera and transmitter developed to allow live imagery of a pilot's concept of motion. This will provide another sensory control output to the pilot.

APPENDICES

Appendix A MATLAB code

The following is MATLAB code developed for the QTUAV. Section A1 presents MATLAB code used to communicate desired set-points to the remote controller using a stereo sound card. Section A2 is a simple map to translate joystick inputs into control set-points. Section A3 is used to create a waveform, in matrix format, suitable to be sent to the soundcard output. Section A4 is non debugged MATLAB code to be eventually used to provide automatic configuration control of the receiver during binding.

A.1 Joystick Input to Control Output (ppm.m)

Desired set-points are determined from a joystick input and a PPM waveform similar to that presented in §5.5 is generated. The program also includes a routine to setup the ESC. The following code uses routines from the Psycho-physics ToolBox[‡‡].

```
% -------------------------ppm.m---------------------------------- %
% This function is used to generate a pulse period modulated signal that  %
% is sent, via the sound port, to the controller. Two seperate routines   %
% are included: The first is a calibration routine used to configure the   %
% bind positions for an input (throttle is the only channel functional    %
% pending purchase of 'bind plugs'); The second is a routine to convert    %
% joystick inputs into motor outputs (a simple relationship matrix, H, is %
% used for the meantime).                                                  %
%                                                                          %
% Codes with LB#.## refer to a log book page and number. Information is    %
% reported on in logbook.                                                  %
%                                                                          %
% Development of a dynamic model and the subsequent Optimal Controller     %
% will provide the information required to translate inputs effectively.   %
% FYI - PPM - Pulse Period Modulation                                      %
% ----------------------------------------------------------------------- %
% Author: Shane Pinder, Cornelis Kok                                       %
% Date Created: 3 June 2008                                                %
% Revision No: 04                                                          %
% Date of Revision: 26 May 2009                                            %
% ----------------------------------------------------------------------- %
% Programmers Notes:                                                       %
%  1)Problem at line 74 observed, program breaking out of switch           %
%    expression incorrectly.                                               %
%  2)If communication with the controller is not observed with the sound   %
%    cable is plugged into the controller, ensure that the volume of the   %
%    sound port is sufficiently loud. (previous tests at 100% volume)      %
%    If there is still insufficient volume, enlarge the value of the       %
%    variable 'volume' (which will increase the amplitude of the waveform %
% ----------------------------------------------------------------------- %

function ppm()
key(32) = 0; % Enter key set to 0.. toggle 1 to end sim
volume = 0.4; % Amplitude of PWM signal
fs = 96000; % Hz % Sample frequency
servos = zeros(1,8); % Initialise servo position
```

[‡‡] Available from www.psychtoolbox.org

```
pulse_duration = [0.4 0.9 1.2 22]; % ms [0end_low_pulse 0min_end_high_pulse
high_pulse_sensitivity overall_train] LB1.86
pulse_length = round(pulse_duration*fs/1000); % samples
pulse_index_raw = repmat([1:pulse_length(1)]', 1, 9);


%Values chosen to be high and low control inputs, (default - low=0, high=1)
high=1;
med=0.5;
low=0;


%Generate and send initial output
fprintf('\nGenerating pulse\n');
y = formPulse(servos, pulse_index_raw, pulse_length, volume); %Call
formpulse function


fprintf('\nPerforming PsychSound opening/initialising routines\n\n');
AssertOpenGL;
InitializePsychSound;
pahandle = PsychPortAudio('Open', [], [], [], fs, 2, pulse_length(4), [],
[]);


PsychPortAudio('FillBuffer', pahandle, y); %Open audio channel and give
pulse function


while KbCheck; end; %Run until no input from user


next_push = PsychPortAudio('Start', pahandle, 0, [], 1) +
(pulse_duration(4) - 10)/1000; %


%Initiate communication with controller
fprintf('\nInitiating communication with receiver.\n');
servos=[0 0 0 0 0 0 0 0];
servos=max(0, min(1, servos)); %check value between 0 and 1
y=formPulse(servos, pulse_index_raw,pulse_length, volume); %create signal
suitable for controller
PsychPortAudio('FillBuffer', pahandle, y, 1); %Fill audio data playback
buffer


% % Select ports to calibrate/utilise
servosActive=[0 1 0 1 1 1 0 0];


% % Select mode (1. User mode   2. Calibration mode) default is user mode
replyMode=input('\nSelect mode: (1)User mode  (2)Calibration mode\n', 's');


switch replyMode
    case '1'
        [fill_success, pahandle] = user(servos, pulse_index_raw,
pulse_length, pulse_duration, volume, fs, pahandle, servosActive, key);
    case '2'
        tunning(servos, pulse_index_raw, pulse_length, volume, pahandle,
high, med, low, servosActive, key);


        replyUsereq = input('\nWould you like to enter user mode now that
you have tuned everything (type "y" for yes)\n');


        if not(strncmpi(replyUsereq, 'y', 1))
            [fill_success, pahandle] = user(servos, pulse_index_raw,
pulse_length, pulse_duration, volume, fs, pahandle, servosActive, key);
        else
            fprintf('\nNon-y value entered, closing\n');
        end


    otherwise
        fprintf('\nInvalid input, initiating user mode in 5 seconds\n');
        pause(5)
        [fill_success, pahandle] = user(servos, pulse_index_raw,
pulse_length, pulse_duration, volume, fs, pahandle, servosActive, key);
end


fprintf('\nInitiating closing routines.\n');
```

```
% Stop playback
PsychPortAudio('Stop', pahandle);
% Close the audio device
PsychPortAudio('Close', pahandle);
% Confirm closure to user
fprintf('\n----------------------------------\nProgram ended.\n');


return
```

A.2 Translator (user.m)

Code to determine and send desired movement to controller

```
% ----------------------------user.m---------------------------------- %
% This code is to accept pilot inputs, and determine control outputs to  %
% be sent to the vehicle.                                                 %
%                      ---------------                                    %
% At present, pilot inputs are obtained from a joystick and keyboard.     %
%                                                                         %
% Inputs consist of trim values and control values that are modified by   %
% the pilot due to direct observation of the rig.                         %
% ----------------------------------------------------------------------- %

function [fill_success, pahandle] = user(servos, pulse_index_raw,
pulse_length, pulse_duration, volume, fs, pahandle, servosActive, key)


fprintf('\nInitiating "user" mode\n');


%INITIALISING-----------------------------------------------------------
fprintf('\nInitialising variables\n');
axes=[0 0 0 0];
trim=[0 0 0 0];
joy=vrjoystick(1);            % Open joystick at address 1
trim_sens=0.1;               % Sensitivity of trim (modifies key
sensitivity)
axes_sens=1.*[0.1 0.1 1.0 0.1]; % Sensitivity of Joystick
%           w1 w2 w3 w4
hmove2propRot=[ 1 -1  1 -1      % roll    hmove2proprot = Matrix relating
joystick
                1  1 -1 -1      % pitch      inputs and expected helicraft
movement
                1  1  1  1      % thrust     (ref LB2.18)
               -1  1  1 -1];    % yaw


key(32) = 0;                 % Enter key set to 0.. toggle 1 to end sim


%wait(10000) = 0;             % Variable used for testing
%fill(10000) = 0;            % Variable used for testing
fill_success(10000) = 0;     % Variable used for testing
s(10000)=0;                  % Preallocation of memory


i(1) = 1;                    % Incrementing variable used for testing
s(1) = 0;                    % Variable used for testing time taken for
cycle
j = 0;                       % Incrementing variable used for testing


key_sens = 1000/fs/pulse_duration(3);
kt_sens = trim_sens.*key_sens;


gs = GetSecs; %Time since windows opened


fprintf('\nAudio playback started, press spacebar key for about 1 second to
quit.\nPress "z" to clear trim values\n');
pause(3);                    % Allow time for user to read message


% Stay in a loop until keypress:
while key(32) == 0
    clc;

    %ACQUIRE and MIX CONTROL INPUTS---------------------------------------
    % Get Joystick/Keyboard values
```

```
    [a b key] = KbCheck; %Acquire status of keyboard
    [axes, buttons, povs]=read(joy); % read struct avail on LB2.26
    %axes(3)=-0.5.*axes(3)+0.2;      % Thrust modifier ref LB2.34
    axes(3)=-1*axes(3)+0.5;


    % Get Trim values
    trim=not(key(90)).*(trim+kt_sens.*(double([key(68) key(83) 0 key(69)])-
double([key(65) key(87) 0 key(81)])))


    % Get Setpoint (Acquiring yaw/roll/thrust/pitch and trim commands
    setpoint=trim+axes_sens.*axes;


    %MODIFICATION OF SETPOINT TO MATCH CHOPPER DYNAMICS-------------------
    %-Dynamic model required-%


    % Use modified setpoint to determine angular rotation control
output,servos
    servos=setpoint*hmove2propRot;
    servos(4:8) = [0 0 servos(4) 0 0];


    %GENERATE AND SEND CONTROL OUTPUT------------------------------------
    % Send control output to reciever
    servos = max(0, min(1, servos))
    y = formPulse(servos, pulse_index_raw, pulse_length, volume);

%   WaitSecs('UntilTime', next_push);
%   next_push = next_push + (pulse_duration(4))/1000;

    a = PsychPortAudio('GetStatus', pahandle);
    disp(a); %Show status of audio variable


    j = j + 1;
    fill_success(j) = PsychPortAudio('FillBuffer', pahandle, y, 1);
end

fprintf('\nSpacebar pressed. User mode ended. Gutted if the plane was in
the air and we made it this easy to disable communication.\n');


return
```

A.3 Produce PWM Signal (formPulse.m)

The following code is used to generate a pulse width modulated signal that is ready to be sent to the controller via the sound card stereo output.

```
    fprintf('\nCalibration complete (hopefully). Returning to zero input.\n');


% ---------------------------formPulse.m------------------------------ %
% Given information about the desired width between pulses (ie desired   %
% control setting) the following generates a Pulse Period Modulated     %
% waveform ready for sending to the controller.                         %
% ------------------------------------------------------------------- %


function pulse_train = formPulse(servos, pulse_index_raw, pulse_length,
volume)


pulse_index = pulse_index_raw + repmat(cumsum([0 round((pulse_length(2) +
pulse_length(3)*[servos]))]), pulse_length(1), 1);


pulse_index = pulse_index + pulse_length(4) - pulse_index(end) - 1;


pulse_train(2, pulse_length(4)) = 0;


pulse_train(1, pulse_index) = -volume; %Generate negative pulse with amp
equal to volume

return
```

A.4 ESC Setup Routines (tunning.m)

```matlab
% ----------------------------tunning.m-------------------------------- %
% The following is a routine to allow semiautomatic calibration of the  %
% ESC.                                                                   %
% --------------------------------------------------------------------- %
function tunning(servos, pulse_index_raw, pulse_length, volume, pahandle,
high, med, low, servosActive, key)


fprintf('\nInitiating calibration mode.\n\nCalibration requires a high
pulse, then, once an acknowledgement tone is heard, a low pulse. Please
follow subsequent instructions.');
%Calibration Mode


%Allow user modification of high and low values for all values
servosHigh=high.*servosActive;
servosMed=med.*servosActive;
servosLow=low.*servosActive;


fprintf('\nWhen you are ready, simultaneously "turn on UAV" and "press any
key (space bar)"\n');
pause         %Wait till any key pressed


%Create sound with controller at chosen high value until enough
%time has passed for next step
servos=servosHigh;
servos=max(0, min(1, servos)); %check value between 0 and 1
y=formPulse(servos, pulse_index_raw,pulse_length, volume); %create signal
suitable for controller
PsychPortAudio('FillBuffer', pahandle, y, 1); %Fill audio data playback
buffer
pause         %Wait till any key pressed


%Create signal for chosen low value until enough time has passed for next
step
fprintf('\nWhen you have heard the confirmation tone please "press any
key".\n');
%Wait till any key pressed
servos=servosLow;
servos=max(0, min(1, servos)); %check value between 0 and 1
y=formPulse(servos, pulse_index_raw,pulse_length, volume); %create signal
suitable for controller
PsychPortAudio('FillBuffer', pahandle, y, 1); %Fill audio data playback
buffer


fprintf('\nSecond confirmation tone will have sounded, do not respond to
the next statement until the confirmation tone is heard. The next step is
to chose the settings for the ESC\n');


%Allow user to select calibration values (feedback for completion of audio
tones
%is through user.. auto feedback is ideal)
%Attain user slection, if enter pressed without entry default is (3)
replyBrake = input('\nSelect Brake Status. (1)Brake disabled, (2)Soft
Brake, (3)Hard Brake<default>\n', 's');
switch replyBrake
    case '1'
        fprintf('\nBrake disabled selected, setting controls to low\n');
        servos=servosLow;
        servos=max(0, min(1, servos)); %check value between 0 and 1
        y = formPulse(servos, pulse_index_raw, pulse_length, volume);
%create signal suitable for controller
        PsychPortAudio('FillBuffer', pahandle, y, 1); %Fill audio data
playback buffer
        pause(2)
    case '2'
        fprintf('\nSoft brake selected, setting controls to medium\n');
        servos = servosMed;
        servos = max(0, min(1, servos)); %check value between 0 and 1
        y = formPulse(servos, pulse_index_raw, pulse_length, volume);
%create signal suitable for controller
        PsychPortAudio('FillBuffer', pahandle, y, 1); %Fill audio data
playback buffer
        pause (2)
```

```matlab
    case '3'
        fprintf('\nHard Brake selected, setting controls to high\n');
        servos = servosHigh;
        servos = max(0, min(1, servos)); %check value between 0 and 1
        y = formPulse(servos, pulse_index_raw, pulse_length, volume);
%create signal suitable for controller
        PsychPortAudio('FillBuffer', pahandle, y, 1); %Fill audio data
playback buffer
        pause (2)
    otherwise
        fprintf('\nInvalid input, default of "Hard Brake" selected\n');
        servos = servosHigh;
        servos = max(0, min(1, servos)); %check value between 0 and 1
        y = formPulse(servos, pulse_index_raw, pulse_length, volume);
%create signal suitable for controller
        PsychPortAudio('FillBuffer', pahandle, y, 1); %Fill audio data
playback buffer
        pause (2)
end


replyTiming = input('\nSelect Timing Status. (1)Low timing <2 pole inrunner
motors> (2)Mid tining <6 pole in/outrunner motors>\n', 's');
switch replyTiming
    case '1'
        fprintf('\nLow timing selected, setting controls to low\n');
        servos = servosLow;
        servos = max(0, min(1, servos)); %check value between 0 and 1
        y = formPulse(servos, pulse_index_raw, pulse_length, volume);
%create signal suitable for controller
        PsychPortAudio('FillBuffer', pahandle, y, 1); %Fill audio data
playback buffer
        pause (2)
    case '2'
        fprintf('\nMid timing selected, setting controls to medium\n');
        servos = servosMed;
        servos = max(0, min(1, servos)); %check value between 0 and 1
        y = formPulse(servos, pulse_index_raw, pulse_length, volume);
%create signal suitable for controller
        PsychPortAudio('FillBuffer', pahandle, y, 1); %Fill audio data
playback buffer
        pause (2)
    case '3'
        fprintf('\nHigh timing selected, setting controls to high\n');
        servos = servosHigh;
        servos = max(0, min(1, servos)); %check value between 0 and 1
        y = formPulse(servos, pulse_index_raw, pulse_length, volume);
%create signal suitable for controller
        PsychPortAudio('FillBuffer', pahandle, y, 1); %Fill audio data
playback buffer
        pause (2)
    otherwise
        fprintf('\nInvalid input, Mid timing has been selected for you\n');
        servos = servosMed;
        servos = max(0, min(1, servos));
        y = formPulse(servos, pulse_index_raw, pulse_length, volume);
%create signal suitable for controller
        PsychPortAudio('FillBuffer', pahandle, y, 1); %Fill audio data
playback buffer
end


replyBattery = input('\nSelect Battery protection status. (1)Low
<70percent> (2)Medium <65percent> (3)High <60percent>\n', 's');
switch lower(replyBattery)
    case '1'
        fprintf('\nLow battery discharge selected, setting controls to
low\n');
        servos = servosLow;
        servos = max(0, min(1, servos)); %check value between 0 and 1
        y = formPulse(servos, pulse_index_raw, pulse_length, volume);
%create signal suitable for controller
        PsychPortAudio('FillBuffer', pahandle, y, 1); %Fill audio data
playback buffer
        pause (2)
    case '2'
        fprintf('\nMedium battery discharge selected, setting controls to
medium\n');
        servos = servosMed;
        servos = max(0, min(1, servos)); %check value between 0 and 1
        y = formPulse(servos, pulse_index_raw, pulse_length, volume);
```

```matlab
%create signal suitable for controller
        PsychPortAudio('FillBuffer', pahandle, y, 1); %Fill audio data
playback buffer
        pause (2)
    case '3'
        fprintf('\nHigh battery discharge selected, setting controls to
high\n');
        servos = servosHigh;
        servos = max(0, min(1, servos));
        y = formPulse(servos, pulse_index_raw, pulse_length, volume);
%create signal suitable for controller
        PsychPortAudio('FillBuffer', pahandle, y, 1); %Fill audio data
playback buffer
        pause (2)
    otherwise
        fprintf('\nInvalid input, default selection of medium has been
selected for you\n');
        servos = servosMed;
        servos = max(0, min(1, servos)); %check value between 0 and 1
        y = formPulse(servos, pulse_index_raw, pulse_length, volume);
%create signal suitable for controller
        PsychPortAudio('FillBuffer', pahandle, y, 1); %Fill audio data
playback buffer
        pause (2)
end
```

Appendix B Derivation of Direction Cosines Matrices

In mathematics, Euler angles represent the rotation of a coordinate system using successive rotations [77]. The order of successive rotations changes the relationship between the defined angles and the inertial coordinate system. Conversion of the body coordinate system to the space coordinate system using the zyx Euler angles, is achieved by successive rotations about the z, y, and x axis Euler angles.

Generally, quadrotor modelling uses xyz Euler angles to allow control of pitch and roll, airplane orientations use zyx Euler angles to allow representation of heading. Zyx Euler angles are used in aerospace. The following is the derivation of two direction cosines matrices (DCM) using zyx Euler angles and xyz Euler angles, which represent usual coordinate systems used for aircraft and helicopters respectively.

B.1 ZYX Direction Cosines Matrix

We define (pitch, roll, yaw) (θ, ϕ, ψ)

- Roll – angle body makes with respect to the vertical plane
- Pitch – angle body makes with respect to horizontal plane
- Heading – angle of rotation about body k axis

In aerospace, coordinate rotations that follow the above convention are called 'Euler angles', this differs to the mathematical definition of Euler angles. The notation zyx, which refer to the order that the rotations are completed, will be used to express the rotation matrix. The body fixed coordinates with respect to the craft are illustrated in Figure 65.

First Rotation, Heading   Second Rotation, Pitch   Third Rotation, Roll
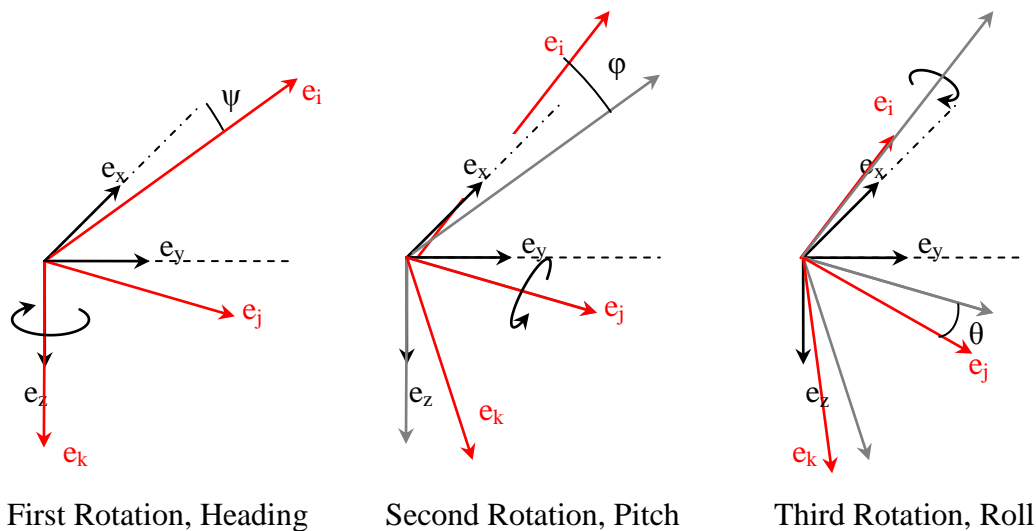
Figure 65: Successive rotations for ZYX Euler angles, where third rotation is 'actual' body coordinate system

A coordinate on the space frame is converted to its representation on the body frame using the direct cosines matrix (DCM), which represents the projection of the body frame components onto the new coordinate system. Each successive rotation has a rotation matrix. Figure 65 above shows the new coordinate system in red, the coordinate system that is being projected onto the new system in grey, and the original body frame in black.

We seek to determine R_{HRP}, a matrix that relates a body fixed frame to an inertial frame with origin at $\mathcal{A}$.

$$[x \quad y \quad z]^T = \boldsymbol{R}_{zyx}[i \quad j \quad k]^T \qquad\qquad 54$$

We use

$$c\vartheta = cos\vartheta, s\vartheta = sin\vartheta \qquad \vartheta\epsilon\{\psi, \theta, \phi\}$$

Rotation about the z-axis, heading

$$\begin{bmatrix} i \\ j \\ k \end{bmatrix}_{1stRot} = \boldsymbol{R}_{heading}\boldsymbol{r}$$

$$\begin{bmatrix} i \\ j \\ k \end{bmatrix}_{1stRot} = \begin{bmatrix} c\psi & s\psi & 0 \\ -s\psi & c\psi & 0 \\ 0 & 0 & 1 \end{bmatrix}\begin{bmatrix} x \\ y \\ z \end{bmatrix} \qquad\qquad 55$$

Rotation about the new y-axis, pitch

$$\begin{bmatrix} i \\ j \\ k \end{bmatrix}_{2ndRot} = \boldsymbol{R}_{pitch}\boldsymbol{R}_{heading}\boldsymbol{r}$$

$$\begin{bmatrix} i \\ j \\ k \end{bmatrix}_{2ndRot} = \begin{bmatrix} c\theta & 0 & -s\theta \\ 0 & 1 & 0 \\ s\theta & 0 & c\theta \end{bmatrix}\begin{bmatrix} c\psi & s\psi & 0 \\ -s\psi & c\psi & 0 \\ 0 & 0 & 1 \end{bmatrix}\begin{bmatrix} x \\ y \\ z \end{bmatrix} \qquad\qquad 56$$

Rotation about the twice rotated x-axis, roll

$$\begin{bmatrix} i \\ j \\ k \end{bmatrix}_{3rdRot} = \boldsymbol{R}_{roll}\boldsymbol{R}_{pith}\boldsymbol{R}_{heading}\boldsymbol{r}$$

$$\begin{bmatrix} i \\ j \\ k \end{bmatrix}_{3rdRot} = \begin{bmatrix} i \\ j \\ k \end{bmatrix} = \begin{bmatrix} 1 & 0 & 0 \\ 0 & c\phi & s\phi \\ 0 & -s\phi & c\phi \end{bmatrix} \begin{bmatrix} c\theta & 0 & -s\theta \\ 0 & 1 & 0 \\ s\theta & 0 & c\theta \end{bmatrix} \begin{bmatrix} c\psi & s\psi & 0 \\ -s\psi & c\psi & 0 \\ 0 & 0 & 1 \end{bmatrix} \begin{bmatrix} x \\ y \\ z \end{bmatrix}$$

57

Solving

$$R_{zyx}r = R_{roll}R_{pitch}R_{heading}$$

58

$$\begin{bmatrix} i \\ j \\ k \end{bmatrix} = \begin{bmatrix} c\theta c\psi & c\theta s\psi & -s\theta \\ s\phi s\theta c\psi - c\phi s\psi & s\phi s\theta s\psi + c\phi c\psi & s\phi c\theta \\ c\phi s\theta c\psi + s\phi s\psi & c\phi s\theta s\psi - s\phi c\psi & c\phi c\theta \end{bmatrix} \begin{bmatrix} x \\ y \\ z \end{bmatrix}$$

59

Define R_{zyx} equal to

$$R_{zyx} = R_{roll}R_{pitch}R_{heading}$$

60

To determine a matrix to determine body coordinates we take the inverse of R_{321}. Because the rotation matrix is orthogonal [91], the inverse is equal to the transpose.

$$\begin{bmatrix} i \\ j \\ k \end{bmatrix} = R_{zyx} \begin{bmatrix} x \\ y \\ z \end{bmatrix}$$

61

$$\begin{bmatrix} x \\ y \\ z \end{bmatrix} = R_{zyx}^{-1} \begin{bmatrix} i \\ j \\ k \end{bmatrix}$$

62

But

$$R^T R = I$$

63

Where I is the identity matrix

$$\begin{bmatrix} x \\ y \\ z \end{bmatrix} = R_{zyx}^T \begin{bmatrix} i \\ j \\ k \end{bmatrix}$$

64

The matrix relating body coordinates to space coordinates is then the transpose of R

$$\begin{bmatrix} x \\ y \\ z \end{bmatrix} = \begin{bmatrix} c\theta c\psi & s\phi s\theta c\psi - c\phi s\psi & c\phi s\theta c\psi + s\phi s\psi \\ c\theta s\psi & s\phi s\theta s\psi + c\phi c\psi & c\phi s\theta s\psi - s\phi c\psi \\ -s\theta & s\phi c\theta & c\phi c\theta \end{bmatrix} \begin{bmatrix} i \\ j \\ k \end{bmatrix}$$

65

$$R = \begin{bmatrix} c\theta c\psi & s\phi s\theta c\psi - c\phi s\psi & c\phi s\theta c\psi + s\phi s\psi \\ c\theta s\psi & s\phi s\theta s\psi + c\phi c\psi & c\phi s\theta s\psi - s\phi c\psi \\ -s\theta & s\phi c\theta & c\phi c\theta \end{bmatrix} \qquad 66$$

Phillips, Hailey et al present a review of attitude representations and show the relationship between the heading-pitch-roll representation of the rotation matrix and other coordinate systems including the quaternion system [77].

B.2 XYZ Direction Cosines Matrix

A body coordinate system obtained by sequential rotations about the x-axis, y-axis then z-axis is termed the xyz (roll-pitch-yaw) Euler angles rotation matrix. This representation is commonly used in the surveyed quadrotor modelling literature. The following is the development of the xyz Euler angles rotation matrix.

Roll, pitch and yaw angles used in the xyz formulation are not equivalent to the heading, pitch, and roll angles used the zyx formulation.

First rotation, roll   Second rotation, pitch   Third rotation, yaw
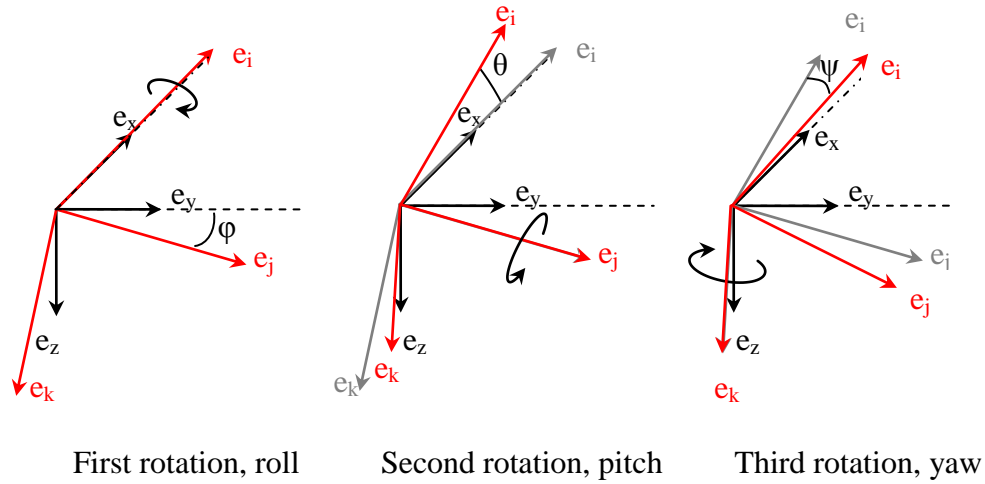
Figure 66: Successive rotations for XYZ Euler angles, where third rotation is 'actual' body coordinate system

Rotate body axis about x-axis

$$\begin{bmatrix} i \\ j \\ k \end{bmatrix}_{rot1} = R_{roll}r = \begin{bmatrix} 1 & 0 & 0 \\ 0 & c\phi & s\phi \\ 0 & -s\phi & c\phi \end{bmatrix} \begin{bmatrix} x \\ y \\ z \end{bmatrix} \qquad 67$$

Rotate 'new axis' about y-axis

$$\begin{bmatrix} i \\ j \\ k \end{bmatrix}_{rot2} = R_{pitch}r = \begin{bmatrix} c\theta & 0 & -s\theta \\ 0 & 1 & 0 \\ s\theta & 0 & c\theta \end{bmatrix} \begin{bmatrix} 1 & 0 & 0 \\ 0 & c\phi & s\phi \\ 0 & -s\phi & c\phi \end{bmatrix} \begin{bmatrix} x \\ y \\ z \end{bmatrix} \qquad 68$$

Rotate 'twice rotated axis' about z-axis

$$\begin{bmatrix} i \\ j \\ k \end{bmatrix}_{rot3} = \begin{bmatrix} i \\ j \\ k \end{bmatrix} = \boldsymbol{R}_{yaw}\boldsymbol{r} = \begin{bmatrix} c\psi & s\psi & 0 \\ -s\psi & c\psi & 0 \\ 0 & 0 & 1 \end{bmatrix}\begin{bmatrix} c\theta & 0 & -s\theta \\ 0 & 1 & 0 \\ s\theta & 0 & c\theta \end{bmatrix}\begin{bmatrix} 1 & 0 & 0 \\ 0 & c\phi & s\phi \\ 0 & -s\phi & c\phi \end{bmatrix}\begin{bmatrix} x \\ y \\ z \end{bmatrix}$$

69

The rotation matrix relating space coordinates to body coordinates is thus

$$\boldsymbol{R}_{xyz} = \begin{bmatrix} c\psi & s\psi & 0 \\ -s\psi & c\psi & 0 \\ 0 & 0 & 1 \end{bmatrix}\begin{bmatrix} c\theta & 0 & -s\theta \\ 0 & 1 & 0 \\ s\theta & 0 & c\theta \end{bmatrix}\begin{bmatrix} 1 & 0 & 0 \\ 0 & c\phi & s\phi \\ 0 & -s\phi & c\phi \end{bmatrix}\begin{bmatrix} x \\ y \\ z \end{bmatrix} \qquad 70$$

$$\boldsymbol{R}_{xyz} = \begin{bmatrix} c\psi c\theta & s\psi c\phi + c\psi s\theta s\phi & s\psi s\phi - c\psi s\theta c\phi \\ -s\psi c\theta & c\psi c\phi - s\psi s\theta s\phi & c\psi s\phi + s\psi s\theta c\phi \\ s\theta & -c\theta s\phi & c\theta c\phi \end{bmatrix} \qquad 71$$

And taking the transpose to determine the rotation matrix relating body coordinates to space coordinates

$$\boldsymbol{R} = \begin{bmatrix} c\psi c\theta & -s\psi c\theta & s\theta \\ s\psi c\phi + c\psi s\theta s\phi & c\psi c\phi - s\psi s\theta s\phi & -c\theta s\phi \\ s\psi s\phi - c\psi s\theta c\phi & c\psi s\phi + s\psi s\theta c\phi & c\theta c\phi \end{bmatrix} \qquad 72$$

Appendix C Singularity in Euler Representation

The calculation of relationship between the non-inertial angular rates and the time rate of change of the Euler angles as shown in Phillips et al is available in [77]. The relationship is

$$\begin{bmatrix} \dot\phi \\ \dot\theta \\ \dot\psi \end{bmatrix} = \begin{bmatrix} 1 & s\phi s\theta/c\theta & c\phi s\theta/c\theta \\ 0 & c\phi & -s\phi \\ 0 & s\phi/c\theta & c\phi/c\theta \end{bmatrix}\begin{bmatrix} \Omega_1 \\ \Omega_2 \\ \Omega_3 \end{bmatrix} \qquad 73$$

The mathematical singularity is caused by the division by zero for four of the terms in the above equation when θ is $\pi/2$ (90 degrees).

Appendix D Expressing dI$_R$/dt with respect to Ω

There is a change in the rotational inertia direction due to rotations of the craft. Assuming rotations of the craft are equal to the rotations of the propellers, the magnitude of the change in rotational inertia is approximately equal to the product of rotational inertia and change in orientation.

$$\Delta I_R = S = I_R \Delta \theta \qquad\qquad 74$$

Where θ is the angle that the propeller has turned through (and can vary) and I_R is the rotational mass moment of inertia for the propeller, which is constant for a body-fixed coordinate system).

We can then determine $\frac{dI_R}{dt}$

$$\frac{\Delta I_R}{\Delta t} = I_R \frac{\Delta \theta}{\Delta t} \qquad\qquad 75$$

$$\frac{dI_R}{dt} = \lim_{x \to 0} I_R \frac{\Delta \theta}{\Delta t} = I_R \Omega \qquad\qquad 76$$

$$QED$$

Appendix E Derivation of the Relationship $\dot{R}$=Rsk(Ω)

The rotation matrix is related to the rate of change in the rotation matrix [91]. A derivation for this relationship is presented below.

The rotation matrix is orthogonal, thus has the relation

$$RR^T = \begin{bmatrix} 1 & 0 & 0 \\ 0 & 1 & 0 \\ 0 & 0 & 1 \end{bmatrix} \qquad\qquad 77$$

Differentiation of the cross product

$$\frac{d(RR^T)}{dt} = \dot{R}R^T + R\dot{R}^T = 0 \qquad\qquad 78$$

$$\dot{R}R^T = -\left(\dot{R}R^T\right)^T \qquad\qquad 79$$

Therefore $\dot{R}R^T$ is a skew symmetric matrix, ie it is equal to the negative of its transpose. The skew symmetric matrix is expressed in terms of components of the body fixed frame rotational velocity.

$$\dot{R}R^T = sk\begin{pmatrix} 0 & \Omega_z & -\Omega_y \\ -\Omega_z & 0 & \Omega_x \\ \Omega_y & -\Omega_x & 0 \end{pmatrix} \qquad\qquad 80$$

$$\dot{R} = sk\begin{pmatrix} 0 & \Omega_z & -\Omega_y \\ -\Omega_z & 0 & \Omega_x \\ \Omega_y & -\Omega_x & 0 \end{pmatrix}R \qquad\qquad 81$$

QED

Appendix F Propeller Forces and $v_{prop/air}$

We construct free body diagrams (FBD's) to illustrate the forces applied to the propeller system. Newton's laws of motion will be used to formulate the relationships between components, combined with the Euler coordinate system. Figure 67 shows a free body diagram for a single propeller (neglecting the propeller mass) and shows the drag and thrust force due to incident air, and the applied motor torque due to electric power.
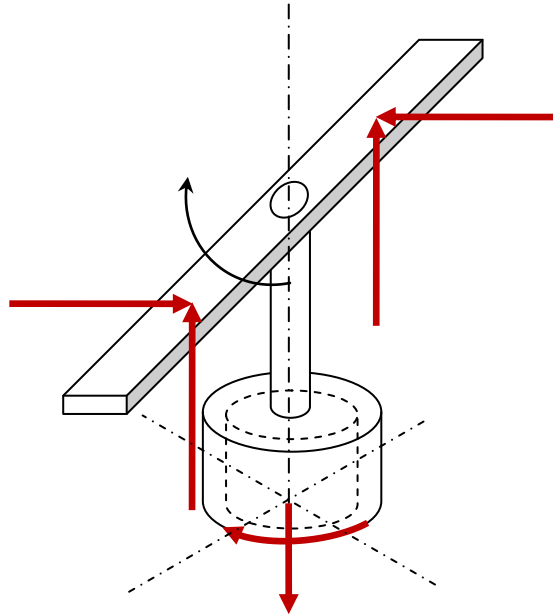
Figure 67: Free body diagram of (motor/hub/prop) propeller assembly

The magnitude of the thrust & drag force generated is dependent on the velocity of the air relative to the propeller. Several influences of the relative velocity of air are described.

Figure 68 shows that there is a change in the velocity of air impacting against the propeller for changes in axial movement. As the axial velocity of the propeller increases, the angle of attack of the propeller decreases.
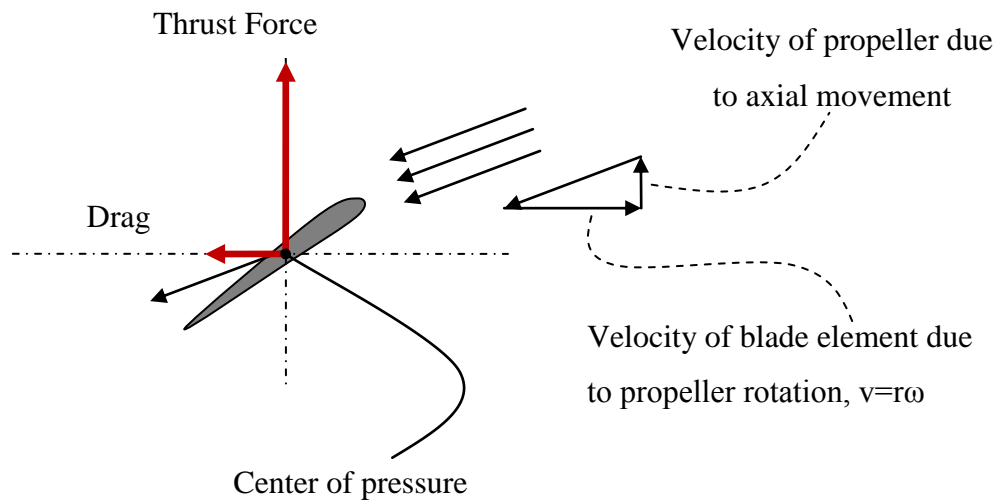
Figure 68: Free body diagram of propeller element

There are additional changes in the air speed (relative to propeller) due to: a difference in velocity at each radial and rotational position due to the combination of a rotating propeller blade and incident flow; and induced air flow (axial flow of air generated). Figure 69 shows a lateral incident air flow and a propeller rotating in the clockwise direction. The air velocity relative to the propeller blade will be larger on the advancing side of the propeller than on the retreating side. This is significant because a larger incident air velocity will produce greater lift (and vice versa), so a difference in thrust for various values of propeller rotation will occur. This difference in thrust causes the blade to flap up and down as it rotates around the hub, and a moment about the propeller hub towards the side with lowest lift.
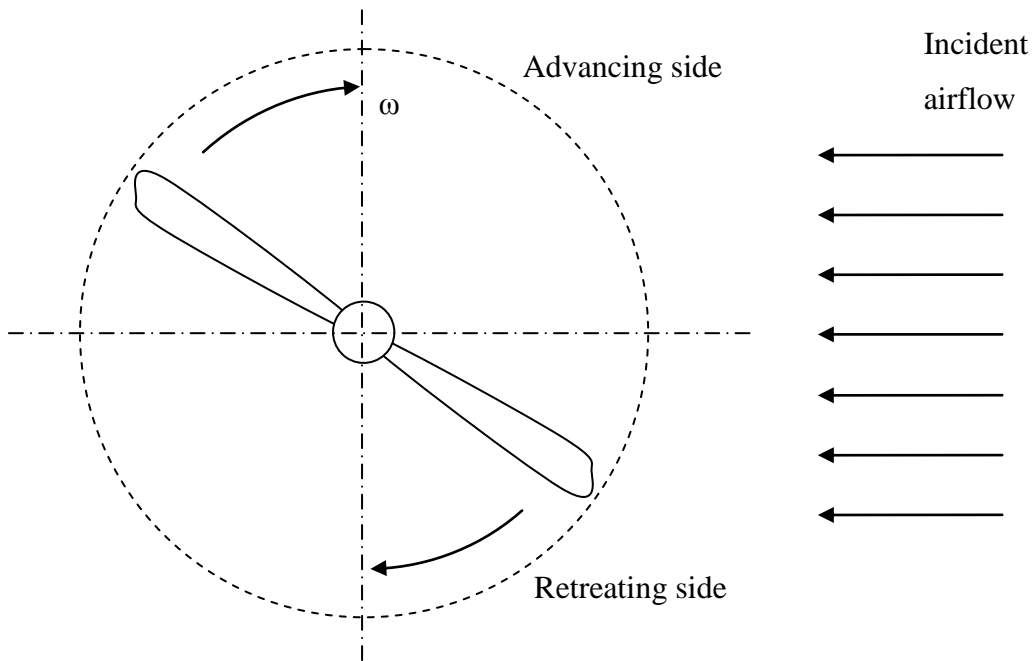
Figure 69: Illustrating the effect of variation of airflow across propeller blade

Figure 70 shows the flow of air induced by a propeller. As the propeller rotates, the air that the propeller impacts with is forced downward. A low pressure region is developed above the propeller blades, and a high pressure region is developed below the propeller blades. An airflow due to the pressure difference is formed which (while providing the pressure difference required for thrust) changes the axial airflow that the propeller blade encounters. Like wingtip vortices in aircraft, this pressure difference creates flow around the tips of the propeller blades and causes a decrease in lift.
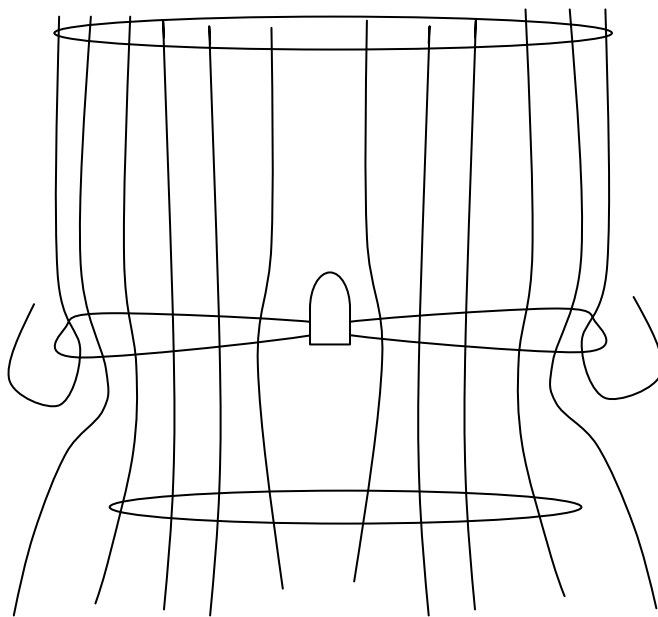
Figure 70: Induced flow on a hovering body (based off readings about flow, tip losses)

The thrust and torque force for a propeller blade are dependent on the velocity of the air that the propeller blade collides with/impacts. The incident air velocity depends on pressure gradients caused by the propeller, propeller shape, and the (axial/lateral) velocity of the propeller assembly.

Appendix G Equipment Information

G.1 Available Motors

- Maximum currents (I_{max}), max voltages (V_{max}), and the proportionality constant between provided voltage and rpm (K_V), are acquired from supplier motor specification sheets.

- Max rotational speed, ω_{max}, is calculated by multiplying K_V by the voltage supplied.

- Maximum power, P_{max}, is calculated by multiplying max current and supplied voltage.

- Maximum storage required, C_{max}, is calculated by the product of the time required (15min=900sec) and max power. This provides a very conservative estimate of the storage required for 15 minutes of flight time at the max current.

Code	I_{max}[§§]	V_{max}	K_V	P_{max}[***]	ω_{max}[†††]	C_{max}
HP-Z1705-11	5.5	3S (3 LiPo cells)	2250	61.1	24975	54945
HP-Z1705-14	4	3S	1800	44.4	19980	39960
HP-Z1709-6	9	3S	2100	99.9	23310	89910
HP-Z1709-9	6.7	3S	1500	74.4	16650	66933
HP-Z2205-34	5	3S	1530	55.5	16983	49950
HP-Z2205-38	4	3S	1340	44.4	14874	39960
HP-Z2209-26	6	3S	1120	66.6	12432	59940
HP-Z2209-32	5	3S	910	55.5	10101	49950
HP-Z2213-20	8	3S	1025	88.8	11378	79920
HP-Z2213-24	6	3S	850	66.6	9435	59940
HP-Z3007-26	15	3S	1240	167	13764	149850
HP-Z3007-30	13	3S	1050	144	11655	129870
HP-Z3013-14	22	3S	1085	244	12044	219780
HP-Z3013-16	17	3S	985	189	10934	169830
HP-Z3019-10	28	3S	1070	311	11877	279720
HP-Z3019-12	24	3S	900	266	9990	239760
HP-Z3025-06	40	3S	1255	444	13931	399600
HP-Z3025-08	32	3S	985	355	10934	319680

[§§] Max current values displayed are continuous values (as opposed to 30 second peak values), 3S LiPo are equivalent to 11.1V (1S = 3.7 volts)
[***] Max power provided to motor
[†††] Assuming enough power is provided to the motor (remember Pin is specific to the load/propeller being rotated), other limits to the rpm include max prop rpm and P_{in}

| HP-Z3025-10 | 27 | 3S | 815 | 300 | 9047 | 269730 |
| HP-Z3025-12 | 20 | 3S | 665 | 222 | 7382 | 199800 |

G.2 Available Propellers

The propellers available have various diameters, pitch, and cross section shapes. A list of available APC propellers is presented.

Code	Brand	Dia	Pitch	Type
APC 4.1x4.1 S4	APC	4.1	4.1	S4
APC 4.7x4.25 S4	APC	4.7	4.25	S4
APC 4.75x4.5 S4	APC	4.75	4.5	S4
APC 4.75x4.75 S4	APC	4.75	4.75	S4
APC 4.75x5.5 S4	APC	4.75	5.5	S4
APC 5x5 S4	APC	5	5	S4
APC 5.1x4.5 E	APC	5.1	4.5	E
APC 5.25x4.75 S4	APC	5.25	4.75	S4
APC 5.25x6.25 S4	APC	5.25	6.25	S4
APC 5.5x4.5 S4	APC	5.5	4.5	S4
APC 6x4 E	APC	6	4	E
APC 6x5.5 E	APC	6	5.5	E
APC 7x5 E	APC	7	5	E
APC 7x5 SF	APC	7	5	SF
APC 8x3.8 SF	APC	8	3.8	SF
APC 8x4 E	APC	8	4	E
APC 8X6 E	APC	8	6	E
APC 9x3.8 SF	APC	9	3.8	SF
APC 9x4.7 SF	APC	9	4.7	SF
APC 9x5 SPORT	APC	9	5	SPORT
APC 9x6 E	APC	9	6	E
APC 10x4.7 SF	APC	10	4.7	SF
APC 10x5 E	APC	10	5	E
APC 10x5 SPORT	APC	10	5	SPORT
APC 10x7 E	APC	10	7	E
APC 10x10 E	APC	10	10	E
APC 11x4.7 SF	APC	11	4.7	SF
APC 11x5.5 E	APCC	11	5.5	E
APC 12x6 E	APC	12	6	E
APC 13x6.5 E	APC	13	6.5	E

Code	Brand	Dia	Pitch	Type
APC 14x7 E	APC	14	7	E
GR 6x3 Fold	GR	6	3	Fold
GR 7.5x4 Fold	GR	7.5	4	Fold
GR 8x4.5 Fold	GR	8	4.5	Fold
GR 9x5 Fold	GR	9	5	Fold
GR 10x6 Fold	GR	10	6	Fold
GR 10x8 Fold	GR	10	8	Fold
GR 12x6 Fold	GR	12	6	Fold
GR 14x9.5 Fold	GR	14	9.5	Fold

G.3 Available Batteries

Data from AlleRC website

LiteStorm VZ Cell Type	$C_{nominal}$	12C	15C	30C cont. max	50C <30 sec
HP-LVZ0700	0.70A/hr	8.4A	10.5A	21.0A	35.0A
HP-LVZ1200	1.20A/hr	14.4A	18.0A	36.0A	60.0A
HP-LVZ2000	2.00A/hr	24.0A	30.0A	60.0A	100.0A
HP-LVZ3200	3.20A/hr	38.4A	48.0A	96.0A	160.0A

LiteStorm VX Cell Type	$C_{nominal}$	12C	15C	20C cont. max	30C <30 sec
HP-LVX0300	0.30A/hr	3.6A	5.0A	6.0A	9.0A
HP-LVX0400	0.40A/hr	4.8A	6.0A	8.0A	12.0A
HP-LVX0800	0.80A/hr	9.6A	12.0A	16.0A	24.0A
HP-LVX1200	1.20A/hr	14.4A	18.0A	24.0A	36.0A
HP-LVX1500	1.50A/hr	18.0A	22.5A	30.0A	45.0A
HP-LVX1800	1.80A/hr	21.6A	27.0A	36.0A	54.0A
HP-LVX2000	2.00A/hr	24.0A	30.0A	40.0A	60.0A
HP-LVX2100	2.10A/hr	25.2A	31.5A	42.0A	63.0A
HP-LVX2200	2.20A/hr	26.4A	33.0A	44.0A	66.0A

LiteStorm VX Cell Type	$C_{nominal}$	12C	15C	25C cont. max	40C <30 sec
HP-LVX2500	2.50A/hr	30.0A	37.5A	62.5A	100.0A
HP-LVX3300	3.30A/hr	39.6A	49.5A	82.5A	132.0A
HP-LVX3700	3.70A/hr	44.4A	59.2A	92.5A	148.0A
HP-LVX4350	4.35A/hr	52.2A	65.25A	108.75A	174.0A
HP-LVX5000	5.00A/hr	60.0A	75.0A	125.0A	200.0A
HP-LVX2500-2P	5.00A/hr	60.0A	75.0A	125.0A	200.0A

LiteStorm CX Cell Type	$C_{nominal}$	12C	15C	18C cont. max	30C <30 sec
HP-LCX2100	2.10A/hr	25.2A	31.5A	37.8A	56.7A
HP-LCX2500	2.50A/hr	30.0A	37.5A	45.0A	67.5A
HP-LCX4250	4.25A/hr	51.0A	63.75A	76.5A	114.75A

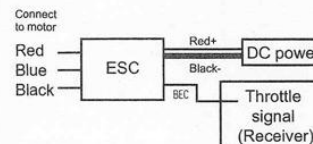| LiteStorm CX Cell Type	$C_{nominal}$	12C	15C	16C cont. max	25C <30 sec
HP-LCX5350	5.35A/hr	64.2A	80.25A	85.6A	133.75A

Appendix H ESC Instructions for use

Product Features

CE FC

1. Small and compact PCB design for light weight and simple installation.
2. Large heat sink for optimum thermal performance.
3. Highly compatible to work with 98% of all brushless motors currently on the market.
4. Ultra-smooth motor start designed to run with all kinds of brushless motors.
5. The power inlet utilizes a Japanese made "Low ESR" capacitor in order to provide stable power source.
6. The BEC power outlet utilizes a Japanese made special polymer aluminum electrolytic capacitor. It provides better noise filtering capability than other BL ESC on the market, delivering stable performance of R/C receiver and BEC.
7. The BEC features dual TO-252 package regulators. They provide superior thermal performance with 2A peak current. (RCE-BL 10A has BEC, current: 1A).
8. The throttle has more than 200 step resolution that provides great throttle response and control.
9. RCE-L25G/RCE-BL35G offers two modes of operation: Normal Airplane Mode and Helicopter Mode (Soft Start, Governor Mode).

Specification

Model	Continuous Current	Burst Current	BEC Output	Dimension	Weight
RCE-BL10A	10A	15A	1A: 2cells Li-ion/6-7cells Ni-Mh→3 servos 3cells Li-ion/8-9cells Ni-Mh→2 servos	45 x 22 x 5	12 g
RCE-BL20A	20A	30A	2A: 2cells Li-ion/6-7cells Ni-Mh→4 servos 3cells Li-ion/8-9cells Ni-Mh→3 servos 4cells Li-ion/10-12cells Ni-Mh→2 servos	45 x 22 x 9	21 g
RCE-BL25G	25A	35A		45 x 22 x11	23 g
RCE-BL35G	35A	45A		45 x 22 x12	25 g

Connect to motor

Red —— Red+ —— DC power
Blue —— ESC —— Black-
Black —— BEC —— Throttle signal (Receiver)

1. **Good temperature situation for working at the maximum current**
2. **Supporting motor types:** 2 ~ 10 pole in/outrunner motors
3. **Supporting maximum RPM:** 2 pole →190,000 rpm ; 6 pole → 630,000 rpm
4. **Input voltage:** 5.5V ~ 16.8V(Lithium 2~4cells/Ni-Mh 6~12cells)

Feature options

1. **Brake Option -** 3 settings that include Brake disabled/Soft brake/Hard brake.
2. **Electronic Timing Option -** 3 settings that include Low timing/Mid timing/High timing.
   Generally, 2 pole motors are recommended to use low timing, while 6 or more poles should use Mid timing. High timing gives more power at the expense of efficiency. Always check the current draw after changing the timing in order to prevent overloading of battery.
3. **Battery Protection Option -** 3 settings that include 70%/ 65% / 60%
   The default setting is 60%, this option will prevent over-discharge of the battery. The following reference is the guideline for setting the Battery Protection option.
   For a 3-Cell Lithium system 4.2V(single cell fully charge voltage) x 3 = 12.6V 12.6V x 60% (factory default) = 7.56V When the voltage of a 3-cell battery drops to 7.56V, the ESC will enable the Battery Protection Option. The power will be reduced to the ESC, and the pilot should land the aircraft immediately.
   NOTE: THIS OPTION IS ONLY SUITABLE FOR A FULLY CHARGED BATTERY PACK IN GOOD WORKING CONDITION.
4. **Aircraft Option (RCE-BL25G/35G):** 3 settings that include Normal Airplane / Helicopter 1 / Helicopter 2.
   Normal Airplane Mode is used for general airplanes and gliders. When flying Helicopters, you can choose Helicopter 1 Mode, or Helicopter 2 Mode. Helicopter 1 Mode provides Soft Start feature. Helicopter 2 Mode provides Soft Start and Governor Mode.
5. **Thermal Protection:** When the ESC temperature reaches 80°C for any reason, it will engage the battery protection circuit, reducing power to the ESC. We recommend mounting the ESC in a location with adequate air flow and ventilation.
6. **Safe Power On Alarm:** When the operator turns on the ESC, it will automatically detect the transmitter signal. The ESC will emit a confirmation tone and enter normal operation mode if the throttle is set to the neutral position. If the throttle position is at full throttle, it will begin to enter Setup Mode. If the throttle is in any other position, the ESC will emit an alarm and not enter into user mode for safety precautions.
7. **Aircraft Locator:** If the aircraft should land or crash in an unexpected location and become lost, the pilot can enable the Aircraft Locator Option. The Aircraft Locator Option is engaged by turning off the transmitter. When the ESC does not receive a signal from the transmitter for 30 seconds, it will start to send an alarm to the motor. The sound of the alarm will aid the pilot to locate the aircraft. This option will not work with a PCM receiver that has SAVE function enabled, or with low noise resistant PPM receivers.

Setup mode

1. **Setup mode:** Make sure to connect the ESC BEC connector to the throttle channel of the receiver. Please refer to the user manual of your radio system. The second step is to connect the 3 power-out signal pins to the brushless motor. Before you turn on the transmitter, please adjust the throttle stick to the maximum full throttle position. Proceed to connect the battery to the ESC. You will hear confirmation sounds as soon as you enter the SETUP MODE. Please refer the attached flow chart for details.

2. **Throttle stick positions in Setup mode:** Setup mode includes four settings: Brake, Electronic Timing, battery protection, and aircraft (RCE-BL25G/BL35G). Every setting has three options. Simply place the throttle stick in the highest, middle, and lowest positions for each setting. For example, first brake setting (Hard): move the stick to the highest position. Then timing setting (mid): move the throttle stick in the middle position.

Mode \ Throttle position	Low	Middle	High
Brake	· Brake disabled(1-1)	Soft brake(1-2)	Hard brake(1-3)
Electronic Timing	Low-timing(2-1)	· Mid-timing(2-2)	High-timing(2-3)
Battery Protection	70% (Low discharge rate)(3-1)	· 65%(Medium discharge rate)(3-2)	60%(High discharge rate)(3-3)
Aircraft(RCE-BL25G/35G)	· Normal Airplane/Glider(4-1)	Helicopter 1 (Soft Start)(4-2)	Helicopter 2 (Soft Start+ Governor Mode)(4-3)

Note : " · " default setting

User Mode

· Ensure the throttle stick to the lowest position. · Switch on transmitter **1**	**Connect battery power to ESC** ♪ ♪ ♪ Power on sound ♪♪♪♪ ♪♪♪♪ Transmitter detected sound **2**	**Setting Status Beeps** First mode sound (Brake) Second mode sound (Timing) Third mode sound (Battery protection) Fourth mode sound (Aircraft) **3**

Setup Instruction

First mode sound Brake Status	Second mode sound Electronic Timing Status	Third mode sound Battery protection Status	Fourth mode sound Aircraft Status
♪ = Brake disabled	♪ Low timing (apply to 2 pole inrunner motors)	♪ = 70% (Low discharge)	♪ = Normal airplane/Glider
♪ ♪ = Soft brake	♪ ♪ Mid timing (apply to 6 pole in/outr unner motors)	♪ ♪ = 65% (Med discharge)	♪ ♪ = Helicopter 1 (Soft start)
♪ ♪ ♪ = Hard brake	♪ ♪ ♪ High timing (apply to high power output) High-timing/big power/power expense	♪ ♪ ♪ = 60% (High discharge)	♪ ♪ ♪ = Helicopter 2 (Soft start + Governor Mode)

Instructions on Aircraft Mode Settings

Normal Airplane/Glider Mode (Option 4-1):
This option is applied to general airplanes and gliders.

Helicopter 1 Mode (Option 4-2):
This option provides a soft start feature and is applied to Helicopters for Normal, Idle Up 1, or Idle Up 2 modes. Please note that the sensitivity of the gyro should be set lower when flying in Idle Up 1 or Idle Up 2 modes if tail hunting (wag) occurs due to higher rotor speed.

Helicopter 2 Mode (Option 4-3):
This option supports soft start as well as Governor Mode features and is applied to Helicopters for Idle Up 1 and Idle Up 2 modes (not suitable for Normal Flight Mode). When Governor Mode is in use, the throttle should be set between 85% and 100%. Again if tail wag occurs, lower the sensitivity of the gyro to eliminate the hunting effect. The Governor Mode may not work properly in cases of insufficient rotor speed (due to improper gear ratio), poor battery discharge capability, and improper setting of gyro sensitivity and the blade pitch, etc. Please make sure all the proper adjustments have been done when using Governor Mode. We suggest the following configurations for the T-REX 450X: Motor- 400LF 2800 KV   Pinion- 15T   Battery- 11.1V 1800 mAH 12C   Main Rotor Blade- 315 Wooden Blades   Pitch- +/- 10 degrees   Throttle Setting in Governor Mode- at least 85%-100% for Idle Up   Head Speed- Approximately 2000 rpm.

Important Notes when using Governor Mode:
1. The Governor mode will keep the main rotor in relatively high speed (85%~100% throttle recommended). Too-low head speed will demand very high rotor pitch angle and cause too much current and overload of the motor.

2. Under Governor Mode, the main rotor speed will be maintained constantly at a preset value automatically. However, the variation of tail blade pitch driven by gyro/rudder servo will also affect main rotor speed. Thus, the ESC and gyro tend to be in racing condition and lock out each other. This situation is getting worse especially when the main rotor speed is set too low in Governor Mode. This is because that variation of tail pitch driven by gyro will be more significant in low rotor speed to achieve the same level of supplementary force to hold the tail. Higher rotor speed is suggested under Governor Mode to eliminate the racing between ESC and gyro. 85%~100% is recommended for the throttle value.

Setup Mode Minimum 4 channel radio is required

· **Place the throttle stick to the highest position.** · **Switch on transmitter** **1**	**Connect battery to ESC** ♪ ♪ ♪ Power on sound ♪♪♪♪ Enter Setup Mode **2**	Throttle channel adjustment process, the highest position acknowledge sound. **3**	Place the throttle stick to the lowest position, the lowest position acknowledge sound. **4**
Use throttle stick to set preferred **Brake mode** within the 5 tones. A confirmation sound will kick in when finish. ♪♪♪♪♪# ♪♪♪♪♪ **5**	Use throttle stick to set preferred **Timing mode** within the 5 tones. A confirmation sound will kick in when finish. ♪♪♪♪♪# ♪♪♪♪♪ **6**	Use throttle stick to set preferred **Battery protection mode** within the 5 tones. A confirmation sound will kick in when finish. ♪♪♪♪♪# ♪♪♪♪♪ **7**	Use throttle stick to set preferred **Aircraft Mode** within the 5 tones. A confirmation sound will kick in when finish. ♪♪♪♪♪# ♪♪♪♪♪ **8**
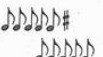
After setup is completed, place the stick to the lowest position to exit Setup Mode and enter User mode (or wait until the User mode beeps finish). The ESC is ready for use.

G20155

Appendix I Inertia Uncertainty Estimation

Estimated uncertainty (w_{IG}) assuming no correlation between m_{tot}, r, and t_{osc} is obtained by assuming using the first order Taylor series approximation of the standard deviation.

$$w_{I_G} = \left[\left(\frac{\delta I_G}{\delta r} w_r\right)^2 + \left(\frac{\delta I_G}{\delta m_{tot}} w_{m_{tot}}\right)^2 + \left(\frac{\delta I_G}{\delta t_{osc}} w_{t_{osc}}\right)^2\right]^{\frac{1}{2}}$$

$$\frac{\delta I_G}{\delta r} = \frac{m_{tot} g t_{osc}^2}{4\pi^2} - 2m_{tot}r$$

$$\frac{\delta I_G}{\delta m_{tot}} = gr\left(\frac{t_{osc}^2}{4\pi^2} - r\right)$$

$$\frac{\delta I_G}{\delta t_{osc}} = \frac{m_{tot} r g t_{osc}}{2\pi^2}$$

Substituting values of m_{tot}, r, t_{osc}, $w_{m_{tot}}$, w_r, $w_{t_{osc}}$ for each axis, the estimated uncertainty of the inertia measurements are obtained as presented in Table 9 below.

Table 9: Estimated inertia uncertainty

Particular	Uncertainty, w_{I_G}
x axis	0.0005 kg.m^2
y axis	0.0011 kg.m^2
z axis	0.0008 kg.m^2

Appendix J MATLAB Quadrotor Dynamic Model

Translational part

$$m_{total}\ddot{\xi} = F_{weight}\hat{e}_z - T_{rotor}R\hat{e}_z \tag{82}$$

where the following constants are determined in Chapter 3, and **R** is the transpose of the xyz rotation matrix (Appendix B)

$$m_{total} = 0.45kg \tag{83}$$

$$F_{weight} = 0.45kg \cdot 9.81ms^{-2} = 4.4145N \tag{84}$$

$$T_{rotor,n} = b\omega_n{}^2 = \omega_n{}^2 \cdot 2.9402 \cdot 10^{-6}N/rpm^2$$

$$T_{rotor} = \sum_{n=1}^{4} b\omega_n{}^2 = 2.9402 \cdot (\omega_1{}^2 + \omega_2{}^2 + \omega_3{}^2 + \omega_4{}^2) \tag{85}$$

therefore the translational quadrotor model is

$$\ddot{\xi} = \begin{bmatrix} \frac{-b \cdot \sin\theta}{0.45}(\omega_1{}^2 + \omega_2{}^2 + \omega_3{}^2 + \omega_4{}^2) \\ \frac{-b \cdot \cos\theta \cdot \sin\phi}{0.45}(\omega_1{}^2 + \omega_2{}^2 + \omega_3{}^2 + \omega_4{}^2) \\ \frac{4.4145}{0.45} - \frac{-b \cdot \cos\theta \cdot \cos\phi}{0.45}(\omega_1{}^2 + \omega_2{}^2 + \omega_3{}^2 + \omega_4{}^2) \end{bmatrix} \tag{86}$$

Eulers law for the conservation of angular momentum for rotor, n

$$\boldsymbol{M_{drag,n}} + \boldsymbol{M_{frame,n}} = \frac{d(I_{rotor,n}\omega_{rotor,n})}{dt}. \tag{.87}$$

where, I_{rotor} does not change direction or size, therefore

$$D\omega_n{}^2\hat{e}_k + \boldsymbol{M_{frame,n}} = \boldsymbol{0} + I_{rotor}\frac{d\omega_n}{dt} \tag{88}$$

$$\boldsymbol{M_{frame,n}} = I_{rotor}\frac{d\omega_n}{dt} - D\omega_n{}^2\hat{e}_k \tag{89}$$

Eulers law for the conservation of angular momentum for the frame

$$\sum_{n=1}^{4}\boldsymbol{M_{frame,n}} + \begin{bmatrix} bj & -bj & bj & -bj \\ bi & bi & -bi & -bi \\ 0 & 0 & 0 & 0 \end{bmatrix}\begin{bmatrix} \omega_1{}^2 \\ \omega_2{}^2 \\ \omega_3{}^2 \\ \omega_4{}^2 \end{bmatrix} = \boldsymbol{I_{frame}}\begin{bmatrix} \dot{\Omega}_i \\ \dot{\Omega}_j \\ \dot{\Omega}_k \end{bmatrix} \tag{90}$$

Substituting $M_{frame,n}$ from equation 89, where the direction of $M_{frame, n}$ is as shown in Figure 53.

$$I_r\begin{bmatrix} \Omega_j & -\Omega_j & -\Omega_j & \Omega_j \\ -\Omega_i & \Omega_i & \Omega_i & -\Omega_i \\ 0 & 0 & 0 & 0 \end{bmatrix}\begin{bmatrix} \omega_1 \\ \omega_2 \\ \omega_3 \\ \omega_4 \end{bmatrix} + \begin{bmatrix} bj & -bj & bj & -bj \\ bi & bi & -bi & -bi \\ -d & d & d & -d \end{bmatrix}\begin{bmatrix} \omega_1{}^2 \\ \omega_2{}^2 \\ \omega_3{}^2 \\ \omega_4{}^2 \end{bmatrix}$$

$$= \begin{bmatrix} I_{ii} & 0 & 0 \\ 0 & I_{jj} & 0 \\ 0 & 0 & I_{kk} \end{bmatrix}\begin{bmatrix} \dot{\Omega}_\iota \\ \dot{\Omega}_j \\ \dot{\Omega}_k \end{bmatrix}$$

Expanding the system of equations and rearranging to group Ω terms

$$I_{ii}\dot{\Omega}_i - I_r\Omega_j(\omega_1 - \omega_2 - \omega_3 + \omega_4) = bj(\omega_1{}^2 - \omega_2{}^2 + \omega_3{}^2 - \omega_4{}^2)$$

$$I_{jj}\dot{\Omega}_j - I_r\Omega_i(\omega_1 - \omega_2 - \omega_3 + \omega_4) = bi(\omega_1{}^2 + \omega_2{}^2 - \omega_3{}^2 - \omega_4{}^2)$$

$$I_{kk}\dot{\Omega}_k = d(-\omega_1{}^2 + \omega_2{}^2 + \omega_3{}^2 - \omega_4{}^2)$$

Applying Laplace transforms, assuming $\Omega_i(0) = \Omega_j(0) = \Omega_k(0) = 0$, and the rotational speed is approximately constant.

$$s\mathcal{L}\Omega_k = d(-\omega_1{}^2 + \omega_2{}^2 + \omega_3{}^2 - \omega_4{}^2) \qquad\qquad 91$$

$$\begin{bmatrix} I_{ii}s & -I_r(\omega_1 - \omega_2 - \omega_3 + \omega_4) \\ I_r(\omega_1 - \omega_2 - \omega_3 + \omega_4) & I_{jj}s \end{bmatrix}\begin{bmatrix} \mathcal{L}\Omega_i \\ \mathcal{L}\Omega_j \end{bmatrix} =$$

$$\begin{bmatrix} bj(\omega_1{}^2 - \omega_2{}^2 + \omega_3{}^2 - \omega_4{}^2) \\ bi(\omega_1{}^2 + \omega_2{}^2 - \omega_3{}^2 - \omega_4{}^2) \end{bmatrix} \qquad\qquad 92$$

Finding the inverse of the coefficients, and rearranging to get an expression for $[\mathcal{L}\Omega_i, \mathcal{L}\Omega_j]^T$

$$\begin{bmatrix} \mathcal{L}\Omega_i \\ \mathcal{L}\Omega_j \end{bmatrix}$$

$$= \begin{bmatrix} \dfrac{I_{jj}bj(\omega_1{}^2 - \omega_2{}^2 + \omega_3{}^2 - \omega_4{}^2)s + I_r bi(\omega_1 - \omega_2 - \omega_3 + \omega_4)(\omega_1{}^2 + \omega_2{}^2 - \omega_3{}^2 - \omega_4{}^2)}{I_{ii}I_{jj}s^2 + I_r{}^2(\omega_1 - \omega_2 - \omega_3 + \omega_4)^2} \\ \dfrac{I_{ii}bi(\omega_1{}^2 + \omega_2{}^2 - \omega_3{}^2 - \omega_4{}^2)s - I_r bj(\omega_1 - \omega_2 - \omega_3 + \omega_4)(\omega_1{}^2 - \omega_2{}^2 + \omega_3{}^2 - \omega_4{}^2)}{I_{ii}I_{jj}s^2 + I_r{}^2(\omega_1 - \omega_2 - \omega_3 + \omega_4)^2} \end{bmatrix}$$

A Simulink model for the quadrotor is provided on the attached CD.

REFERENCES

1. Pinder, S., *Control Strategy for a Four-Rotor VTOL UAV*, in *46th AIAA Aerospace Sciences Meeting and Exhibit*. 2008: Reno, Nevada.
2. US-DOD, *Unmanned Aircraft Systems Roadmap 2005-2030*, D.O.D., Editor. 2005, Office of the Secretary of Defense.
3. Kroo, I. and P. Kunz. *Development of the mesicopter: A miniature autonomous rotorcraft*. 2000.
4. Kroo, I., *Meisocopter Image*, http://adg.stanford.edu/mesicopter/imageArchive/images/mesicopter%205.jpg, Editor. 2009.
5. Wong, K.C., et al. *Attitude stabilization in hover flight of a mini tail-sitter UAV with variable pitch propeller*. in *Intelligent Robots and Systems, 2007. IROS 2007. IEEE/RSJ International Conference on*. 2007.
6. Grasmeyer, J.M. and M.T. Keennon, *Development of the Black Widow Micro Air Vehicle*. 2001.
7. Espinoza, O., *MV-22 Osprey (Hover)*, in *Boeing: Multimedia - Image Gallery*. 2007, Boeing.
8. Kin, A.M., *MV-22 Osprey (Forward flight)*, in *Boeing: Multimedia - Image Gallery*. 2007, Boeing.
9. Unknown, *Convair XFY-1 Pogo*. 1954, Smithsonian National Air and Space Museum.
10. Kermode, A.C., *Flight without formulae*. 1989, Harlow, Essex: Longman Scientific & Technical.
11. Field, M., *LAPD_Bell_206_Jetranger.jpg*. 2006.
12. Lehmann, M., *KamowK32A*. 2006, Wikipedia.
13. Unknown, *De Bothezat Quadrotor*. 1923, Edison National Historic Site archives.
14. Frank, A., et al., *Hover, Transition, and Level Flight Control Design for a Single-Propeller Indoor Airplane*, in *To appear in the Proceedings of the AIAA Guidance, Navigation Control Conference and Exhibit*. 2007: Myrtle Beach, SC.
15. Stone, R.H. *Control Architecture for a Tail-Sitter Unmanned Air Vehicle*. in *Proc. of the 5th Asian Control Conference*. 2004. Melbourne, Australia.
16. Phillip, A., *Design of a Multi-Rotor VTOL UAV*. 2005, Department of Mechanical Engineering, University of Waterloo.
17. Tremblay, R., *Propulsion System for a Multi-Rotor VTOL*. 2005, Department of Mechanical Engineering, University of Waterloo.
18. Phillip, A., *Dynamic Model of a Multi-Rotor VTOL*. 2006, Department of Mechanical Engineering, University of Waterloo.
19. Wilson, J. and S. Pinder, *Control Strategy for a Four-Rotor VTOL UAV*. 2006, AUT University: Auckland.
20. Boy, G.A. *Evolution of socio-cognitive models supporting the co-adaptation of people and technology*. in *Proceedings of HCI International*. 2001. New Orleans, USA.
21. Arnaud, *Image of a Cessna 172*. 2007, Wikimedia.

22. Norman, D.A. and S.W. Draper, *User centered system design: New perspectives on Human-computer interation*. 1986, Hillsdale, NJ: Erlbaum Associates. 526.

23. Stengel, R.F., *Toward intelligent flight control.* Systems, Man and Cybernetics, IEEE Transactions on, 1993. **23**(6): p. 1699-1717.

24. Phillips, W.F., *Mechanics of Flight*. 2004: John Wiley and Sons.

25. Grant, P.R. and B. Haycock, *The Effect of Jerk and Acceleration on the Perception of Motion*, in *AIAA Modeling and Simulation Technologies Conference and Exhibit*. 2006: Keystone, Colorado.

26. Zain, M.Z., N. Mohamad, and Z.M. Ali, *Redesign of the Bothezat Helicopter: the way Forward for the Rotorcraft Industry*, in *43rd AIAA/ASME/ASCE/ASH/ASC Structures, Structural Dynamics and Materials Conference*. 2002: Denver, Colorado.

27. Leishman, J.G., *The Breguet-Richet Quad-Rotor Helicopter of 1907*. 2009.

28. *De Bothezat helicopter - development history, photos, technical data*. 2009.

29. Ardema, M.D., *Vehicle Concepts and Technology Requirements for Buoyant Heavy-Lift Systems*. 1981, NASA, Scientific and Technical Information Branch, Ames Research Center: Moffett Field, California.

30. Jenkins, D.R., T. Landix, and J. Miller, *American X-Vehicles: An Inventory of X-1 to X-50*, in *Monographs in Aerospace History No. 31*. 2003, AIAA.

31. DeTore, J. and S. Martin Jr, *Multi Rotor Options for Heavy Lift.* 1979.

32. Nagabhushan, B.L. and N.P. Tomlinson, *Dynamic Stability of a Buoyant Quad-Rotor Aircraft.* Journal of Aircraft, 1983. **20**(3): p. 243-249.

33. Kroo, I. and P. F, *Proposal - Mesicopter: A Meso-Scale Flight Vehicle for Atmospheric Sensing*. 1998, Stanford: California.

34. Kroo, I. and P. Kunz, *Mesoscale flight and miniature rotorcraft development.* Fixed and flapping wing aerodynamics for micro air vehicle applications, 2001: p. 503-517.

35. Kroo, I., *Innovations in aeronautics.* AIAA Paper, 2004. **1**.

36. Kroo, I., et al., *The Mesicopter: A Miniature Rotorcraft Concept - Phase II Interim Report*. 2000, Stanford University.

37. *About Draganfly Innovations Inc. - Innovative UAV Aircraft & Aerial Video Systems*. 2009 [cited 2009 16 April].

38. Altug, E., J.P. Ostrowski, and R. Mahony. *Control of a quadrotor helicopter using visual feedback*. in *Robotics and Automation, 2002. Proceedings. ICRA '02. IEEE International Conference on*. 2002.

39. Pounds, P., et al. *Design of a four-rotor aerial robot*. 2002.

40. Roberts, J.M., P.I. Corke, and G. Buskey. *Low-cost flight control system for a small autonomous helicopter*. in *Robotics and Automation, 2003. Proceedings. ICRA '03. IEEE International Conference on*. 2003.

41. Pounds, P., R. Mahony, and P. Corke. *Small-Scale Aeroelastic Rotor Simulation, Design and Fabrication*. in *Proceedings of Australasian Conference on Robotics and Automation*. 2005. Sydney, Australia.

42. Pounds, P., R. Mahony, and P. Corke. *Modelling and control of a quad-rotor robot*. in *Proceedings of the Australasian Conference on Robotics and Automation*. 2006.

43. Altug, E., J.P. Ostrowski, and C.J. Taylor, *Control of a quadrotor helicopter using dual camera visual feedback.* The International Journal of Robotics Research, 2005. **24**(5): p. 329.

44. Altug, E., J.P. Ostrowski, and C.J. Taylor. *Quadrotor control using dual camera visual feedback*. 2003.

45. Erginer, B. and E. Altug. *Modeling and PD Control of a Quadrotor VTOL Vehicle*. in *Intelligent Vehicles Symposium, 2007 IEEE*. 2007.

46. Bouabdallah, S., P. Murrieri, and R. Siegwart. *Design and control of an indoor micro quadrotor*. in *Robotics and Automation, 2004. Proceedings. ICRA '04. 2004 IEEE International Conference on*. 2004.

47. Bouabdallah, S., A. Noth, and R. Siegwart. *PID vs LQ control techniques applied to an indoor micro quadrotor*. in *Proceedings of the 2004 IEEE/RSJ International Conference on Intelligent Robots and Systems*. 2004. Sendal, Japan.

48. Bouabdallah, S. and R. Siegwart. *Full control of a quadrotor*. in *Intelligent Robots and Systems, 2007. IROS 2007. IEEE/RSJ International Conference on*. 2007.

49. Tayebi, A. and S. McGilvray. *Attitude stabilization of a four-rotor aerial robot*. in *Decision and Control, 2004. CDC. 43rd IEEE Conference on*. 2004. Atlantis, Paradise Island, Bahamas.

50. Tayebi, A. and S. McGilvray, *Attitude stabilization of a VTOL quadrotor aircraft.* IEEE Transactions on Control Systems Technology, 2006. **14**(3): p. 562-571.

51. Tayebi, A., et al. *Attitude estimation and stabilization of a rigid body using low-cost sensors*. in *Proceedings of the 46th IEEE Conference on Decision and Control*. 2007. New Orleans, LA, USA.

52. Tayebi, A. *Unit Quaternion-Based Output Feedback for the Attitude Tracking Problem*. in *IEEE Transactions on Automatic Control*. 2008. unknown.

53. Derafa, L., T. Madani, and A. Benallegue. *Dynamic Modelling and Experimental Identification of Four Rotors Helicopter Parameters*. in *Industrial Technology, 2006. ICIT 2006. IEEE International Conference on*. 2006.

54. Bouchoucha, M., et al. *Step by step robust nonlinear PI for attitude stabilisation of a four-rotor mini-aircraft*. in *Control and Automation, 2008 16th Mediterranean Conference on*. 2008.

55. Bouadi, H., M. Bouchoucha, and M. Tadjine, *Sliding Mode Control based on Backstepping Approach for an UAV Type-Quadrotor.* International Journal of Applied Mathematics and Computer Sciences, 2008. **4**(1): p. 12-17.

56. Dunfied, J., M. Tarbouchi, and G. Labonte. *Neural network based control of a four rotor helicopter*. in *Industrial Technology, 2004. IEEE ICIT '04. 2004 IEEE International Conference on*. 2004.

57. Coza, C. and C.J.B. Macnab. *A New Robust Adaptive-Fuzzy Control Method Applied to Quadrotor Helicopter Stabilization*. in *Fuzzy Information Processing Society, 2006. NAFIPS 2006. Annual meeting of the North American*. 2006.

58. Nicol, C., C.J.B. Macnab, and A. Ramirez-Serrano. *Robust neural network control of a quadrotor helicopter*. in *Electrical and Computer Engineering, 2008. CCECE 2008. Canadian Conference on*. 2008.

59. Kong Wai, W. and M.S.B. Abidin. *Design and Control of a Quad-Rotor Flying Robot For Aerial Surveillance*. in *Research and Development, 2006. SCOReD 2006. 4th Student Conference on*. 2006.

60. Hoffmann, G., et al. *The Stanford testbed of autonomous rotorcraft for multi agent control (STARMAC)*. in *Digital Avionics Systems Conference, 2004. DASC 04. The 23rd*. 2004.

61. Hoffmann, G.M., et al. *Quadrotor helicopter flight dynamics and control: Theory and experiment*. in *Proceedings of the AIAA Guidance, Navigation, and Control*. 2007. unknown.

62. Waslander, S.L., et al. *Multi-agent quadrotor testbed control design: integral sliding mode vs. reinforcement learning*. in *Intelligent Robots and Systems, 2005. (IROS 2005). 2005 IEEE/RSJ International Conference on*. 2005.

63. Earl, M.G. and R. D'Andrea. *Real-time attitude estimation techniques applied to a four rotor helicopter*. in *Decision and Control, 2004. CDC. 43rd IEEE Conference on*. 2004.

64. Breheny, S.H., R. D'Andrea, and J.C. Miller. *Using airborne vehicle-based antenna arrays to improve communications with UAV clusters*. in *Decision and Control, 2003. Proceedings. 42nd IEEE Conference on*. 2003.

65. Gurdan, D., et al. *Energy-efficient Autonomous Four-rotor Flying Robot Controlled at 1 kHz*. in *Robotics and Automation, 2007 IEEE International Conference on*. 2007.

66. Escareno, J., S. Salazar-Cruz, and R. Lozano. *Embedded control of a four-rotor UAV*. in *Proceedings of the 2006 Americal Control Conference*. 2006. Minneapolis, Minnesota, USA: IEEE.

67. Amir, M.Y. and V. Abbass. *Modeling of Quadrotor Helicopter Dynamics*. in *Smart Manufacturing Application, 2008. ICSMA 2008. International Conference on*. 2008.

68. Madani, T. and A. Benallegue. *Control of a Quadrotor Mini-Helicopter via Full State Backstepping Technique*. in *Decision and Control, 2006 45th IEEE Conference on*. 2006.

69. Berbra, C., S. Lesecq, and J.J. Martinez. *A multi-observer switching strategy for fault-tolerant control of a quadrotor helicopter*. in *Control and Automation, 2008 16th Mediterranean Conference on*. 2008.

70. Tretyakov, V. and H. Surmann. *Hardware architecture of a four-rotor UAV for USAR/WSAR scenarios*. in *Workshop Proceedings of SIMPAR 2008 - International Conference on Simulation, Modeling and Programming for Autonomous Robots*. 2008. Venice, Italy.

71. Ng, T.T.H. and G.S.B. Leng, *Application of genetic algorithms to conceptual design of a micro-air vehicle.* Engineering Applications of Artificial Intelligence, 2002. **15**(5): p. 439-445.

72. Ng, T.T.H. and G.S.B. Leng, *Design of small-scale quadrotor unmanned air vehicles using genetic algorithms.* Proceedings of the Institution of Mechanical Engineers - Part G: Journal of Aerospace Engineering, 2007. **221**(5): p. 893-905.

73. Young, L.A., et al. *New concepts and perspectives on micro-rotorcraft and small autonomous rotary-wing vehicles*. in *AIAA 20 th Applied Aerodynamics Conference*. 2002. St Louis, MO.

74. Knoebel, N.B. and T.W. McLain. *Adaptive quaternion control of a miniature tailsitter UAV*. in *American Control Conference, 2008*. 2008.

75. Colgren, R. and R. Loschke, *Effective Design of Highly Maneuverable Tailless Aircraft.* Journal of Aircraft, 2008. **45**(4): p. 1441-1449.

76. Stone, R.H., et al., *Flight Testing of the T-Wing Tail-Sitter Unmanned Air Vehicle.* Journal of Aircraft, 2008. **45**(2).

77. Phillips, W.F., C.E. Hailey, and G.A. Gebert, *Review of Attitude Representations Used for Aircraft Kinematics.* Journal of Aircraft, 2001. **38**(4).

78.   Chao, H., Y. Cao, and Y. Chen. *Autopilots for Small Fixed-Wing Unmanned Air Vehicles: A Survey*. in *Proceedings of the 2007 IEEE International Conference on Mechatronics and Automation*. 2007. Harbin, China.

79.   Chao, H., Y. Cao, and Y. Chen, *Autopilots for Small Fixed-Wing Unmanned Air Vehicles: A Survey*, in *International Conference on Mechatronics and Automation*. 2007: Harbin, China. p. 3144-3149.

80.   Martin, P. and E. Salaun. *Invariant observers for attitude and heading estimation from low-cost inertial and magnetic sensors*. in *Decision and Control, 2007 46th IEEE Conference on*. 2007.

81.   Fay, A., *A knowledge-based system to translate control system applications.* Engineering Applications of Artificial Intelligence, 2003. **16**: p. 567-577.

82.   Frazzoli, E., M.A. Dahleh, and E. Feron. *Robust hybrid control for autonomous vehicle motion planning*. in *Decision and Control, 2000. Proceedings of the 39th IEEE Conference on*. 2000.

83.   Zhang, Y., et al., *Development of the model and hierarchy controller of the quad-copter.* Proceedings of the Institution of Mechanical Engineers -- Part G -- Journal of Aerospace Engineering, 2008. **222**(1): p. 1-12.

84.   Robinson, J., *Development of an Aerofoil for a VTOL UAV*. 2008, AUT University: Auckland, New Zealand.

85.   Pounds, P., et al. *Towards dynamically-favourable quad-rotor aerial robots*. 2004.

86.   Abbott, I.H. and A.E. Von-DoenHoff, *Theory of wing sections: Including a summary of airfoil data*. Second Edition ed. 1959, New York, NY: Dover Publications Inc.

87.   Richards, R.J., *An introduction to dynamics and control*. 1979: Longman Scientific and Technical.

88.   Hamel, T., et al. *Dynamic modelling and configuration stabilization for an X4-flyer*. in *15th Triennial World Congress*. 2002. Barcelona, Spain.

89.   Diebel, J., *Representing Attitude: Euler Angles, Unit Quaternions, and Rotation Vectors*. 2006, Stanford University: Stanford, California.

90.   Nice, E.B., *Design of a Four Rotor Hovering Vehicle*, in *Graduate School*. 2004, Cornell Univeristy.

91.   Levine, W.S., ed. *The Control Handbook*. 1996, CRC press: Boca Raton, Fl. 1305.

92.   Stengel, R.F., *Flight Dynamics*. 2004: Princeton University Press.

93.   Bramwell, A.R.S., G. Done, and D. Balmford, *Bramwell's Helicopter Dynamics*. Second edition ed. 2001, Woburn, MA: Buterworth Heinemann.

94.   Pinder, S., *Aircraft Takeoff Performance Monitoring in Far-Northern Resions: An Application of the Global Positioning System*, in *Mechanical Engineering*. 2002, Univeristy of Saskatchewan.

95.   Ogata, K., *Modern Control Engineering*. Fourth Edition ed. 2002, Upper Saddle River, NJ: Prentice Hall.

96.   Jackson, E.B., *Manual for a Workstation-based Generic Flight Simulation Program (LaRCsim) - Version 1.4*. 1995, Langley Research Center, NASA: Hampton, Viginia.

97.   Campa, G., *Airlib - The aircraft library*. 2003, Mathworks. p. Airlib is a library of aircraft models to be used with Simulink 3.1. It includes a model for the Cessna 172 and Boeing 747., http://www.mathworks.com/matlabcentral/fileexchange/3019 (retrieved 15 June 2009).

98.   Brumbaugh, R.W., *Aircraft model for the AIAA controls design challenge.* Journal of Guidance Control and Dynamics, 1994. **17**(4): p. 747-752.

99.   Kim, S.K. and D.M. Tilbury, *Mathematical Modeling and Experimental Identification of an Unmanned Helicopter Robot with Flybar Dynamics.* Journal of Robotic Systems, 2004. **21**(3): p. 95-116.

100.   Mahony, R. and T. Hamel, *Adaptive compensation of aerodynamic effects during takeoff and landing manoeuvres for a scale model autonomous helicopter.* European Journal of Control, 2001. **7**(1): p. 43-57.

GLOSSARY OF TERMS

Command: User inputs to a HMI that correspond to user desired states

Conceptual model: A model, internal to a user, that relates their control inputs to desired control outputs

Control: Manipulation of independent states to achieve dependent desired states

Controller setting: Value displayed on radio controller indicating a set-point

Pilot: Human who provides command of a system

Quadrotor: Four-propeller helicopter with all propellers in the same plane and with two propellers rotating clockwise and two propellers rotating counter-clockwise (ie with configuration shown in Figure 5).